ISBN 978-82-471-1956-3 (printed ver.)
ISBN 978-82-471-1957-0 (electronic ver.)
ISSN 1503-8181

Doctoral theses at NTNU, 2009:267

Cécile Barrère

Integrated geophysical modelling and tectonic evolution of the western Barents Sea

NTNU
Norwegian University of
Science and Technology

Cécile Barrère
Doctoral Thesis

Doctoral theses at NTNU, 2009:267

NTNU
Norwegian University of
Science and Technology

Thesis for the degree of
philosophiae doctor

Department of Petroleum Engineering and Applied
Geophysics
NTNU, University of Trondheim

NTNU
Norwegian University of
Science and Technology

Cécile Barrère

Integrated geophysical modelling and tectonic evolution of the western Barents Sea

Thesis for the degree of philosophiae doctor

Trondheim, August 2009

Norwegian University of
Science and Technology
Department of Petroleum Engineering and Applied Geophysics
NTNU, University of Trondheim

NTNU
Norwegian University of
Science and Technology

NTNU
Norwegian University of Science and Technology

Thesis for the degree of philosophiae doctor

Department of Petroleum Engineering and Applied Geophysics
NTNU, University of Trondheim

ISBN 978-82-471-1956-3 (printed ver.)
ISBN 978-82-471-1957-0 (electronic ver.)
ISSN 1503-8181

Doctoral Theses at NTNU, 2009:267

Printed by Tapir Uttrykk

Cécile Barrère

NTNU, University of Trondheim
Department of Petroleum Engineering and Applied Geophysics

Integrated geophysical modelling and tectonic evolution of the western Barents Sea

Dissertation for the degree of philosophiae doctor (PhD)

Submitted in August 2009

Table of contents

Appendix

Slagstad, T., Barrére, C., Davidsen, B. and Ramstad, R. K. (2008) Petrophysical and thermal properties of pre-Devonian basement rocks on the Norwegian continental margin. NGU Bulletin, 448, 1-6.

Acknowledgements

First I would like to thank Jan Reidar Skilbrei and Odleiv Olesen who gave me the opportunity to develop my scientific skills through this PhD at NGU. Thank you for the way you welcomed me and set me up in my new life in Norway. I would like to extend a special thanks to Odleiv who has followed closely my work and who allowed me to join the scientific cruise around Svalbard in 2006. This wonderful trip remains as one of my best memories.

Great thanks go to my official supervisor Jörg Ebbing and my none-official supervisor Laurent Gernigon for their professionalism and the friendship we have developed during these years. Thank you for encouraging and supporting me during my thesis, sharing your experience, knowledge and reviewing the papers, and for respecting and trusting me.

Special thanks go to Hermann Zeyen who collaborated with me despite a busy schedule! The enthusiasm he showed when sharing his knowledge was amazing and terribly contagious.

I would like to kindly thank the members of StatoilHydro who helped me get the data I needed to complete my thesis and showed me a bit of the incredibly beautiful Lofoten Islands. Special thanks go to Arild Ingebrigtsen and Peter Midbøe.
I would like to express my acknowledgments to Mai-Britt Mørk, Christine Fichler and Manel Fernandez who accepted assessing the thesis and who provided helpful comments, which have improved the quality of the thesis.
Also, I would like to congratulate and thank all the researchers who have worked to understand the geology of the Barents Sea. All their publications have directly contributed to the success of this PhD.

I warmly thank all of my team members and colleagues from NGU who had a word, an action, a smile to cheer me up every day. Working in this ambience was an immense chance and I wish to all PhD. candidates a similar experience. I would like to express my gratitude to David Roberts who have corrected the english and commented the content of several of the papers included in my thesis. My gratitude goes also to Morten Often who has been a colleague, landlord, taxi-driver, cross-country skiing teacher and a friend. Thank you for introducing me to Norwegian culture through the music, dance and food.

I would like to especially embrace my favourite Icelander (Fjalar), Iranian (Aziz) and Italian (Laura) PhD mates and friends for the good times we have shared together.

I knew no one in Trondheim when I arrived in August 2005. I do not know whom I should thank for introducing me to the numerous other nice people I have had the chance to meet in the city… the fates maybe! I would like to affectionately embrace the Spanish team, the Italian troop, the German delegation, the French band and more largely the French-speaking league, the Norwegian Club and the English, American, Portuguese, Danish, Belgian, and others who offered me friendship and made my stay unforgettable.

I also give hugs to my numerous friends in France who supported me from a distance. Lately, a new group of supporters appeared at my new company, Beicip-Franlab. I would like to thank them for encouraging me during the last months of my PhD.

I thank my family and my boyfriend's family for their love and psychological support that were essential to the success of my PhD. I finally thank Thomas, who was in France but has shared all the highs and lows of these years with me, who always found the right words, who never complained and was just nothing less than perfect.

Trondheim, August 2009

Cécile Barrère

Chapter 1. Introduction

The Barents Sea Shelf is located in northernmost Europe and extends from the eastern boundary of North Atlantic and Svalbard archipelago in the west to Novaya Zemlya in the east, over a distance of about 1000 km (Fig. 1.1). In the west and north, the Barents Sea is bounded by Cenozoic passive margins. The Barents Sea is divided into the eastern Barents Sea belonging to Russia and the Norwegian western Barents Sea. The eastern and western continental shelves have very different basin structures with long-wavelength basins in the east and narrower rift basins in the west, more particularly in the southwestern part of the Barents Shelf. In this area, sedimentary rocks in the basins range in age from Late Palaeozoic to Quaternary. Locally, the sedimentary rock successions have a thickness of more than 14 km.

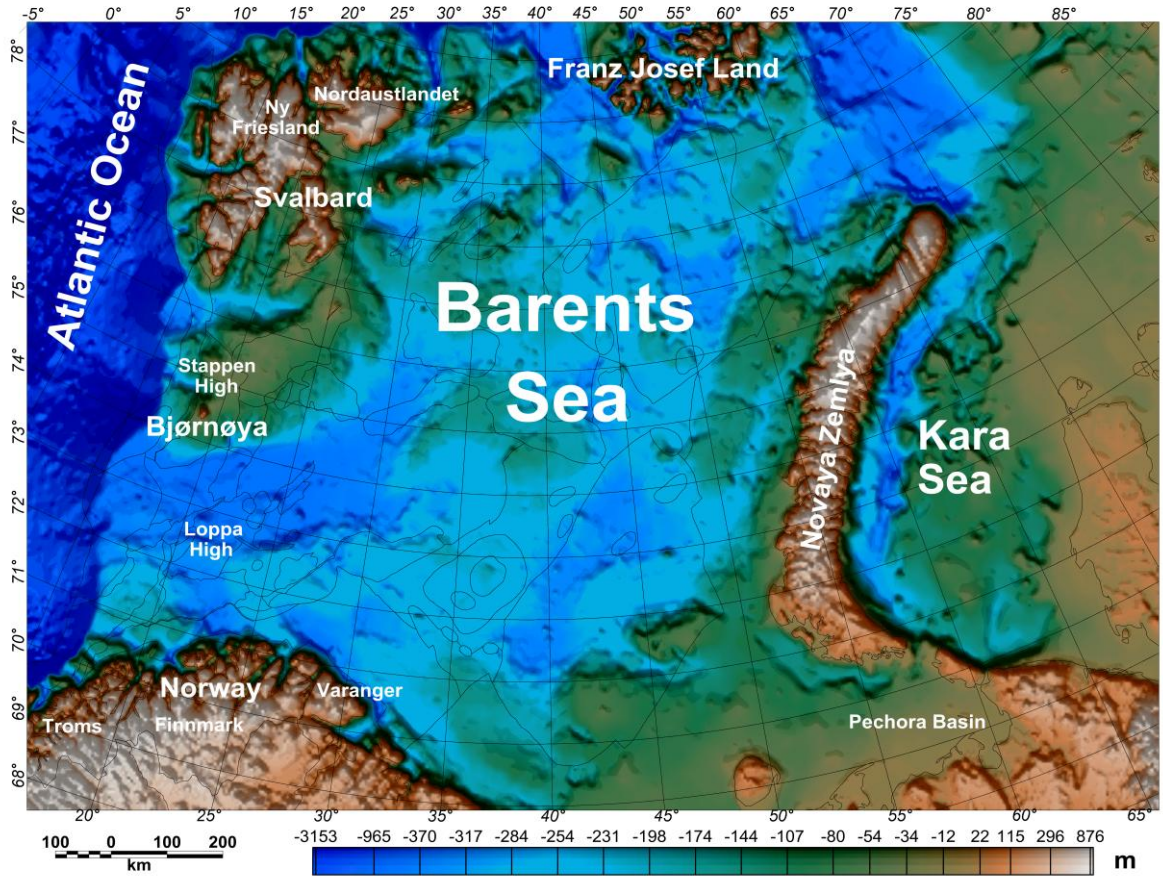

Figure 1.1: Barents Sea shelf and surrounding land masses: bathymetry-topography. The study area is the southwestern (SW) Barents Sea (69 °N – 75 °N and 13 °E – 30 °E). The thin black lines show the tectonic units as defined by the Norwegian Petroleum Directorate).

Exploration of the Barents Sea is of increasing interest for academic and economic reasons due to the hydrocarbon potential of the area (Doré, 1995; Gautier et al., 2009). Among the productive areas, the eastern Barents Sea sedimentary basins have yielded significant gas reserves.

In the western Barents Sea, exploration efforts were focused on the Finnmark Platform, the Nordkapp Basin and the Western Margin. The first major discovery was the Snøhvit gas field in the middle of the 80s and the last was the Goliath oil field discovered in 2000.

In order to improve the geological knowledge mandatory to permit new discoveries, numerous geological and geophysical studies have been funded in Norway during the last 30 years. The present study aims to increase the understanding of the geology of the Norwegian Barents Shelf and to optimise the choice of the exploration focus. This study has been carried out as part of the project HeatBar (Basement Heat Generation and Heat Flow in the western Barents Sea – Importance for hydrocarbon systems) and has been funded by the PETROMAKS programme of the Research Council of Norway and StatoilHydro.

The thesis is motivated by the observation that the maturation of hydrocarbonreservoirs is dependent on the paleo-temperatures, which are influenced among other things by heat production in the basement (e.g. Nadeau et al., 2005). Therefore, knowledge of the basement is of huge importance to estimate the thermal state of sedimentary basins. The thesis aims at characterising the basement lithological variations underlying the deep basins and understanding the relationships between structural highs and basins and the deep crustal configuration.

The characterisation of the basement structure and lithology has also allowed a re-assessment of the offshore prolongation of the Caledonian structures observed onshore Norway. The tectonic framework proposed has implication for the Mesozoic to Cenozoic sedimentary basin evolution.

This thesis presents crustal integrated modelling by implementing a procedure that couples 2D and 3D joint gravity and magnetic modelling with isostatic and thermal analysis. The integrated modelling of aeromagnetic, gravity, and seismic data constrains the basement architecture as well as the intra-basement lithology variations. Thermal modelling involving joint modelling of the geoid, gravity and topography data permits testing the crustal structure obtained by joint gravity and magnetic modelling in terms of surface heat flow estimation.

The following section starts with an introduction to the different geological topics addressed in the thesis. Then, the theoretical background regarding potential field forward modelling, not presented in the individual chapter is developed. At the end, I describe in short the content of the individual chapters.

1.1 Topics addressed in the thesis

1.1.1 Basement structure and composition

From seismic studies it has been shown that the basement in the western Barents Sea is characterized by structural highs and lows (e.g., Faleide et al., 1988, 1991, 1993, 1996; Gabrielsen et al., 1984, 1990). However, the crystalline basement is often difficult to recognize on seismic sections (e.g. Hospers and Ediriweera, 1991) due to low acoustic impedance contrast between sedimentary rocks and basement, multiples and signal-to-noise ratio at greater depths.

Gravity and magnetic data are potential fields containing, among other signals, the signature of the top basement configuration. Due to the ambiguity of the gravity and magnetic fields interpretation inherent to the depth and shape of the density contrast and magnetic source, respectively; the interpretation of these fields requires constraining data. Therefore, in recent studies, the basement structures offshore are indirectly investigated through the combination of potential field data with seismic reflection and refraction data in addition to well data penetrating the top basement. Also, samples from the closest onshore area to the study area can provide petrophysical values useful for modelling leading to proposition of onshore-offshore correlations.

The Geological Survey of Norway (NGU) has covered large parts of the Barents Sea and Svalbard with aeromagnetic measurements (Åm, 1975; Skilbrei, 1990, 2000; Olesen et al., 2006), which provide insights into the basement geometry. In the southwestern Barents Sea, two different basement surfaces were first mapped from aeromagnetic data by Åm (1975). A relatively shallow "refraction and magnetic basement" surface was interpreted to represent the top of the Palaeozoic rocks, and

a deeper "magnetic basement surface" was considered to represent the top of the Precambrian rocks.

Efforts have previously been made to improve the depth-to-top basement estimates from combination of seismic information and 2D gravity modelling (Gudlaugsson et al., 1987, 1994, 1998; Breivik et al., 2002, 2003, 2005; Mjelde et al., 2002; Ritzmann et al., 2004, 2007) giving rise to a new generation of depth to top basement maps constrained by a sparse net of 2D refraction and reflection seismic data (Skilbrei, 1991, 1995; Ritzmann et al., 2007).

1.1.2 The Barents Sea basins evolution

Extensive work regarding the southwestern Barents Sea basins initiated at Palaeozoic times (Ziegler, 1988; Doré, 1991; Gudlaugsson et al, 1998; Ritzmann et al., 2007) and their later development at Mesozoic and Cenozoic times (Faleide et al., 1988, 1993, 1996; Breivik et al., 1998; Gabrielsen et al., 1984, 1990) has been carried out. These studies mainly proposed basin evolution models based on seismic interpretation of the sedimentary reflectors and lead to estimation of time of the basins formation. Nevertheless, due to the lack of good crustal imaging, little is known about the rifting processes at the origin of the southwestern Barents Sea basins and no clear reason of the diversity of basin orientation is proposed in the literature. Also, the crustal stretching history remains poorly understood.

1.1.3 Thermal state of the Barents Shelf lithosphere

The thermal state of the lithosphere reflects the tectonic history and geological processes controlling its evolution through time. The maturation of organic matter in the sedimentary succession is linked to the present and past temperature. Despite the importance of addressing these issues and in spite of the increasing industrial interest in the Barents Sea, a model of the thermal state of this area had previously not been generated. For the study area, only few heat flow measurements have been collected in shallow wells made by IKU in the 80s (Zielinski et al., 1986; Sættem et al., 1988; Løseth et al., 1992). These data can help constraining surface heat flow

estimations. The new knowledge regarding basement structure and composition brought by the presented study found the basis for an improved heat flow modelling.

1.1.4 Prolongation of the Caledonian structures in the Barents Sea

Plate reconstruction and earlier geological models supported the idea of Norwegian Caledonides propagating northward through the Barents Shelf. Three main geometries of this Barentsian extension have been proposed.

The geophysical studies of Breivik et al. (2002, 2003 and 2005) (Fig. 1.2) led them to propose a two branches extension with a NE-trending orogen lying to the east of Franz Josef Land and a NNW-trending orogen including the Bjørnøya Island and Svalbard.

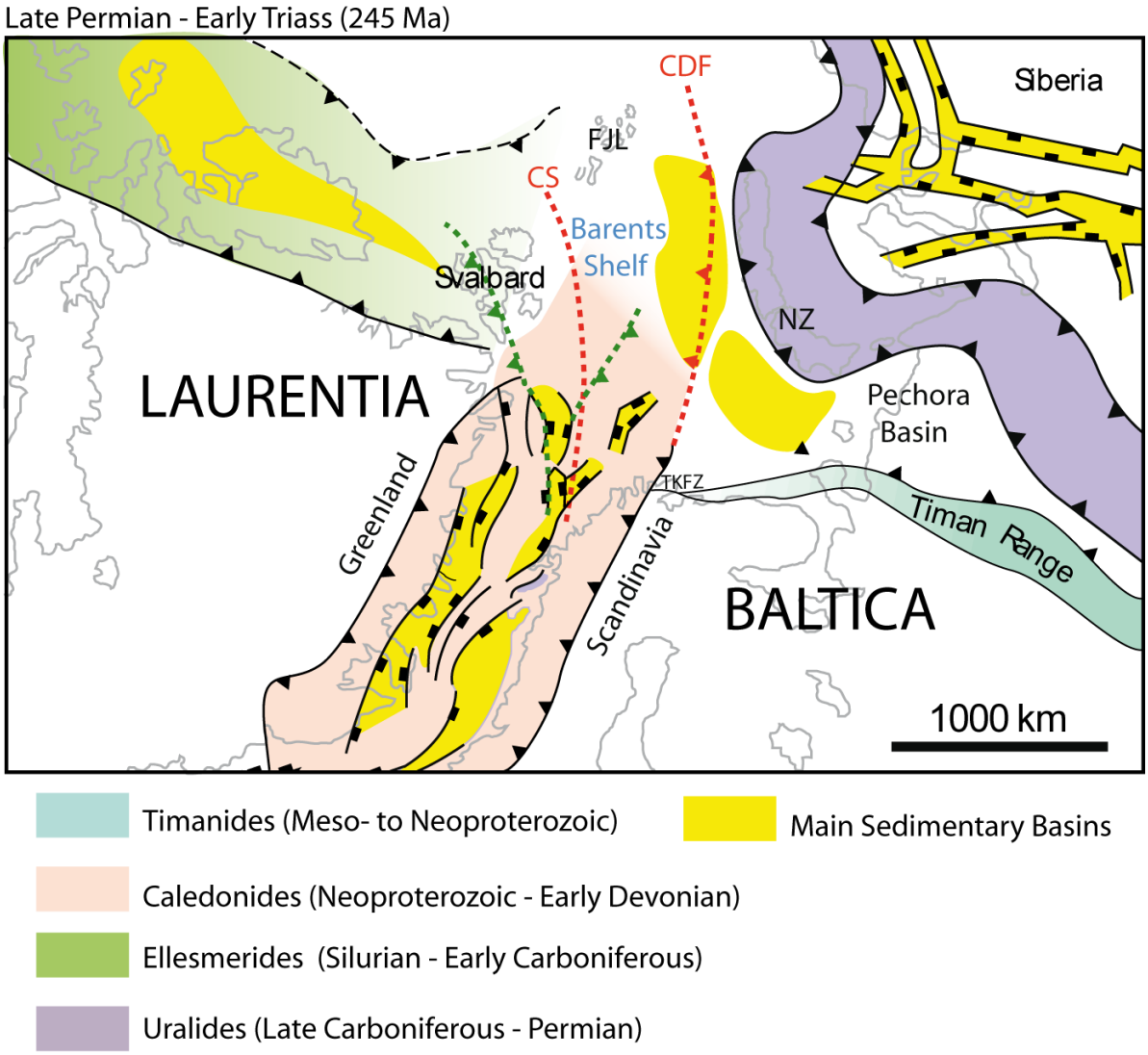

Figure 1.2: The Barents Sea Shelf in the Late Permian-Early Trias (245 Ma). The extension of the Timanides, Caledonides, Ellesmerides and Uralides ranges, as well as the main sedimentary basins, are represented. FJL (Franz Josef Land), BFZ (Billefjorden Fault Zone), TKFZ (Trollfjorden-Komagelva Fault Zone), NZ (Novaya Zemlya). The interpreted offshore prolongation of the Norwegian Caledonides into the Barents Sea as proposed by Gee (2005) is schematically represented with the red dashed lines. The proposed Caledonian sutures by Breivik et al. (2005) based on OBS profiles by Breivik et al. (2002, 2003 and 2005) and the Caledonidian model modified from Gudlaugsson et al. (1998) are represented with the green dashed lines.

Another hypothesis has been developed by Gee and co-workers (Gee, 2005; Gee et al., 2006) based on geological investigations including a careful analysis of outcrops from all around the Barents Sea (Roberts and Gee 1985; Stephens and Gee 1989; Gee et al., 1995; Gee and Pease, 2004; Gee and Tebenkov, 2004; Gee, 2005; Gee and Stephenson, 2006; Gee et al., 2006). In their model based on differentiation between terranes from Laurentia and Baltica, they propose a one-branch extension with a Caledonian suture trending NE and located between the Svalbard and Franz Josef Land (Fig. 1.2).

Finally, on the basis of integrated geophysical data analysis Ritzmann and Faleide (2007) proposed an offshore continuation of the Caledonides into the Barents Sea with Caledonian structures widening substantially in the southwestern Barents Sea (Fig. 1.3).

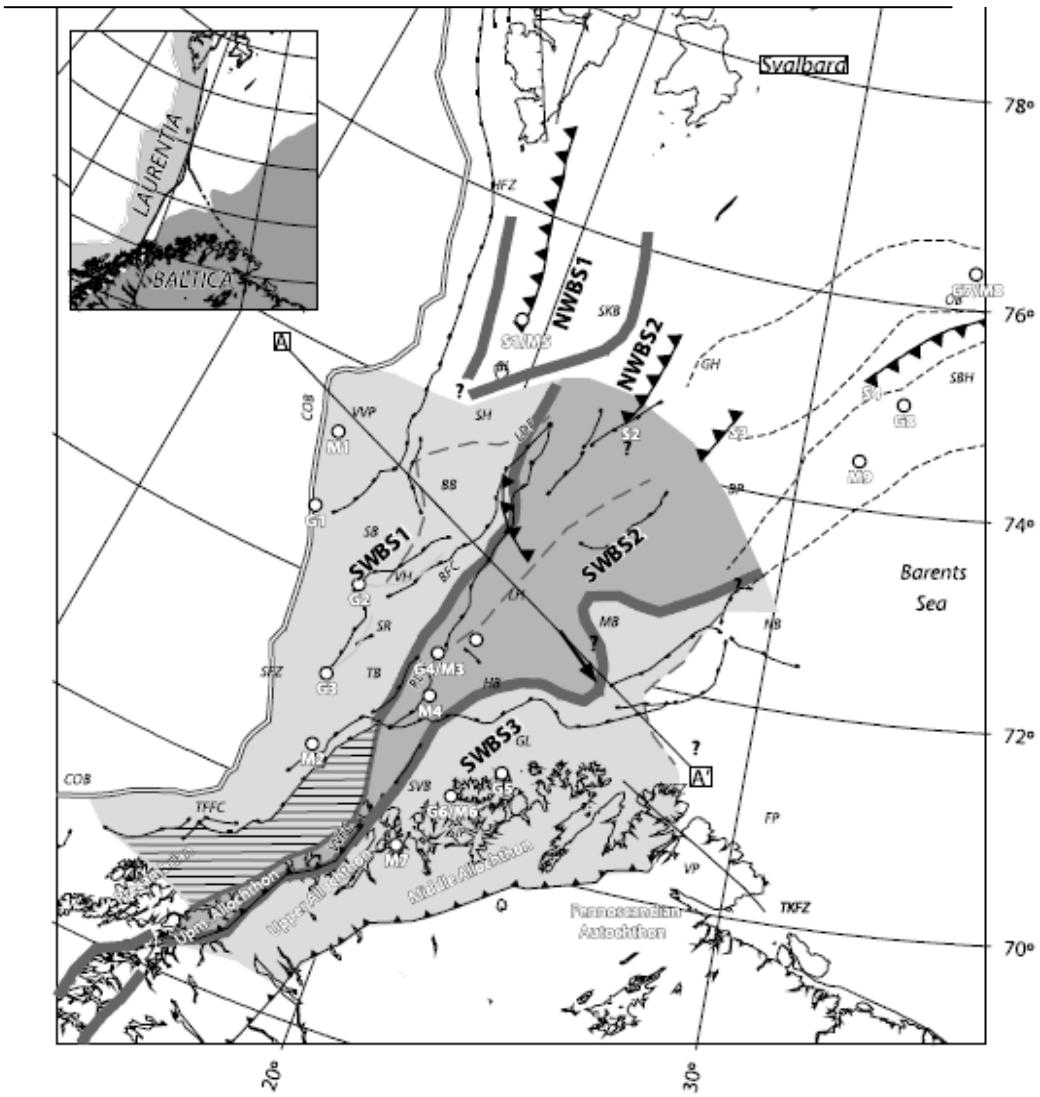

Figure 1.3: Map showing the tectonic units of the western Barents Sea, southwest Barents Sea (SWBS) 1–3 and northwest Barents Sea (NWBS) 1/2, according to the geophysical data interpretation (picture from Ritzmann and Faleide, 2007). Thick grey lines are main boundaries. Dots labeled with G*/M* are selected gravity and magnetic anomalies. Lineaments suggested from earlier studies are labeled with S*. The thin dashed lines in the surrounding of S4 are mapped by gravity and magnetic data and outline a possible connection of the Olga Basin main thrust to the units SWBS 2/3. The NW-SE trending thrust in the center of the plot is constrained by a steep Moho topography along profile IKU-F oriented towards the Trollfjord-Komagelva Fault Zone (arrow). Unit SWBS 3 and the onshore regions comprising the Lower to Upper Allochthons have affinity to Baltica. Unit SWBS 2 is covered by the Scandian Uppermost Allochthon. East of the Troms-Finnmark Fault Complex (TFFC), Precambrian rocks were possibly overlain by Uppermost Allochthon rocks prior to

their uplift in the Late Jurassic–Early Cretaceous (horizontal hatched). Unit SWBS 1 is a Laurentian fragment.

The state of the art potential field models as well as the modern seismic profile interpreted here focus on deciphering the crustal domains based on their density and magnetic properties. Particularly, the models intend at deciphering between Laurentia and Baltica terranes involved during the Caledonian orogeny. The suture between these terranes is also seeked. Suture zones have a width from few hundred meters to a couple of kilometers. They can be networks of mylonitic shear zones and associated brittle fault zones. The Caledonian suture is probably an ensemble of igneous intrusions and tectonic lenses of all kind of lithologies, from plutonic rocks to ophiolitic fragments inherited from the former ocean separating Laurentia and Baltica and the colliding terranes. More specifically, the Caledonian suture zone may involve metamorphic gneiss complexes originating from large volumes of crust buried during the orogeny. Because of the Western Gneiss Region outcropping in southern Norway (Cuthbert et al., 2000), we do not exclude a possible eclogisation of the rocks involved in the Caledonian suture. In consequence, the Caledonian suture is likely made of high-density rocks (2950-3300 kg/m3). Due to the variety of rocks involved in the suture and the uncertainty regarding the distribution and degree of metamorphism reached by these rocks, the magnetic properties are uncertain. Nevertheless, a suture zone may separate terranes of contrasted magnetic properties and becomes a major weakness zone within the crust.

1.2 Theoretical background

In the following I will outline in short the theoretical background for the studies presented in the thesis.

1.2.1 Potential fields

Magnetic and gravitational attractions are potential fields. A potential field is a vector fields varying in three dimensions that can be described by (Blakely, 1996):

$$F(x,y,z) = (\frac{\partial W}{\partial x}, \frac{\partial W}{\partial y}, \frac{\partial W}{\partial z}) = \nabla W \qquad (1)$$

By definition, the work in any direction is equal to the component of force in that direction. The vector field is completely specified by the scalar field W, the work function of F.

$$\frac{\partial W}{\partial x} = Fx \qquad (2)$$

The derivative of the work in any direction is equal to the component of force in that direction:

$$W = (P, P_0) = \int_{P_0}^{P} F.ds \qquad (3)$$

$$W = (P, P_0) = \int_{P_0}^{P} (\frac{\partial W}{\partial x} dx + \frac{\partial W}{\partial y} dy + \frac{\partial W}{\partial z} dz)$$

$$W = (P, P_0) = \int_{P_0}^{P} dW$$

$$W = (P, P_0) = W(P) - W(P_0)$$

Where W is the work required to move the particle from point P_0 to P. A potential field is conservative, thus, its work is independent of the path between P and P_0 but depends on the difference in potential between the two points. ϕ is the potential energy of a particle (i.e, charge, masse). The potential ϕ of the vector field F is defined as the work function:

$$F = \nabla \phi \qquad (4)$$

In regions where there are no particules of energy (i.e, charges/masses), potential field also satisfies the Laplace's equation of homogeneity:

$$\frac{\partial^2 \phi}{\partial x^2} + \frac{\partial^2 \phi}{\partial y^2} + \frac{\partial^2 \phi}{\partial z^2} = 0 \quad (5)$$

This mean that in the three dimensions, the potential ϕ is never more or less concentrated than all surrounding part of the region.

Geophysical instruments generally measure only the vertical component of a potential field. That single component constitutes a continuous scalar field (e.g., g_z) varying in three dimensions.

The amplitude and wavelength of gravity and magnetic data are influenced by the source geometry (depth and dimension) and the contrast of the relevant physical parameters density and magnetization, respectively, to the surrounding.

A variety of methods (i.e., Peter half slope, Euler deconvolution) exist to estimate the source depth and geometry (Reid et al., 1990; Skilbrei, 1993). Such inverse methods suffer from the ambiguity of the gravity and magnetic fields. An alternative is forward modelling of the potential fields, particular if constraints from seismic and bore holes are available. In forward modelling, one does between distinguish 2D modelling (e.g. on profiles) and 3D modelling.

1.2.2 Gravity field

The gravitational potential U and gravitational attraction g at point P due to a volume of mass with density ρ is defined as (Blakely, 1996):

$$U(P) = \gamma \int_R \frac{\rho}{r} dv \qquad (6)$$

$$g(P) = \nabla U = -\gamma \int_R \rho \frac{\hat{r}}{r^2} dv \qquad (7)$$

Where r is the distance from the point of observation P to an element of the body dv, and γ is the gravitational constant. $\hat{r}$ is a unit vector pointing from an element of the mass to P.

$$r = \sqrt{(x-x')^2 + (y-y')^2 + (z-z')^2}$$

Gravimeters measure the vertical attraction of gravity. In Cartesian coordinates the gravity data can be expressed as:

$$g(x,y,z) = \frac{\partial U}{\partial z} = -\gamma \iiint \rho(x',y',z') \frac{(z-z')}{r^3} dx'dy'dz' \qquad (8)$$

With an observed point P(x,y,z) and a 3D body with density The forward modelling requires the repeated calculation of g (x, y, z). The general expression of g(x, y, z) is:

$$g(x,y,z) = \iiint \rho(x',y',z') \psi(x-x', y-y', z-z') dx'dy'dz'$$

Where ψ is named the Green's function, the gravitational attraction at (x, y, z) of a point mass located at (x', y', z'):

$$\psi(x,y,z) = -\gamma \frac{z}{(x^2+y^2+z^2)^{3/2}} \qquad (9)$$

2D modelling computes the vertical attraction of gravity created by a two dimensional structure. The geologic structures are often lineated in a particular horizontal direction (e.g., simple rift zone, simple anticline). In that context, the key is to model along a profile perpendicular to the main structural axis. Consequently, the y-axis is directed parallel to the invariant direction leaving only the x and z dimension to consider.

$$U = 2\gamma \int \rho(S) \log \frac{1}{r} dS \qquad (10)$$

Where S is the cross-sectional surface and r the perpendicular distance to an element of the body.

$$r = \sqrt{(x - x')^2 + (z - z')^2}$$

For a surface of constant density, the vertical attraction of gravity is given by:

$$g(P) = \frac{\partial U}{\partial z} == 2\gamma\rho \iint \left(\frac{z'\, dx'\, dz'}{x'^2 + z'^2} \right) \qquad (11)$$

2D modelling requires that no significant changes in the third dimension occur close to the 2D geometry. Complex geological structures require a 3D definition of their geometry. The 3D geometry is approximated by rectangular prisms or polyhedrons (i.e., IGMAS; Götze and Lahmeyer 1988). For each prism or polyhedron a constant density is defined. For the homogeneous polyhedron, the volume integral (Equ. 8) is transformed into a sum of line integrals (Equ. 12, 13) to calculate the gravity field (Götze and Lahmeyer, 1988):

$$g(x, y, z) = \frac{\partial U}{\partial z} = -\gamma\rho(x', y', z') \iiint \frac{\partial}{\partial z} \left(\frac{1}{r} \right) dV = -\gamma\rho(x', y', z') \iint \cos(\vec{n}, z) \left(\frac{1}{r} \right) dS \qquad (12)$$

The surface integral has to be calculated for the whole polyhedron surface S_j and the $\cos(\vec{n}_j, z)$ (j=1, 2,… m, the number of surfaces) determines the direction of the surface element ds with regards to the Cartesian coordinates system. Since $\cos(\vec{n}_j, z)$ is constant for any polyhedron surface, the attraction effect of a polyhedron by the superposition of gravity effect of its individual surfaces S_j is expressed by:

$$g(x, y, z) = \frac{\partial U}{\partial z} == -\gamma\rho(x', y', z') \sum_{j=1}^{m} \cos(\vec{n}_j, z) \iint \left(\frac{1}{r} \right) dS_j \qquad (13)$$

1.2.3 Free-air gravity field and Bouguer anomaly

Measured gravity data (Δg_{obs}) contain superposed short wavelength (shallow) and

long wavelength (deep) information, and reflect density contrasts along different boundaries. The differentiation of the sources is not straight forward but different anomalies can be computed to enhance the ground densities distribution.

The free air (FA) anomaly is the difference between observed gravity and theoretical, normal Earth gravity and corrected for the elevation relative to the ellipsoid, and Earth tides.

Latitude correction (γ_o) and free-air correction (FAC) give the free-air anomaly (Δg_{FA}):

$$\Delta g_{FA} = g_{obs} - \gamma_o + FAC \qquad (14)$$

The Bouguer anomaly ($\Delta g_{B;}$ named after the French scientist Pierre Bouguer) is computed from the free-air anomaly by removing the attraction of the masses above the sea-level. For the Bouguer correction the mass distribution is approximated by a flat plate of thickness H (height of the gravity measurement location above sea-level) and constant density.

The Bouguer correction is defined as followed:

$$\Delta g_B = g_{obs} - \gamma_o + FAC + BC \qquad (15)$$

With BC = Bouguer Correction.

The Bouguer anomaly corrects the free air anomaly for the mass of rock that exists between the station elevation and the sea-level. Offshore, the Bouguer correction is equivalent to substituting the water layer by a sedimentary or rock infilling layer. The reduction density is traditionally 2670 kg/m^3 onshore and is between 2670 and 2200 kg/m^3 offshore depending on the use of the computed map. The Bouguer reduction used is already a part of the modelling. The application of a Bouguer reduction offshore removes the bathymetric signature from the gravity data. In the Barents Sea, the shallow and regular water layer does not prevent from viewing the crustal signature in the gravity data.Free air anomalies were used when modelling along 2D profiles in paper I, paper III and paper IV; consequently, the water was modelled with a density of 1030 kg/m^3. However,as the 3D model covers a large area including the continental slope, we applied more accurate modelling of the gravity data using the the Bouguer anomalies calculated with a reduction density of 2200 kg/m^3 similar to the uppermost sediments.

The complete Bouguer anomaly includes the terrain correction:

$$\Delta g_{BC} = g_{obs} - \gamma_o + FAC + BC + TC \qquad (16)$$

The terrain correction corrects for the non-planar topography surrounding, In principal the terrain correction is always negative.

The (complete) Bouguer anomaly is conventionally used for regional modelling and interpretation. But also the isostatic anomaly is often used (see below).

1.2.4 Isostatic computations

A correction of the Bouguer anomaly for isostasy can be computed. This correction (IC) removes from the Bouguer anomaly the gravity effects of a theoretical isostatic Moho from the Bouguer anomaly. The remaining contribution (isostatic gravity residual) originates from the crustal mass that is unrelated to isostatic local compensation of topographic load. The isostatic gravity residual anomaly is:

$$\Delta g_I = g_{obs} - \gamma_o + FAC + BC + TC + IC \qquad (17)$$

Two models of local isostatic compensation co-exist; for both models there is no rigidity compensation beneath the load. In the concept of Airy-Heiskanen isostasy topographic heights are accommodated by changes in crustal thickness. The Pratt-Hayford model proposed that different topographic heights are accommodated by lateral changes in rock density. The depth of compensation is at the lithosphere/asthenosphere boundary and its undulation is due to the lateral variations of load. At the depth of compensation the pressure exerted is constant.

$$Load = P = \rho \cdot g \cdot h = cst \quad (18)$$

From under the deepest root to the base of the lithosphere there are parallel isobars lines that can be use as computation level. These computations ignore the strength of the crust and the upper mantle.

In the concept of regional or Vening-Meinesz isostasy, the load is on top of a rigid plate and the compensation of the load is said "regional". In the context of regional isostatic compensation the lithosphere has a finite rigidity. The supporting lithospheric material with rigidity is flexured distributing the load over a broad region. Vening-Meinesz (1939) isostasy implies the lithosphere behaves as a perfect elastic material and that its flexure depends on the topographic load and internal loads. The most important factor that controls the bending is the flexural rigidity. The loading of a plate with a high flexural rigidity will lead to a very limited deflection of the plate whereas

the loading of a plate with a low flexural rigidity will lead to a larger deflection of the plate. For the extreme case where the flexural rigidity is zero the plate will behave as in the case of Airy isostasy.

The basic equation for the deformation of an elastic beam overlying an inviscid fluid, in our case represented by the Mantle, is given by Gunn (1943) a differential equation of the 4th order:

$$D\frac{d^4w(x)}{dx^4} + (\rho_m - \rho)g \times w(x) = 0 \quad (19)$$

Where

D flexural rigidity

w vertical deflection of the plate at x

ρ the average density above the plate (i.e. crust)

ρ_m the average density o below the plate (i.e. mantle)

g gravitational acceleration

The rigidity modulus enter in the computation of the Young Modulus (E):

$$E = 2G(\upsilon + 1) \quad (20)$$

Where υ is the Poisson ratio.

G, the rigidity modulus relates shear stress to shear strain (τ= Gγ).

A link has been established between the temperature and the rigidity modulus G (Kusznir and Karner, 1985). Kusznir and Karner (1985) suggested that the continental flexural rigidity is controlled by crustal thickness and lithospheric thickness through the thermal structure. The elastic thickness parameter (Te) tends to express the relation between the lithospheric thickness of the plate and the plate rigidity. The flexural rigidity D varies as a function of the lithospheric elastic thickness (Te) of the plate through the relation:

$$D = \frac{E \times Te^3}{12(1-\nu^2)} \quad (21)$$

Where

E Young modulus

Te Elastic lithosphere thickness

v Poisson coefficient

1.2.5 Magnetic field modelling

Magnetic data collected by magnetometers measure the strength of T, the intensity of the geomagnetic field (or total field) in the vicinity of the instrument. The geomagnetic field strength is described with inclination, declination and field strength dependent of the location on the Earth surface and time of the data acquisition. The geomagnetic field is mostly composed of the magnetic field produced by currents in the liquid outer core of the Earth. It also includes magnetic fields caused by currents flowing in the ionosphere triggered by solar winds and a crustal magnetic field due to outcropping and buried magnetic rocks. The total field anomaly ΔT is calculated by substracting the magnitude of a suitable modelled regional field F (IGRF: Interntional Geomagnetic Reference Field) from the total field:

$$\Delta T = |T| - |F| \quad (22)$$

Aeromagnetic data processing tends to isolate the residual crustal magnetic field component linked to rock magnetisation. Aeromagnetic data modelling aims at understanding the depth to the magnetic source as well as the magnetic susceptibility lateral variation.

According to the Helmholtz theorem, if no currents exist in the region of investigation, then B is a potential field and has a scalar potential V such that:

$$B = -\nabla V \qquad (23)$$

As the gravitational field, the magnetic field respects the Laplace's equation of homogeneity.

At an observation point P, the magnetic field of a volume of magnetic material is:

$$B(P) = -Cm\nabla_P \int_R M \cdot \nabla_Q \frac{1}{r} dv \qquad (24)$$

with $Cm = \frac{\mu_0}{4\pi} = 10^{-7}\, henry.meter^{-1}$ (S.I)

Where μ_0 is the permeability of free space, M is the magnetisation, and r the distance from the observation points P to element dv of the body situated at point Q.

In magnetic modelling, similarly to what is explained in the gravity-modelling paragraph, the concept surface magnetic charges is applied and the magnetic effect of a homogeneous magnetised polyhedron can be modelled by magnetic charge on the body's surface. Summing the effects of the prisms approximates the magnetic

anomaly. The magnetic field of a uniformly magnetised body with volume R and surface S is:

$$\int_R \nabla \cdot B dv = \int_S B \cdot \hat{n} dS \qquad (25)$$

$$B = -Cm \int_S \frac{M \cdot \hat{n}}{r^2} \hat{r} dS = Cm \sum_{i=1}^{N} (M \cdot \hat{n}_i) \int_{S_i} \frac{\hat{r}}{r^2} dS \qquad (26)$$

Where S_i represents the surface of the ith facet and $\hat{n}_i$ its outward normal.

The magnetic scalar potential is only defined in regions of space in the absence of currents. These special conditions are approximately obtained in typical geophysical measurement of the magnetic field. The total field anomaly is approximated by:

$$\Delta T = -Cm\vec{F} \nabla_P \int_R M \cdot \nabla_Q \frac{1}{r} dv \qquad (27)$$

Where R is the radius over the volume of particles.

1.2.6 Rock magnetisation

Rock magnetic properties originate from an imbalance in the structural arrangement of iron ions. This arrangement causes a transfer of electrons between the different irons in a structured path or vector. This electric vector generates a magnetic field. The most common minerals defining this rock property are magnetite (Fe_3O_4) and titanomagnetite $Fe(Fe,Ti)_2O_4$.

The magnetization M is the vector sum of the induced and remanent components of magnetization. Indeed, two types of magnetisation co-exist within a rock, the induced (Mi) and remanent magnetization (Mr).

The magnetic particles are generally oriented in random directions but an external field can provoke alignment of the magnetic particles and induce magnetisation. The magnetic susceptibility of a rock is its ability to become magnetised by an external magnetic field. The magnetic susceptibility is dimensionless. Induced magnetization aligns with the direction of the Earth's magnetic field H and is proportional to the magnetic susceptibility χ so that:

$$M_i = \chi H \qquad (28)$$

The magnetic remanence is the magnetization left behind in a medium after an external magnetic field is removed. In our case it is related to the total magnetic field existing during the rock formation.

The relative importance of remanent magnetisation (Mr) vs. induced magnetisation (Mi) is expressed by the Koenigsberger ratio (Q-ratio).

$$Koenigsberger\_ratio = Q = \frac{|Mr|}{|Mi|} = \frac{Mr}{\chi H} \qquad (29)$$

With χ = magnetic susceptibility and H=induced magnetic field in A/m.

1.2.7 Thermal modelling

The physical properties to describe the lithosphere are among others: density and flexural rigidity. These properties depend on rock composition but also on temperature and pressure. While the best information about the geometry of the lithosphere can be taken from seismic studies, the determination of the other parameters is far more complex. Between temperature distribution, density and flexural rigidity, however, relationships can be found (Zeyen and Fernàndez 1994; Zeyen et al., 2005).

Temperature distribution is generally calculated from measured geothermal gradients and, based on it, the surface heat flow. However, these data can only be directly measured by drilling and drill holes do in general not exceed 3-5 km in depth. At these relatively shallow depths, and particularly in polar areas, the temperatures are perturbed by near-surface processes like ground water flow, erosion, sedimentation or paleoclimate. In addition, the surface heat-flow is affected by the composition of the lithosphere through thermal conductivity variations and radioactive heat production that affects strongly the temperature distribution. It is thus impossible to obtain reliable estimations of temperature distribution based only on thermal data. Therefore, the focus of the thermal modelling in the thesis is on the combined interpretation of the density and thermal structure using the influence of the temperature on rock density.

To introduce the equations used for thermal modelling described within Chapter 5 we remind the fundamentals of heat flow in the next paragraphs.

The Earth's heat flow is the amount of heat escaping from the interior across a unit area of the Earth surface. The heat interior is cooling off by a combination of thermal conduction through the basement crust and the delivery of cold material to the interior by slabs, a form of advection. Within the crust, crustal contribution comes from the crustal radioactivity that is a major contributor to the continental crust heat flow and its lateral variation. The crustal heat production is related to radioactive decay of predominantly the following isotopes: thorium 232 (^{232}Th), uranium 238, (^{238}U), potassium 40 (^{40}K). Continental heat flow is usually plotted as a function of crustal age since the last tectonic, magmatic or thermal metamorphic event and the long term asymptotic value is taken to be the background heat flow.
A little of heat is transferred to the surface by hydrothermal circulation.

The conducted heat trough the surface can be decomposed as following:

$$\rho \cdot c \cdot \frac{\partial T}{\partial t} = \nabla(\lambda \nabla T) + A(x, z) - \rho \cdot c \cdot \vec{v} \cdot \nabla T \quad (30)$$

Where $\rho \cdot c \cdot \vec{v} \cdot \nabla T$ represents heat advection by material movement, ρ is density (kg/m^3), c is heat capacity parameter (J/K.kg), $\vec{v}$ is material velocity (m/s), and T temperature (K), $\nabla = (\partial / \partial x, \partial / \partial z)$. $A(x, z)$ stands for crustal contribution, A is volumetric radiogenic heat production and $\nabla(\lambda \nabla T)$ corresponds to diffusion term (background heat flow), λ is thermal conductivity (W.m^{-1}.K^{-1}).

The program used in Chapter 5 calculates the thermal steady state of the lithosphere considering no change of temperature distribution over time as if the crust would has attained thermal equilibration since the last period of tectonic activity. In consequence, the transient component is neglected: $\frac{\partial T}{\partial t}$ =0 and v=0.

The equation of steady state heat transport used in chapter 5 is the following:

$$\nabla(\lambda \nabla T) + A(x, z) = 0 \quad (31)$$

Also in chapter 5, the influence of the temperature on mantle rock density is

expressed through a thermal expansion parameter relating mantle densities to changes in volume in response to changes in temperature. Heat production and thermal conductivity values are attributed to mantle, lower crustal and crustal bodies.

1.3 Organisation and outlines of the thesis

The thesis contains four main papers (Chapters 2-6), where I have been the first author and a fifth paper in the appendix, where my contribution was minor. This paper is included in the thesis for completion as it presents the petrophysical data offshore Norway, which are crucial to constrain the outlined models and concepts. The successive papers follow the path taken by the flow of ideas all along the study.

Chapter 2 presents a paper published in 2009 in Tectonophysics (Barrère; C. Ebbing, J., Gernigon, L., 2009. Offshore prolongation of Caledonian structures and basement characterisation in the Western Barents Sea from geophysical modelling. Tectonophysics, 470, 71-88).
The paper presents 2D models built along regional transects (the IKU profiles A, B and C), which are at the basis to evaluate the petrophysical values applied in the 3D and thermal model. These 2D models were used to evaluate how to distinguish different crustal units: the Achaean to Palaeoproterozoic shield, the Caledonian nappes and the mafic rocks locally occurring in the Precambrian or involved in the nappes. It was established that this distinction is possible by a joint modelling of the density and magnetic susceptibility and more specifically by the joint interpretation of the density, magnetic susceptibility and Q-ratio of the basement blocks. In addition, the paper introduces a discussion about the offshore prolongation of the Norwegian Caledonides and the link between the Caledonian structures and the development of the sedimentary basins in the western Barents Sea.

Chapter 3 presents a paper submitted to Geophysical Journal International in August 2009 (Barrère; C. Ebbing, J., Gernigon, L. 3D density and magnetic crustal characterisation of the southwestern Barents Shelf: implications for the offshore prolongation of the Norwegian Caledonides. *GJI, subm.).*

In this chapter, a new 3D crustal model for the southwestern Barents Sea is presented. The density/magnetic crustal model integrates a wealth of geophysical and geological data available in the southwestern Barents Sea. The model is constrained by well data, industrial depth-converted horizons, seismic data and petrophysical data from onshore Norway samples. From the model a new top basement and Moho maps are extracted and compared to previous compilations. Different crustal domains are characterised by their density and magnetic properties and interpreted with respect to their geological history. The paper introduces also for the first time a thinning factor map for the entire south-western Barents Sea that highlights variations in crustal thickness. In the southwestern Barents Sea, a severe crustal thinning is modelled west of the Loppa High, below the western marginal basins. The integration of the basement units map with the potential fields maps leads to a re-evaluation of the tectonic framework and triggers a discussion about sedimentary basin evolution. We propose a asymmetric Caledonian collisional prism with a unique Caledonian arm, and a Caledonian suture to the west of the Loppa High propagating northward between Svalbard and Franz Josef Land. In addition, on the one hand, we suggest that pre-existing Caledonian and Timanian weakness zones exerted a strong control on basin evolution east of the Loppa High. On the other hand, we interpret that the formation of the western basins (i.e., the Tromsø and Bjørnøya Basins) has been controlled mostly by the reactivation of the Caledonian suture, which coincides with the alignment of the Bjørnøyrenna and Ringvassøy-Loppa Fault Complexes.

The study presented in **Chapter 4** has been submitted in august 2009 to Geological Society of America Bulletin (Barrère C., Gernigon L. and Ebbing J., The tectonic evolution of the Bjørnøya Basin and Loppa High, southwestern Barents Sea - new insights into post-Caledonian features, *GSA Bulletin subm*.).

The study focuses on the structural relationship between the Bjørnøya Basin and the Loppa High. The study is based on the interpretation of an integrated geological model built along the seismic profile NBR07-232849. The integrated model reveals the crustal thinning system developed to the west of the Loppa High and links the detailed basin structure to the deep crust. We interpret post Caledonian features affecting the Barents Shelf crust and discuss the stretching model implied by the interpreted geometry and lithologies. Finally, a scenario for the Bjørnøya Basin and

Loppa High development is presented, which illustrates its evolution from Late Devonian to the present-day.

The **Chapter 5** is a manuscript in preparation (Barrère C. and Zeyen H., Integrated modelling and heat flow estimations, case study along a 2D profile across the southwestern Barents Shelf, *in prep.*).
Here, the use of an integrated model as input for heat-flow modelling is demonstrated. The input crustal structure is a combination of the IKU_B (chapter 2) and NBR07-232849 (chapter 3) joint gravity and magnetic models. The thermal model allows us to compare modelled heat-flow with observed heat-flow in the southwestern Barents Sea. The model provides also heat-flow estimates at top basement and a discussion of the heat-transfer from the mantle into the crust. The model allows us to discuss and provide preliminary insights into the depth of the oil- and gas window in the Barents Sea.

The **Appendix** presents the petrophysical data, published by Slagstad et al. in the NGU Bulletin 448. (Slagstad, T., Barrére, C., Davidsen, B. and Ramstad, R. K. (2008) Petrophysical and thermal properties of pre-Devonian basement rocks on the Norwegian continental margin. NGU Bulletin, 448, 1-6).
These are key data to constrain the density and magnetic modelling and the related geological interpretations. I sampled the cores originating from the Barents Sea crust and carried out a part of the petrophysical measurements.

References

Blakely, R.,1996, J., Potential Theory in Gravity and Magnetic Applications, Cambridge University press, Trumpington street/Cambridge-United kingdom.

Breivik, A.J., Faleide, J.I. and Gudlaugsson, S.T., 1998, Southwestern Barents Sea margin: late Mesozoic sedimentary basins and crustal extension, Tectonophysics, 293, 21-44.

Breivik, A.J., Mjelde, R., Grogan, P., Shimamura, H., Murai, Y., Nishimura, Y. & Kuwano, A., 2002, A possible Caledonide arm through the Barents Sea imaged by OBS data, Tectonophysics, 355, 67-97.

Breivik, A.J., Mjelde, R., Grogan, P., Shimamura, H., Murai, Y. & Nishimura, Y., 2003, Crustal structure and transform margin development south of Svalbard based on ocean bottom seismometer data, Tectonophysics, 369, 37-70.

Breivik, A.J., Mjelde, R., Grogan, P., Shimamura, H., Murai, Y. & Nishimura, Y., 2005, Caledonide development offshore-onshore Svalbard based on ocean bottom

seismometer, conventional seismic, and potential field data, Tectonophysics, 401, 79-117.
Cuthbert, S. J., Carswell, D. A., Krogh-Ravna, E. J. & Wain A., 2000, Eclogites and eclogites in the Western Gneiss Region, Norwegian Caledonides Lithos, v. 52, no. 1-4, pp. 165-195.
Doré, A.G., 1991, The structural foundation and evolution of Mesozoic seaways between Europe and the Arctic: Palaeogeograhy, Palaeoclimatology, Palaeoecology, v. 87, pp. 441–492.
Doré, A.G., 1995, Barents Sea geology, petroleum resources and commercial potential: Arctic,v. 48, no. 3, p. 207-221.
Faleide, J.I., Myhre, A.M., and Eldholm, O., 1988, Early Tertiary volcanism at the western Barents Sea margin, in Morton, A. and Parson, L.M., eds., Early Tertiary volcanism and the opening of the NE Atlantic: Geological Society Special Publications, v. 39, pp. 135–146.
Faleide, J.I., Gudlaugsson, S.T., Eldholm, O., Myhre, A.M. & Jackson, H.R., 1991, Deep Seismic Transects across the Sheared Western Barents Sea-Svalbard Continental-Margin, Tectonophysics, 189, 73-89.
Faleide, J.I., Vågnes, E. and Gudlaugsson, S.T., 1993, Late Mesozoic-Cenozoic Evolution of the South-Western Barents Sea in a Regional Rift Shear Tectonic Setting, Marine and Petroleum Geology, 10, 186-214.
Faleide, J.I., Solheim, A., Fiedler, A., Hjelstuen, B.O., Andersen, E.S. and Vanneste, K., 1996, Late Cenozoic evolution of the western Barents Sea-Svalbard continental margin, Global and Planetary Change, 12, 53-74.
Gautier, D.L., Bird, K.J., Charpentier, R.R., Grantz, A., Houseknecht, D.W., Klett, T.R. Moore, T.E., Pitman, J.K., Schenk, C.J., Schuenemeyer, J.H., Sørensen, K., Tennyson, M.E., Valin, Z.C., Wandrey, C.J., 2009, Assessment of Undiscovered Oil and Gas in the Arctic. Science 29 May 2009: Vol. 324. no. 5931, pp. 1175 – 1179.
Gabrielsen, R.H., 1984, Long-lived fault zones and their influence on the tectonic development of the southwestern Barents Sea., Journal of the Geological Society, 141, 651-662.
Gabrielsen, R.H., Færseth, R.B., Jensen, L.N., Kalheim, J.E. & Riis, F., 1990, Structural elements of the Norwegian continental shelf. Part I: The Barents Sea Region., Norwegian Petroleum Directorate Bulletin.
Gee, D.G., 2005, Scandinavian Caledonides (with Greenland). pp. 64-74, eds Selley, R. C., Cocks, L. R. M. & Plimer, I. R. Encyclopedia of Geology.
Gee, D.G., Johansson, A., Ohta, Y., Tebenkov, A.M., Krasilschikov, A.A., Balashov, Y.A., Larionov, A.N., Gannibal, L.F. and Ryungenen, G.I., 1995, Grenvillian Basement and a Major Unconformity within the Caledonides of Nordaustlandet, Svalbard, Precambrian Research, 70, 215-234.
Gee, D.G., and Pease, V.L., 2004, The Neoproterozoic Timanide Orogeny of Eastern Baltica, Geological Society London Memoirs, 30, 191-207.
Gee, D.G., and Tebenkov, A., 2004, Svalbard: a fragment of the Laurentian margin. in The Neoproterozoic Timanide Orogen of eastern Baltica: introduction, pp. 191-206, eds Gee, D. G. & Pease, V. L. Geological Society London.
Gee and Stephenson (eds.), 2006, European Lithosphere Dynamics, Geological Society, London, Memoirs, 32, 507-521.
Gee, D.G., Bogolepova, O.K. and Lorenz, H., 2006, The Timanide, Caledonide and Uralide orogens in the Eurasian high Arctic, and relationships to the palaeo-

continents Laurentia, Baltica and Siberia. in European Lithosphere Dynamics, pp. 507-521, eds Gee & Stephenson. Geological Society of London.
Götze, H.J. and Lahmeyer, B., 1988, Application of three-dimensional interactive modeling in gravity and magnetics. Geophysics Vol. 53 No. 8, pp. 1096–1108.
Gudlaugsson, S.T. and Faleide, J.I., 1994, The continental margin between Spitsbergen and Bjørnøya. in Seismic Atlas of Western Svalbard, Medd, pp. 11-13, ed Eiken, O. Norwegian Polarinstitut.
Gudlaugsson, S.T., Faleide, J.I., Fanavoll, S. and Johansen, B., 1987, Deep Seismic-Reflection Profiles across the Western Barents Sea, Geophysical Journal of the Royal Astronomical Society, 89, 273-278.
Gudlaugsson, S.T., Faleide, J.I., Johansen, S.E. and Breivik, A.J., 1998, Late Palaeozoic structural development of the South-western Barents Sea, Marine and Petroleum Geology, 15, 73-102.
Gunn, R., 1943, “A quantitative evaluation of the influence of the lithosphere on the anomalies of gravity”, Journal of the Franklin Institute, 236, p. 373.
Hospers, J. and Ediriweera, K.K., 1991, Depth and configuration of the crystalline basement in the Viking Graben area, Northern North Sea. Journal of the Geological Society, London, 148, 261-265.
Kuznir, N. and Karner, G., 1985, Dependence of the flexural rigidity of continental lithosphere on rheology and temperature. Nature 316, pp. 138–142.
Løseth, H., Lippard, S. J., Sættem, J., Fanavoll, S., Fjerdingstad, V., Leith, T.L., Ritter, U., Smelror, M., and Stylta, Ø., 1992, Cenozoic uplift and erosion of the Barents Sea -evidence from the Svalis Dome area. In: Vorren, T. O., Bergsaker, E., Dahl-Stamnes, O. A., Holter, E., Johansen, B., Lie, E. & Lund, T. B. (eds) Artic Geology and Petroleum Potential. Norwegian Petroleum Society Special Publication, 2, 643-664.
Mjelde, R., Breivik, A.J., Elstad, H., Ryseth, A.E., Skilbrei, J.R., Opsal, J.G., Shimamura, H., Murai, Y. & Nishimura, Y., 2002, Geological development of the Sorvestsnaget Basin, SW Barents Sea, from ocean bottom seismic, surface seismic and gravity data, Norwegian Journal of Geology, 82, 183-202.
Nadeau P.H., Bjørkum P.A. and Walderhaug O. 2005, Petroleum system analysis: Impact of shale diagenesis on reservoir fluid pressure, hydrocarbon migration and biodegradation risks. In Doré, A.G. and Ving, B. (eds), Petroleum Geology: North-West Europe and Global Perspectives – Proceedings of the 6th Petroleum Conference, 1267-1274. Petroleum Geology Conferencees Ltd., Published by the Geological Society.
Olesen, O., Gernigon, L., Ebbing, J., Mogaard, J.O., Pascal, C. & Wienecke, S., 2006, Interpretation of aeromagnetic data along the Jan Mayen Fracture Zone, JAS-05., Geological Survey of Noway (NGU) Report 2006.018 (confidential to 17.02.2011), 162.
Reid, A.B., Allsop, J.M., Granser, H., Millett, A.J. and Somerton, I.W., 1990, Magnetic interpretation in three dimensions using Euler deconvolution, Geophysics, v 55, 80-91.
Ritzmann, O., Jokat, W., Czuba, W., Guterch, A., Mjelde, R. And Nishimura, Y., 2004, A deep seismic transect from Hovgård Ridge to northwestern Svalbard across the continental-ocean transition: A sheared margin study: Geophysical Journal International, v. 157, pp. 683–702.
Ritzmann, O. and Faleide, J.I., 2007, Caledonian basement of the western Barents Sea, Tectonics, 26.

Ritzmann, O., Maercklin, N., Faleide, J.I., Bungum, H., Mooney, W.D. & Detweiler, S.T., 2007, A three-dimensional geophysical model of the crust in the Barents Sea region: Model construction and basement characterization, Geophysical Journal International, 170, 417-435.

Roberts, D. and Gee, D.G., 1985, An introduction to the structure of the Scandinavian Caledonides. In Gee, D.G. & Sturt, B.A. (eds) The Caledonide Orogen – Scandinavia and related areas. John Wiley & Sons,Chichester, 55-68.

Skilbrei, J.R., 1990, Flymagnetiske målinger over Barentshavet. NGU Årsmelding 1989, 18-19.

Skilbrei, J.R., 1991, Interpretation of Depth to the Magnetic Basement in the Northern Barents Sea (South of Svalbard), Tectonophysics, 200, 127-141.

Skilbrei, J.R., 1993, Short Note: The straight-slope method for basement depth determination revisited. Geophysics, Vol. 58, NO. 4 (April 1993), P. 593-595.

Skilbrei, J.R., 1995, Aspects of the geology of the southwestern Barents sea from aeromagnetic data. Norges geologiske undersøkelse Bulletin 427, 64-67.

Skilbrei, J.R., Kihle, O., Gellein, J., Solheim, D., Nyland, B., 2000, Gravity anomaly map, Norway and adjacent ocean areas. M 1:3 000 000. Geological Survey of Norway.

Stephens, M.B., and Gee, D.G., 1989, Terranes and polyphase accretionary history in the Scandinavian Caledonides, in Dallmeyer, R.D. (ed) Terranes in the Circum-Atlantic Paelozoic Orogens. Geological Society of America Special Paper 230, 17–30.

Sættem, J., 1988, Varmestrømsmålinger i Barentshavet. 18. Nordiske Geologiske Vintermøde, Geological Survey of Denmark (extended abstract), 406-408.

Zeyen, H. and Fernandez, M. 1994, Integrated lithospheric modeling combining thermal, gravity, and local isostasy analysis: application to the NE Spanish Geotransect. Journal of Geophysical Research, 99, 18089–18102.

Zeyen, H., Ayarza, P., Fernandez, M. and Rimi, A., 2005, Lithospheric structure under the western African–European plate boundary: a transect across the Atlas Mountains and the Gulf of Cadiz. Tectonics, 24, TC2001.

Ziegler, P.A., 1988, Evolution of the Arctic-North Atlantic and the western Tethys, Am. Assoc. Petrol. Geol. Mem., 48, 198.

Zielinski, G.R., Gunleiksrud, T., Sættem, J., Zuidberg, H.M., and Geise, J. M., 1986, Deep heat flow measurements in Quaternary sediments on the Norwegian continental shelf. Offshore Technology Conference Houston, TX 1986, 277-282.

Åm, K., 1975, Aeromagnetic basement complex mapping north of latitude 62 N, Norway, Norges geologiske undersøkelse, 316, 351-374.

Chapter 2

Offshore prolongation of Caledonian structures and basement characterisation in the western Barents Sea from geophysical modelling

Cécile Barrère, Jörg Ebbing and Laurent Gernigon

Published in Tectonophysics in 2009:
Barrère, C., Ebbing, J. & Gernigon, L., 2009a. Offshore prolongation of Caledonian structure and basement characterisation in the western Barents Sea from geophysical modelling, Tectonophysics, 470, 71-88.

Abstract

This study interprets the potential field of the western Barents Shelf at a crustal scale and characterises the basement underlying the deep basins in the southwestern Barents Sea. Comparing potential fields with onshore geology shows that Archaean to Palaeoproterozoic basement and mafic complexes are related to regional magnetic highs while Caledonian nappes are associated with lower magnetic anomalies. It also shows that crustal structures such as major fault zones can be extended offshore. Interpretation of the magnetic data suggests an elbow-shaped offshore prolongation of the Caledonides linking structures striking N 50º in northern Norway with the N-S structures on Svalbard. The basic interpretation has been tested by 2D free air gravity and magnetic forward modelling along selected seismic transects. Seismic interpretation is integrated with density and magnetic modelling to investigate the crustal and deep-crustal configuration of the southwestern Barents Sea. The distribution of density, magnetic susceptibility and Q-ratio values allows us to distinguish different basement units.

Compiling onshore information with the inter-profile correlations of the 2D models has allowed us to compile a map of basement units. The distribution of basement lithologies leads to a new regional understanding of the crustal architecture of the Barents Shelf. The shape and strike of the offshore prolongation of the Caledonian structures suggest that terranes affected by the Timanian orogeny propagate across the Barents Shelf farther to the northwest than have been interpreted previously.

2.1 Introduction

The Barents Sea Shelf is located in northernmost Europe and extends from the North Atlantic and the Svalbard Archipelago in the west to Novaya Zemlya in the east, over a distance of 1000 km (Fig. 2.1). In the west, the Barents Sea is bounded by its Cenozoic passive margins that were formed during the final stages of North Atlantic break-up in the Early Eocene (Doré, 1991; Lundin and Doré, 2002).

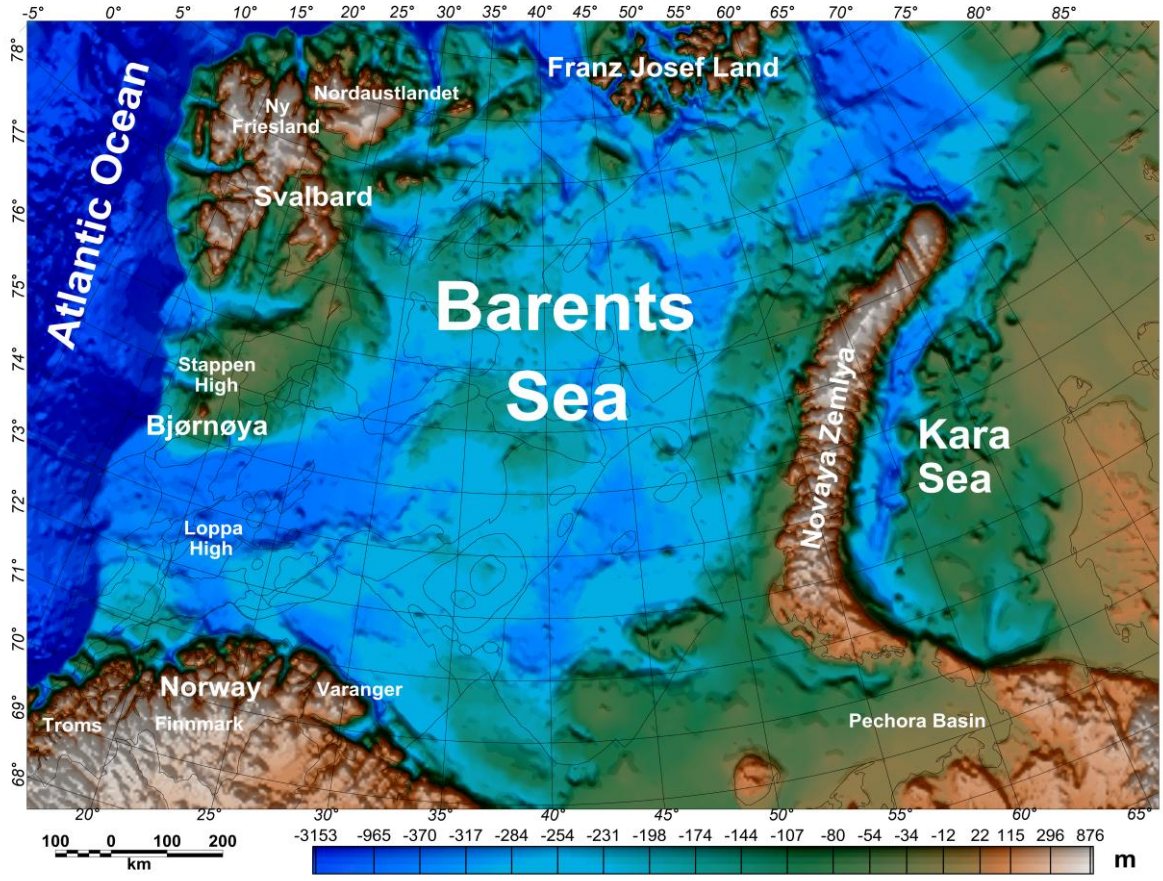

Figure 2.1: Barents Sea shelf and surrounding land masses: bathymetry-topography. The study area is the southwestern (SW) Barents Sea (69 °N – 75 °N and 13 °E – 30 °E). The thin black lines show the tectonic units as defined by the Norwegian Petroleum Directorate).

Exploration of the Barents Sea is of great interest for both academic and economic purposes due to the hydrocarbon potential in the area. In such a context, a detailed knowledge of the basement is fundamental as its geometry and composition provide important constraints for basin analysis and heat flow studies.

A dense grid of industrial seismic reflection data exists in the area and the western Barents Sea has been the subject of many previous investigations and interpretations (Breivik et al., 1998; Faleide et al., 1993; Gabrielsen, 1984; Gabrielsen et al., 1990; Gabrielsen et al., 1997; Gudlaugsson and Faleide, 1994; Gudlaugsson et al., 1987; Gudlaugsson et al., 1998; Johansen et al., 1994; Ritzmann et al., 2007; Skilbrei, 1991). On the Barents Shelf, sedimentary thicknesses locally reach to more than 14 km; therefore, conventional seismic reflection data do not allow reliable mapping below the Permian succession and the complex structure of the deep basement still remains poorly constrained. Little information about the regional structure of the crust is available from published models based mainly on Ocean Bottom Seismometer (OBS) data (Fig. 2.2). Seismic refraction data (Breivik et al., 2003; Breivik et al., 2005; Breivik et al., 2002; Mjelde et al., 2002) had already been presented as an alternative method for constraining the sub-sedimentary crustal structure.

The present study aims to investigate the nature and complex history structure and lithology of the Barents Shelf using potential field data. Our specific study area for basement characterisation is the southwestern (SW) Barents Sea (69 °N – 75 °N and 13 °E – 30 °E). Situated offshore from northern Norway where Caledonian thrust sheets are well-exposed (Ramsay et al., 1985; Siedlecka and Roberts, 1996; Sturt et al., 1975), this area encompasses major structural highs, platforms and basins (Fig. 2.2; (Gabrielsen et al., 1990; Gudlaugsson et al., 1998)). Offshore, most of the sedimentary rocks in the basins range in age from Late Palaeozoic to Quaternary. The investigations offshore started at the most prominent basement high of the area, the Loppa High (Fig. 2.2), which is surrounded by individual faults or fault complexes that were activated during the formation of the positive basement feature observed at present day (Gabrielsen, 1984; Gabrielsen et al., 1990).

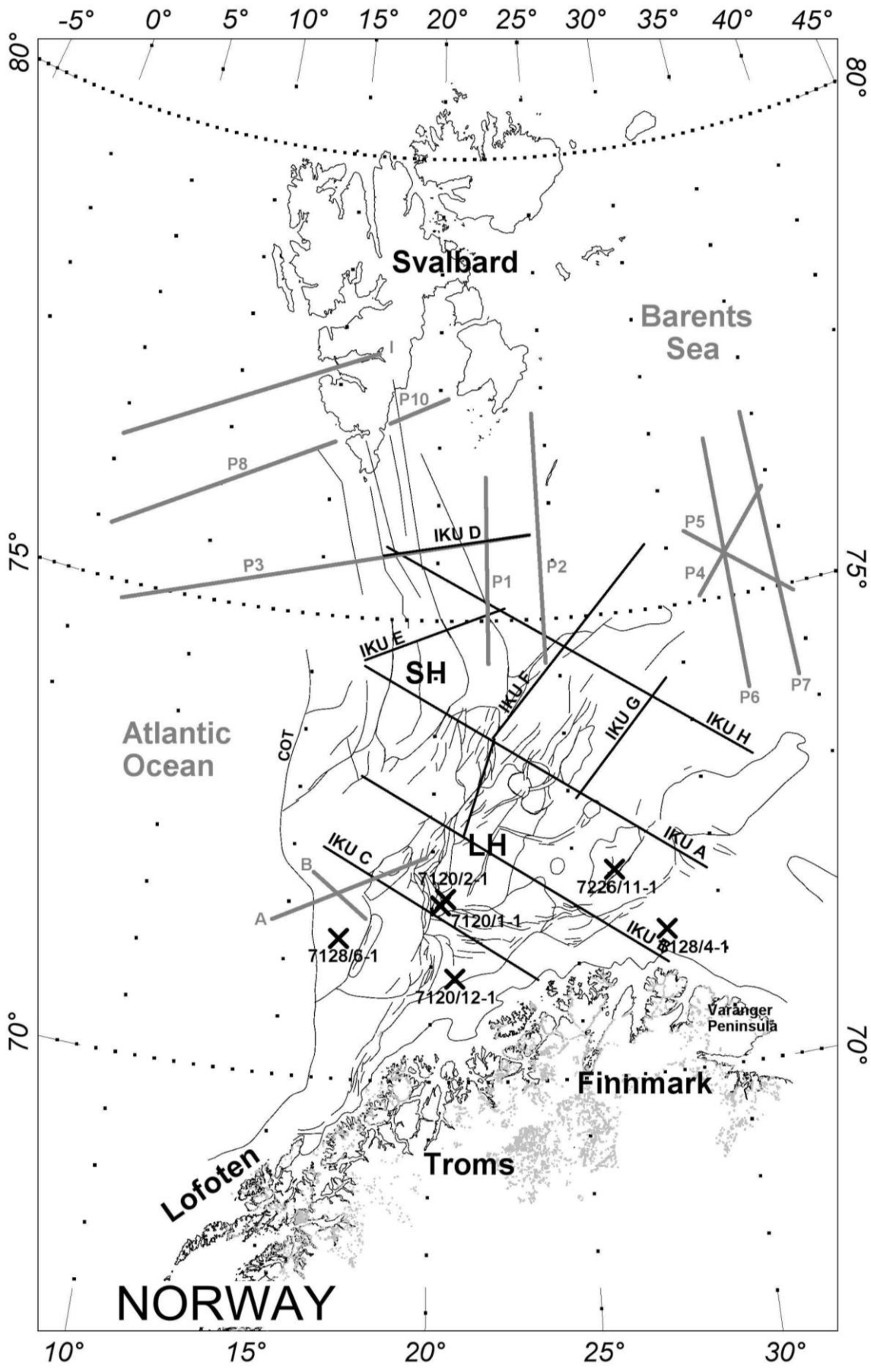
-5°
0°
5°
10°
15°
20°
25°
30°
35°
40°
45°
80°
75°
70°
10°
15°
20°
25°
30°
Svalbard
Barents Sea
Atlantic Ocean
NORWAY
Lofoten
Troms
Finnmark
Varanger Peninsula
P1
P2
P3
P4
P5
P6
P7
P8
P10
I
IKU A
IKU B
IKU C
IKU D
IKU E
IKU F
IKU G
IKU H
COT
SH
LH
7120/2-1
7120/1-1
7120/12-1
7128/6-1
7128/4-1
7226/11-1
A
B

Figure 2.2: Simplified structural and location map. Onshore, the locations of the petrophysical samples used to constrain the modelling parameters (Olesen et al., 1990) are plotted in grey.
Offshore, the solid lines indicate a simplified structural map. The main structural highs are the LH (Loppa High) and the SH (Stappen High). The crosses locate the wells that reach down to the basement rocks, and straight solid lines show the seismic data used as constraints in this study. The IKU deep reflection data is in black. The more significant wide-angle data is in grey: P1, P2, P3, P4, P5, P8 and P10 are from Breivik et al. 2002, 2003 and 2005; A and B are from Mjelde et al, 2002; I is from Ritzmann et al. 2002.

Following a brief presentation of the geological setting, we correlate the geological information both available onshore and offshore with the regional potential field data. Maps are interpreted using different filtering techniques, onshore-offshore relationships and potential field modelling. Reliable crustal models across the SW Barents Sea are constructed by integrating structural information derived from seismic data and petrophysical constraints. A map showing principal basement units and a regional interpretation focusing on the prolongation of Caledonian structures offshore and the origin of sedimentary basins are presented.

2.2 Geological setting

The tectonic evolution of the Barents Sea area was strongly influenced by the Palaeoproterozoic (Svecofennian) orogeny, which established the stable Russian-European platform adjacent to the northern Archaean part of the Fennoscandian Shield (Alsgaard, 1993; Gee et al., 2006; Gee and Tebenkov, 2004; Roberts and Olovyanishnikov, 2004; Torsvik et al., 1996).

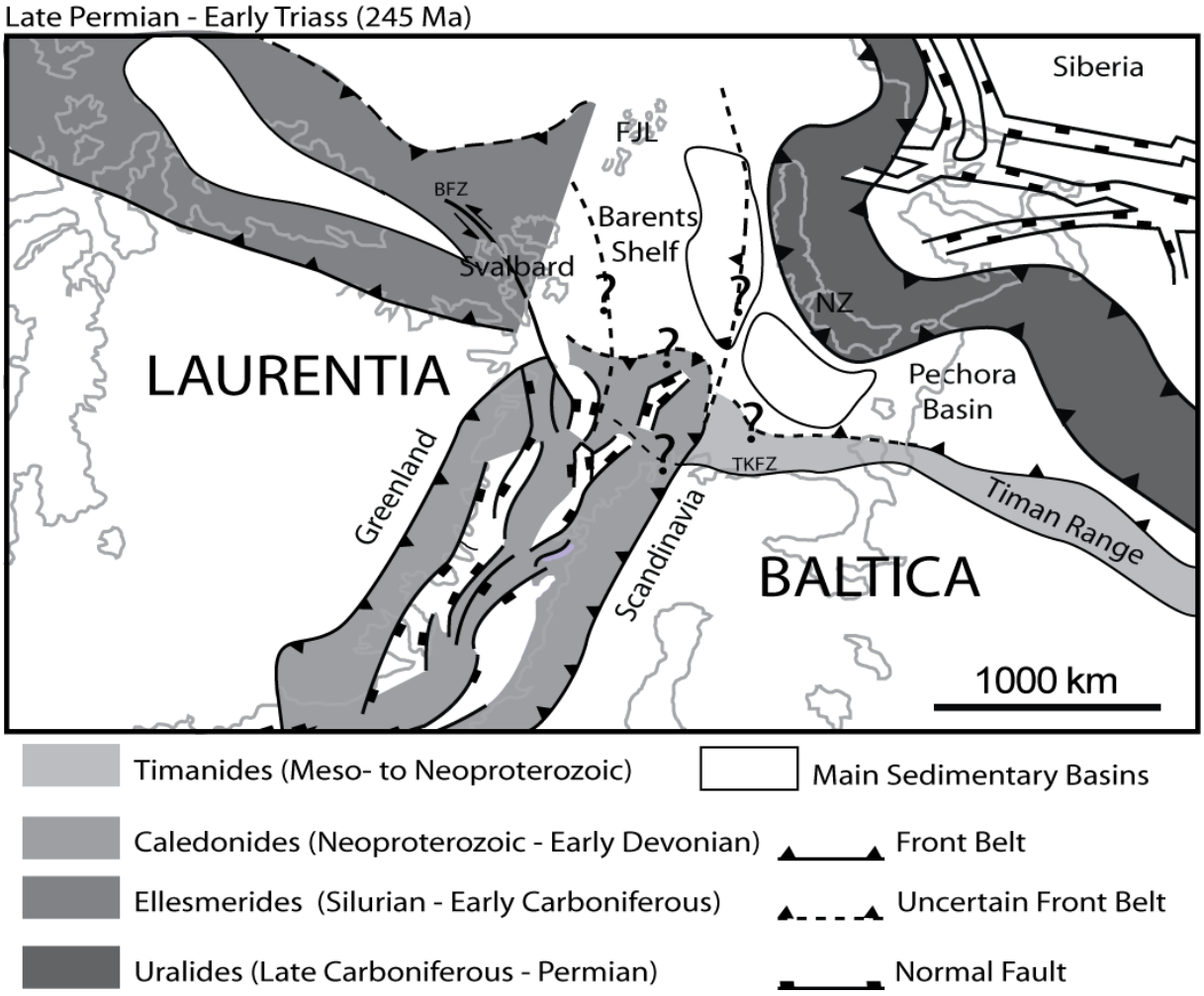

Figure 2.3: The Barents Sea Shelf in the Late Permian-Early Trias (245 Ma). The extension of the Timanides, Caledonides, Ellesmerides and Uralides ranges, as well as the main sedimentary basins, are represented. The question marks highlight the uncertain positions of structural boundaries such as the Caledonian suture and front and the Timanian front belt. FJL (Franz Josef Land), BFZ (Billefjorden Fault Zone), TKFZ (Trollfjorden-Komagelva Fault Zone), NZ (Novaya Zemlya).

The north- to northeastward extension of the Norwegian Caledonides into the Barents Sea – generally referred to as the Barentsian Caledonides (e.g., Siedlecka 1975) is flanked to the east by the late Neoproterozoic Timanide fold belt (Fig. 2.3), recognised as far north as on Novaya Zemlya. Accreted and superimposed, Neoproterozoic (Timanian) orogenic trends are usually oriented NW-SE (e.g., Timan Range, Timan-Varanger Belt), and Timanian basement is present in the western and central Pechora Basin (Gee et al., 2006; Ivanova, 2001). On Varanger Peninsula in Norway, the Trollfjorden-Komagelva Fault Zone (Fig. 2.3) separates the Baltican

platform domain terranes from the Timanian basinal terranes and can be followed south-eastwards into the Timan Range (Olovyanishnikov et al., 2000; Roberts and Olovyanishnikov, 2004; Roberts and Siedlecka, 2002).

From Late Cambrian time and over a period of 80 Myr, the gradual closure of the Iapetus Ocean (Gee, 2005; Gee et al., 2006; Roberts, 2003; Roberts and Gale, 1978; Torsvik et al., 1996) involved subduction zones, associated magmatic activity in island arcs and several tectonic events along the margins of both Laurentia and Baltica. The major collision between Baltica and Laurentia (forming the Larussia plate) began in the Silurian and extended until the Early Devonian, and is known as the Scandian orogeny.

Several studies on Spitsbergen have shown that the Caledonian basement terranes and structures (Harland et al, 1994) correlate with similar terranes, faults and thrusts mapped on the East Greenland margin (Gee and Tebenkov, 2004; Scott and Turton, 2001). The affinity of terranes on Svalbard and in East Greenland to the Laurentian plate (Torsvik and Cocks, 2005) is well known. Nevertheless, the relative positions of these two terranes are still a matter of debate.

From Silurian to Early Carboniferous time, the Innuitian or Ellesmerian Orogeny (Fig. 2.3) affected Laurentia (Filatova and Khain, 2007; Piepjohn et al., 2007). Thereafter, the deformation regime changed from compression and lateral shortening to regional extension (Gee, 2005).

The Late Palaeozoic and Mesozoic tectonic history of the western Barents Sea was mostly dominated by several rifting episodes. Agreement exists about two main extensional periods, respectively in Early-Mid Devonian to Early-Mid Carboniferous and Permian to Early Triassic times (Gabrielsen et al., 1990; Lippard and Roberts, 1987).

The late- to post-Scandian collapse of the Caledonides is recognised throughout much of Scandinavia (Andersen, 1998; Fossen, 2000; Roberts, 1983) and in East-Greenland (Higgins et al., 2004). Gudlaugsson et al. (1998) argued for a post-Caledonian extensional collapse to the southeast of Bjørnøya. On Svalbard, Chorowicz (1992), Manby and Lyberis (1992) and Skilbrei (1991) interpreted the Devonian graben of Spitsbergen as a post-orogenic basin.

With respect to the stratigraphic records on Svalbard and the Barents shelf, it seems that both were subjected to broadly similar extensional regimes (Bugge et al., 1995;

Gabrielsen et al., 1990; Larssen et al., 2005). These observations provide evidence of a regional subsidence leading to the formation of a large interior sag basin, which they interpret as the first stage of the rift system formation in the southwestern Barents Sea. Gudlaugsson et al. (1998) proposed that the fan-shaped structural configuration of the rift system is inherited from the structural axis of the Scandinavian and East-Greenland Caledonides (and Barentsian Caledonides) interfering with the northerly oriented Caledonian-Innuitian orogenic trend.

Rifting episodes have also been documented in Carboniferous, Permian, Triassic and Late Jurassic to Early Cretaceous times (Johansen et al., 1994). These episodes led to the formation of the major rift basins on the Barents Shelf.

Subsidence and salt tectonics occurred throughout the Triassic period and affect the regional depositional patterns of the area (Breivik et al., 1995; Gabrielsen et al., 1990; Lind, 1987).

During Mid Jurassic time, rifting and block tilting occurred once again and increased through to the Early Cretaceous (Faleide et al., 1993). During this period, up to 3 km of sedimentary rocks were eroded (Dimakis et al., 1998), leaving little Cretaceous and Jurassic rocks preserved on the Loppa High, but creating well defined Jurassic depocentres in adjacent basins.

The Late Jurassic-Early Cretaceous period was dominated by a composite rifting episode, which gave rise to prominent NE-SW trending structures in the Northeast Atlantic, such as the Bjørnøya Basin. Following rifting, a wide region subsided and was covered by thick Cretaceous strata.

During Early Cretaceous time, the northern part of the Barents Shelf was affected by a significant magmatic event (Grogan et al., 1998), which is considered to have been part of the Large Igneous Province (Maher, 2001) linking Greenland, Svalbard, Franz Josef Land and adjacent shelf areas. During the Late Cretaceous, "reverse faulting and folding, combined with extensional faulting along Bjørnøyrenna Fault Complex, became still more common, even though extension may have prevailed on the regional scale" (Gabrielsen et al., 1997).

The main continental break-up and the development of the western Barents Sea Margin occurred in Mid Cenozoic (Oligocene) time.

The last episode of the complex western Barents Sea history is the uplift of the westernmost Barents Shelf that started in Late Cenozoic and led to the removal of 3 kilometres of sediments (Nyland et al., 1992).

2.3 Databases

2.3.1 Seismic data

We had access to depth-converted industrial seismic profiles including regional deep-seismic reflection lines (alias, the IKU lines) (Fig. 2.2). Acquired in the mid-1980s, these seismic data have been interpreted in several studies (Breivik et al., 1998; Breivik et al., 2005; Faleide et al., 1993; Gudlaugsson and Faleide, 1994; Gudlaugsson et al., 1987; Sanner, 1995). Velocity models derived from seismic refraction data are used to constrain the deep crustal structures (Breivik et al., 1998; Breivik et al., 1995; Breivik et al., 2003; Breivik et al., 2005; Breivik et al., 2002; Mjelde et al., 2002).

2.3.2 Gravity data

Gravity data are available from the compilation published by Skilbrei et al. (2000). To make the correlation between the onshore and offshore structures possible, terrain-corrected Bouguer anomaly values were calculated using a Bouguer reduction density of 2670 kg/m^3 (Fig. 2.4A).

2.3.3 Magnetic data

Aeromagnetic data are available from a magnetic compilation of the western Barents Sea (Olesen et al., 2006) (Fig. 2.4B). The dataset was compiled from reprocessed aeromagnetic surveys. The line spacing ranges from 0.5 to 2.5 km over mainland Norway and from 3 to 8 km over the continental shelf. To investigate the crustal sources, the data are reduced to the pole and upward continued to 600 m.

Further correlations between tectonic units and magnetic anomalies can be detected by looking at trends from derivative-filtered magnetic data. The tilt derivative is useful for mapping shallow basement structures. The tilt derivative is defined as the first vertical derivative of the total magnetic intensity, T, divided by the total horizontal

derivatives of T. It enhances the geometrical contrast existing in the internal basement structure (Verduzco et al., 2004).

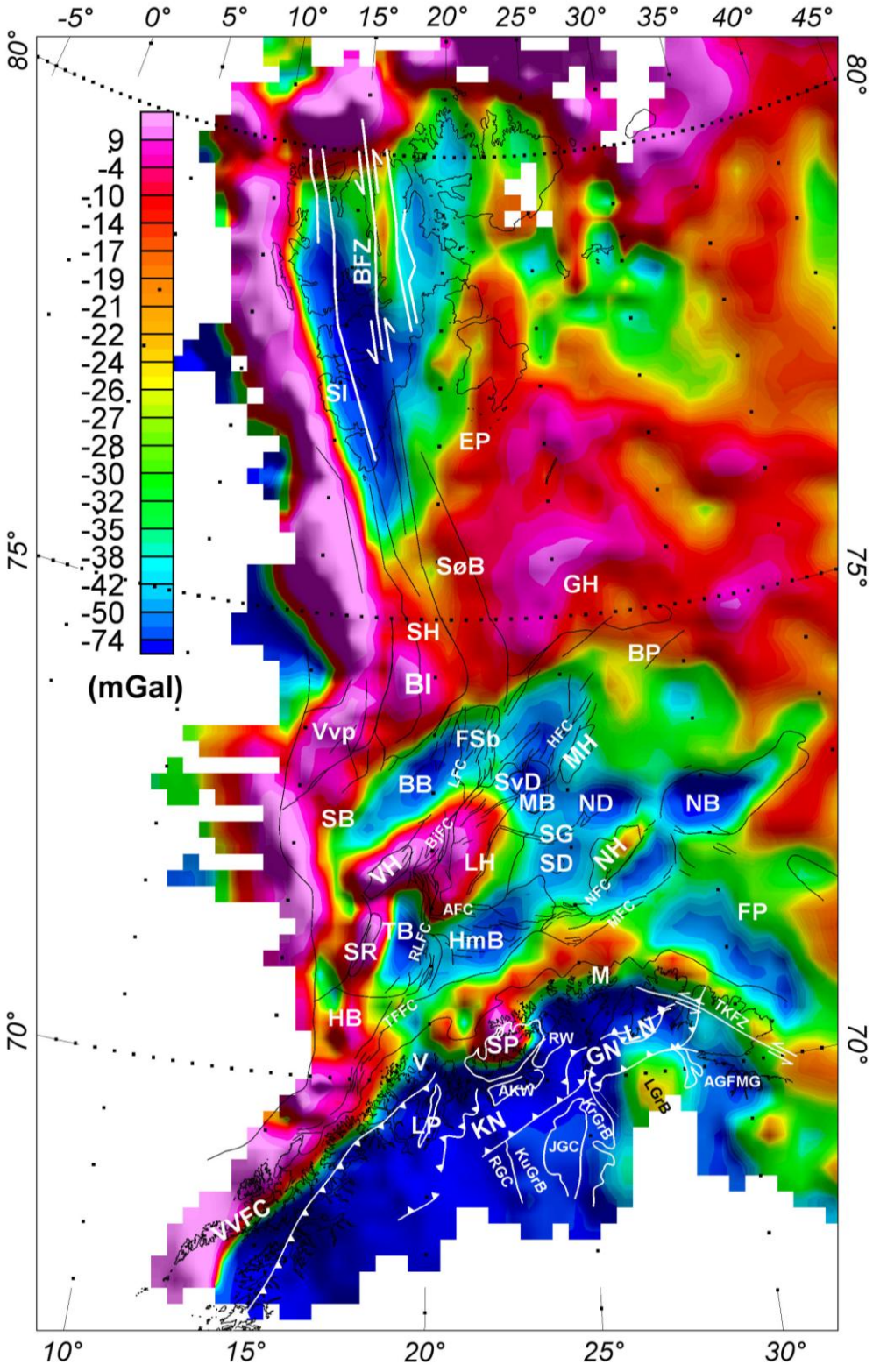

Figure 2.4A: Bouguer anomaly and simplified structural map

Overlay of the Bouguer anomaly (mGal) (Bouguer density = 2670 kg/m^3) and simplified structural map.

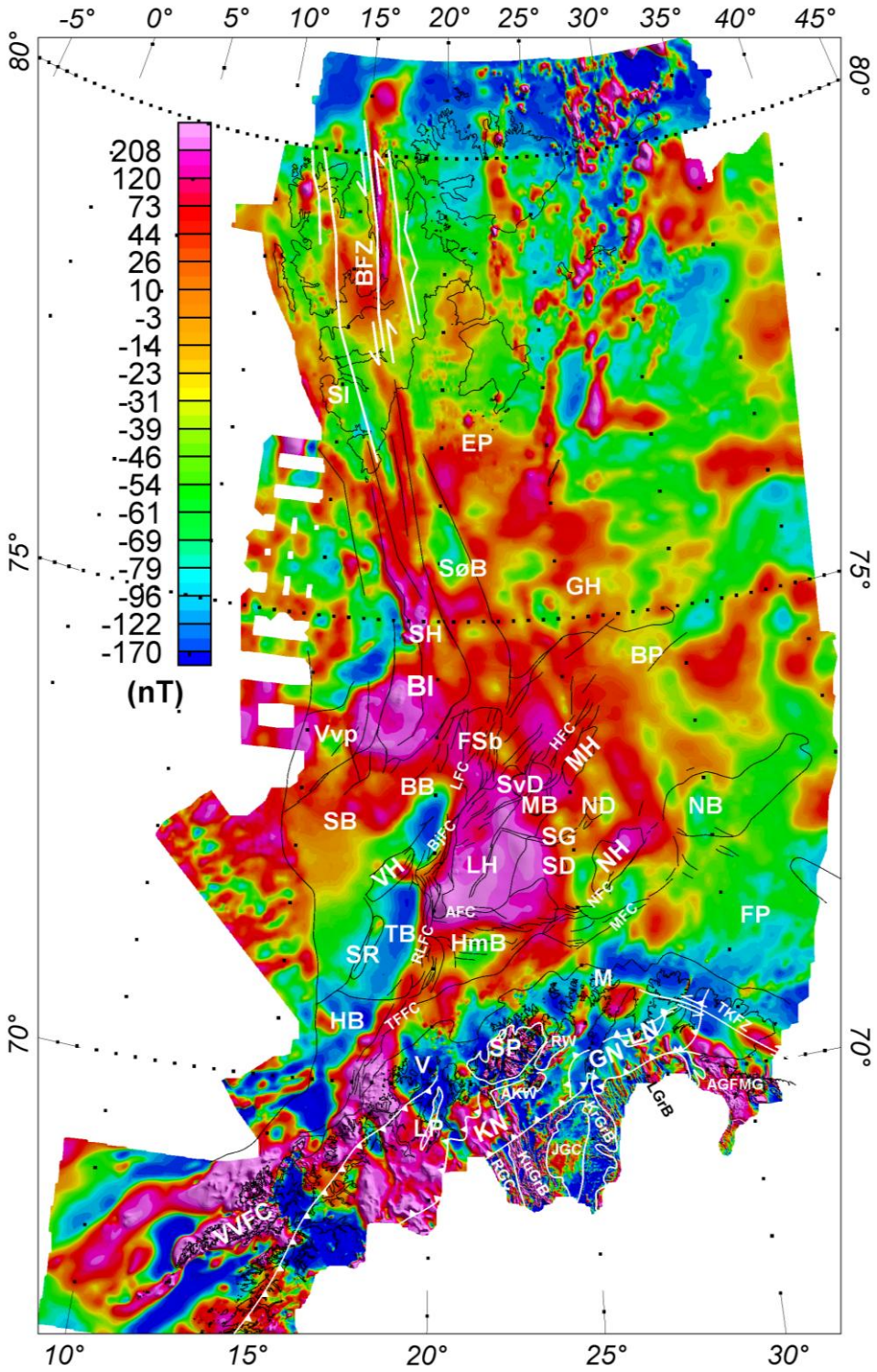

Figure 2.4B: Total magnetic field (nT) (pole-reduced and upward-continued to 600m) and simplified structural map.

Overlay of the total magnetic field (TMF) reduced to the pole (D=24.4º I=7.3º) and a simplified structural map. (Refer to the abbreviation list at the end of the paper, page 81)

2.3.4 Petrophysical information

Petrophysical constraints were derived from the literature (Olesen et al., 1990; Skilbrei, 1991; Skilbrei et al., 1991; Tsikalas, 1992) (Fig. 2.2). Density, magnetic susceptibility and remanence values from onshore samples (Troms and Finnmark regions) (Olesen et al., 1990) were used to choose starting values in the models (Table 2.1).

Starting values for the modelling				
Unit	Density (kg/m^3)	Mag. Susc. (SI)	Mag. Rem. (A/m)	Q-ratio
Sediments	1800 to 2710	0.00	0.00	0.00
Archaean to Palaeoproterozoic rocks	2750 to 2800	0.01 to >0.1	0.20	0.05 to 0.5
Caledonian nappes	2750	1.10^{-4} to 0.01	0.01	0.25 to 21
Mafic rocks	2800 to 3000	0.01	0.2	0.50
Lower crust	2950	1.10^{-4}	0.00	0.00
Mantle	3300	0.00	0.00	0.00
Interpreted values				
	Density (kg/m^3)	Mag. Susc. (SI)	Mag. Rem. (A/m)	Q-ratio
B1 Archaean to Palaeoproterozoic rocks	2750-2800	0.010→0.200	0.20	Q<1.00
B2 Caledonian nappes on top of Archaean to Palaeoproterozoic rocks	2750	0.001→0.010	0.01	Q>1.00
B3 Deep crustal high density body	3100-3200	1.10^{-4}	0.00	0.00
B4 None-magnetic basement	2750-2800	0.000	0.00	0.00
B5 Basement affected by magmatism	2800-2900	0.007	0.20	0.60
MI (Mafic Intrusions)	3000	0.015	0.20	0.30→0.35

Table 2.1: Starting values: density (kg/m^3), magnetic susceptibility, magnetic remanence (A/m) and Q-ratio for all geological layers were determined from published papers (Tsikalas, 1992; Olesen et al., 1990; Breivik et al, 1998, 2002, 2003, 2005 and Bungum et al., 2006)

Interpreted values: The different basement units were defined by a combination of petrophysical values obtained by density and magnetic modelling.

Along a profile the density is constant within a body. The density value intervals originate from the inter-profile correlations and gathering of bodies of compatible gravity and magnetic properties.

2.4 Onshore-offshore correlations of gravity and magnetic anomalies

The geology of Finnmark and Troms, northern Norway regions, was studied by examining the available geological maps. The Fennoscandian Shield in that region is partly covered by Caledonian nappes, of which the Kalak, Laksefjord and Gaissa nappes complexes locally reach up to 5 km in thickness (Olesen et al., 1990; Ramsay et al., 1985; Rice et al., 1989; Siedlecka and Roberts, 1996).
In many of the nappes, the metasedimentary rocks are intruded by mafic dykes of Vendian or Devonian age, and at some levels of the tectonostratigraphy there are major, mafic-ultramafic, plutonic complexes such as the Vendian-age Seiland Igneous Province (Roberts et al., 2006) and the Early Silurian, Honningsvåg Igneous Complex (Corfu et al., 2006; Robins, 1998). On the island of Magerøya there are also a few mafic dykes of Carbonifereous age (Lippard and Prestvik, 1997).

2.4.1 Geology / Bouguer anomalies

The Bouguer anomaly reflects the density contrast of the anomalous masses with respect to normal densities. The correlation between Bouguer anomalies and onshore geological units is not obvious (Fig. 2.4A and 2.5A), only the Seiland Igneous Province creates a pronounced gravity high (Olesen et al., 1990).
A series of gravity highs is located along the outer part of the Finnmark area, facing the Barents Sea. They could possibly be related to the ultramafites and gabbros of Silurian age that occur on Magerøya (Corfu et al., 2006; Robins, 1998).

The Stappen High, the Veslemøy High and the Senja Ridge are also well delimited by positive Bouguer anomalies ranging from 30 to 100 mGal. The Loppa High is characterised by a prominent ellipsoidal Bouguer anomaly of 70 mGal striking roughly N-S and focused along the Bjørnøyrenna Fault Complex and the Ringvassøy-Loppa Fault Complex. The Norsel and the Gardarbanken Highs, as well

as the Bjarmeland and the Finnmark Platforms are represented by medium gravity anomalies from 20 to 30 mGal.

Gravity lows between -20 mGal and -40 mGal outline the Tromsø, Maud and Nordkapp Basins as well as the Norvarg and Svalis Domes. The Hammerfest, Bjørnøya and Sørvestsnaget Basins and the Samson Dome correlate with medium Bouguer anomalies of around –10 mGal. The Bouguer anomaly map (Fig. 2.4A) highlights a few trends. The regional N 50˚ tectonic trends are perceptible in lineaments along the Vestfjorden-Vanna, the Troms-Finnmark and Måsøy Fault Complexes as well as along the axis of the Nordkapp Basin. The gravity highs of the Veslemøy High and the Senja Ridge do not correlate with magnetic highs.

2.4.2 Geology / magnetic anomalies

A comparison of the main geological units with the magnetic data (Fig. 2.4B and 2.5B) highlights correlations between Archaean to Palaeoproterozoic gneiss complexes and magnetic highs, e.g., the Raisædno and Jergol Gneiss Complexes (amphibolites facies), the Tanaelv Migmatite Complex, the Varanger Gneiss Complex (amphibolite to granulite facies) and the Levajok Granulite Complex, all trending at N 150˚ (marked as AGFMG in Fig. 2.5B). There is a good correlation between magnetic highs and the gabbro and ultramafic rocks of the Seiland Igneous Province, as well as with the ophiolitic rocks of the Lyngen Province. The Kautokeino and Karajok Greenstone Belts (greenschist to amphibolite facies) are associated with magnetic highs and represent distinct linear features striking N 165˚ that can be followed beneath the Caledonian nappes (Fig. 2.5B) (Olesen et al., 1990; Åm, 1975).

Even where the samples from Caledonian nappes are magnetic (Table 1), the do not produce a significant magnetic anomaly. Therefore, Palaeoproterozoic, mafic and felsic, medium- and high-grade metamorphic rocks are recognised as the sources of significant regional magnetic anomalies. These rocks are characterised by different ranges of density and magnetic pattern.

Offshore, the upward-continued and pole-reduced total magnetic field (Fig. 2.4B) does not show any good correlation with the offshore tectonic units. It is there assumed to reflect a combination of top basement topography (i.e., tilted blocks, undulations of erosional surfaces) and intra-basement sources (i.e., high-magnetic plutons, mafic dykes).

The Loppa and Stappen Highs, identified as basement highs (Gabrielsen et al., 1990), are represented by strong magnetic anomalies ranging from 100 nT to 900 nT. In the Loppa High region, two different provinces are distinguished from potential field data. The western part of the basement high is characterised by a pronounced Bouguer anomaly (70 mGal) and a moderate magnetic anomaly (100 nT). In contrast, the eastern part is marked by a gradual decrease in Bouguer anomalies down to 0 mGal and an increase in magnetic anomalies up to 900 nT.

Some magnetic anomalies are clearly limited in their spatial extension, such as in the northern part of the Norsel High and the Veslemøy High. A low-amplitude but well-focused magnetic high is located in the northern part of the Senja Ridge. The Hammerfest Basin is surrounded by several intense magnetic highs. In the northern part of the basin, the magnetic high is related to the Loppa High. In the southeast, the magnetic high correlates with the junction of three fault complexes: the Tromsø-Finnmark Fault Complex, the Asterias and the Nysleppen Fault Complexes. In the west, the magnetic high involves the Ringvassøy-Loppa and Tromsø-Finnmark Fault Complexes. The gravity lows of the Maud Basin and the faults striking NE-SW to the north of the Maud Basin correlate with high-magnetic anomalies. The Sørvestsnaget Basin presents an anomaly gradually increasing northwards from -100 to 0 nT. Strong and aligned magnetic lows, in the range -100 to -160 nT, strike N 25˚ and correspond to the Harstad Basin, the Tromsø Basin and the eastern part of the Bjørnøya Basin.

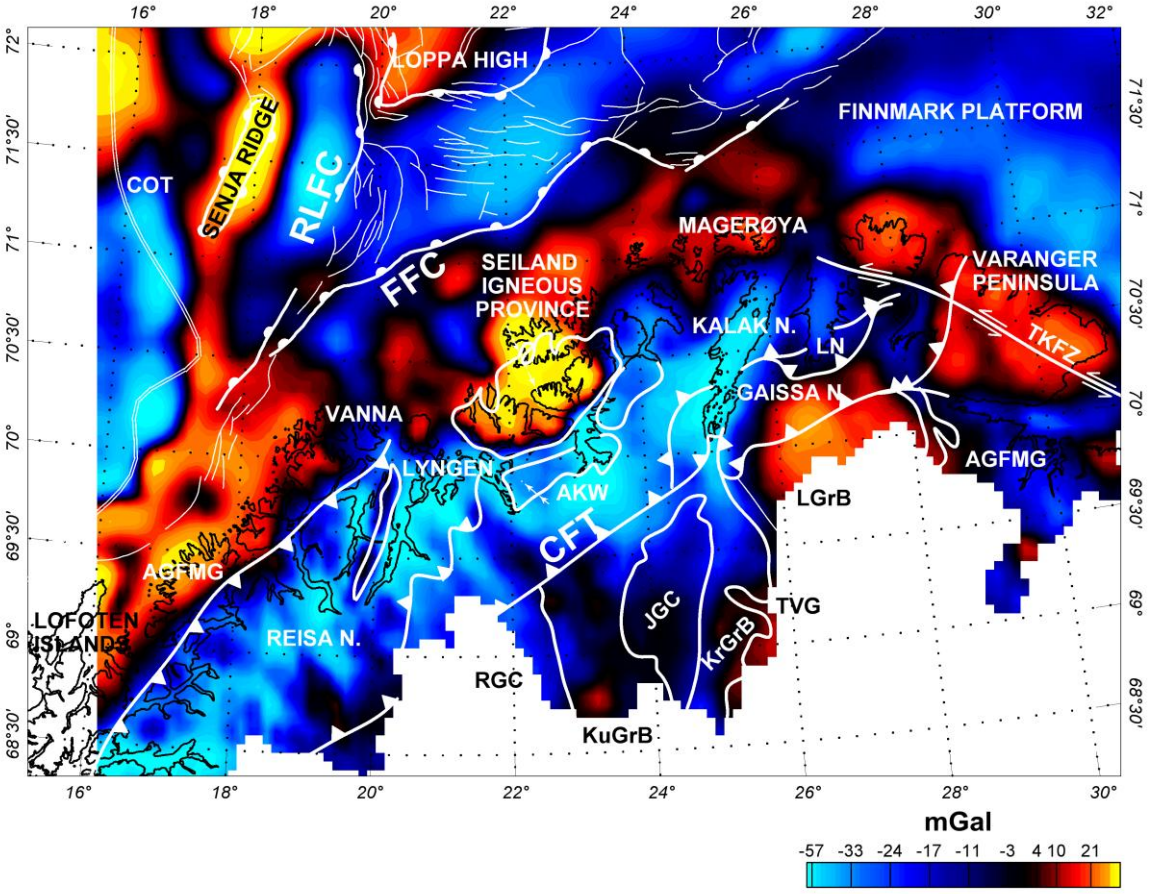
LOPPA HIGH
FINNMARK PLATFORM
SENJA RIDGE
RLFC
COT
FFC
SEILAND
IGNEOUS
PROVINCE
MAGERØYA
VARANGER
PENINSULA
TKFZ
KALAK N.
LN
GAISSA N.
VANNA
LYNGEN
AKW
CFT
AGFMG
LGrB
JGC
KrGrB
TVG
LOFOTEN
ISLANDS
REISA N.
RGC
KuGrB
mGal
-57 -33 -24 -17 -11 -3 4 10 21

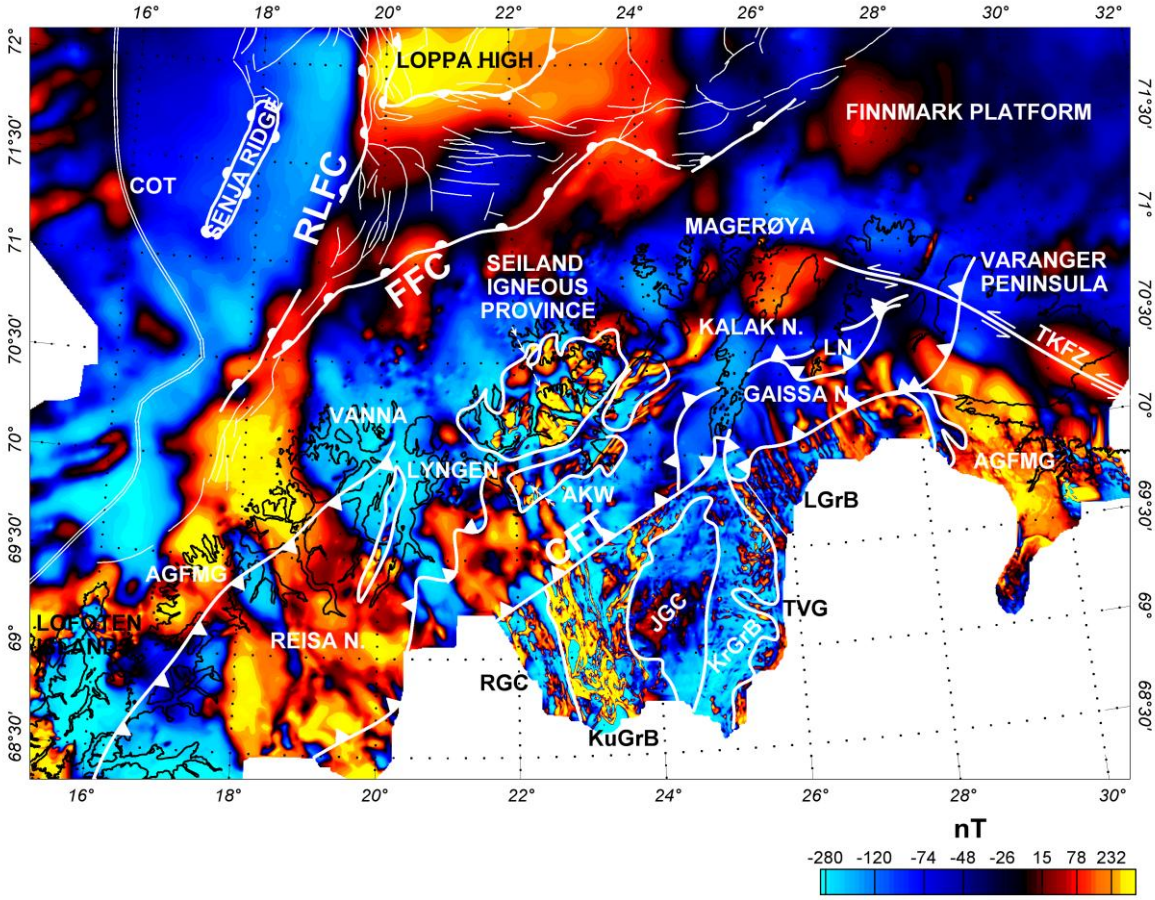
LOPPA HIGH
FINNMARK PLATFORM
SENJA RIDGE
RLFC
COT
FFC
SEILAND
IGNEOUS
PROVINCE
MAGERØYA
VARANGER
PENINSULA
TKFZ
KALAK N.
LN
GAISSA N.
VANNA
LYNGEN
AKW
CFT
AGFMG
LGrB
JGC
KrGrB
TVG
LOFOTEN
ISLANDS
REISA N.
RGC
KuGrB
nT
-280 -120 -74 -48 -26 15 78 232

Figure 2.5: Correlation between geological information and potential field maps (TMF- High Pass 50 km and Bouguer anomaly)
A. Bouguer anomalies, Bouguer reduction density = 2670 kg/m^3
B. Total magnetic field (TMF), high-pass filter (50 km) applied. The high-pass filtering tends to better focus the magnetic anomalies.

2.4.3 Onshore-offshore magnetic domains established from magnetic trends

Because a magnetic anomaly has a petrophysical and/or structural origin, the magnetic trends outline the pattern of magnetic sources and/or structural elements as contacts between magnetic and less magnetic rocks. We overlay the trends of the total magnetic field (Fig. 2.6A) with the trends of its tilt derivative version (Fig. 2.6B). Five domains have thus been identified (Fig. 2.6C).

1. Onshore northern Norway, short-wavelength magnetic anomalies of the Archaean to Palaeoproterozoic gneisses and greenstone belts strike N 150˚ to N 165˚ (Fig. 2.6C, domain D1). These anomalies can be traced beneath the Caledonian nappes.
2. In the southwest, sea-floor spreading anomalies strike approximately N 50˚; they are bounded by a magnetic high related to the continental/oceanic strike-slip system boundary (Fig. 2.6C, D2).
3. The northeast region east of Svalbard was affected by Cretaceous magmatism (Grogan et al., 2000; Maher et al., 2001); on the map it exhibits pronounced, focused, high-frequency magnetic anomalies striking from N-S to N 20˚ (Fig. 2.6C, D3).
4. In the east, a group of trends is noticeably different and depicts a semicircular shape abutting the N 150˚ trends of the central part of the area (Fig. 2.6C, D4).
5. The central area is defined by N-S trends seen on land in Svalbard. These anomalies swing towards N 165˚ to N 150˚ trends south of the Svalbard archipelago and cross the southwestern Barents Sea to the south Loppa High where they bend to N 50˚ and extend along the Norwegian coast. Together, these trends form an elbow shape and link the N-S trends on Svalbard with the 150˚ trends of the southwestern Barents Sea and the N 50˚ trends of the Finnmark, Måsøy and Nysleppen Fault Complexes (Fig. 2.6C, D5). The fault zones defining the Utrøst Ridge (Lofoten), the Finnmark Fault Complex and the Nordkapp Basin are also aligned N 50˚. Onshore, the N 50˚ trend corresponds to the general strike of the Caledonian thrusts. We

propose that the elbow-shaped trends offshore are due to a combined effect of the strike of the Archaean to Palaeoproterozoic gneisses and Caledonian structures such as Scandian thrusts.

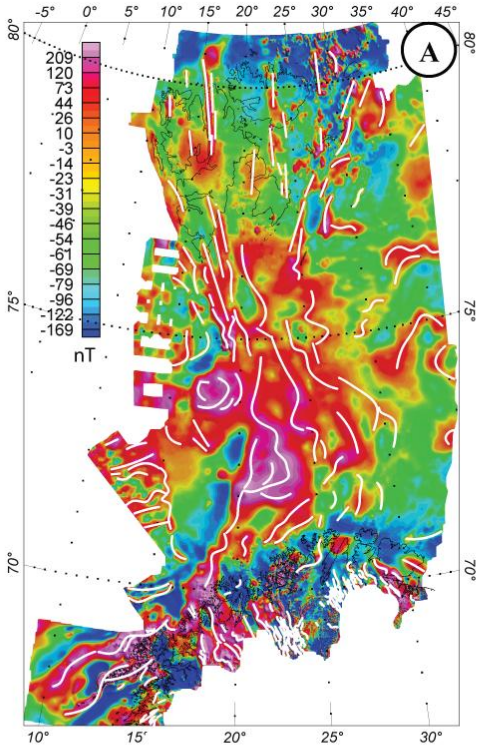

Total Magnetic Field (TMF)
(TMF trends, white lines)

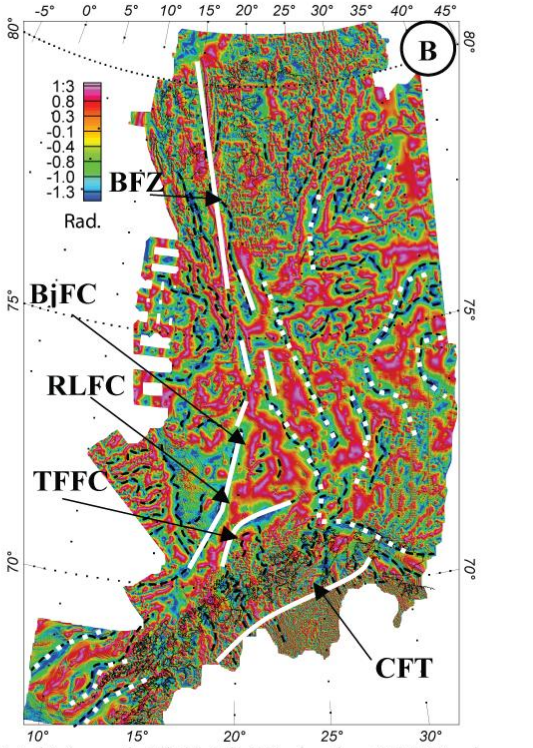

Total Magnetic Field, Tild Derivative (TD) Version
(TD trends, black dash; interpretation, white and arrows)

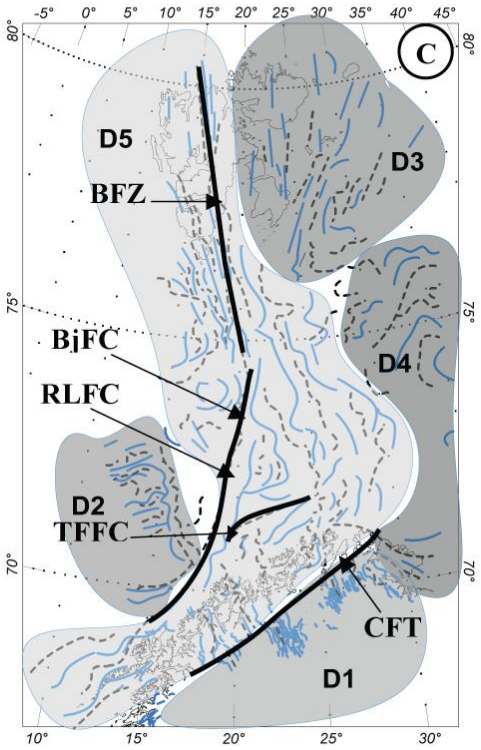

Magnetic domains established from the magnetic trends

Figure 2.6: Magnetic data interpreted

A. Reduced to the pole and upward-continued total magnetic field (TMF) - magnetic trends in blue lines.

B. Tilt derivative version of the TMF - trends in black dashed lines.

C. Magnetic domains established from the magnetic trends of Fig. 2.6A and 2.6B. The interpretation of the boundaries of D5 are open to discussion.

2.5 Forward modelling

The preliminary interpretation of the maps is now tested by forward modelling along three selected seismic transects, IKU A, B and C using the software GM-SYS 2D (Geosoft 2005).

2.5.1 Method

The shallow geometry of the models is based on the interpretation of major seismic reflectors including the 1) base Quaternary, 2) base Tertiary, 3) intra Upper Cretaceous, 4) intra Lower Cretaceous, 5) base of Upper Jurassic, 6) top Triassic, 7) near top Permian and near top basement. The top basement is determined by means of seismic interpretation where possible. The existence of a continuous mid-crustal boundary at around 20 km depth was inferred from seismic refraction velocity models. At this depth, P-wave velocities locally reach 7 km/s and basement reflectivity changes.

Density values were applied to all layers (Table 2.1). The densities of the sedimentary layers are based on a review of the available well data (Tsikalas, 1992). Tables published by Ritzmann and Faleide (2007) based on velocity-density relationships of sedimentary units obtained from the seismic refraction and reflection/gravity studies are also used (Breivik et al., 1998; Breivik et al., 2003; Breivik et al., 2005; Breivik et al., 2002; Mjelde et al., 2002). In our model we chose a density of 2950 kg/m^3 for the lower crust, and determined the crustal structure by density modelling. Then, the magnetic modelling helps to split the crust into blocks of contrasting magnetic properties.

The remanent magnetisation of the Archaean to Palaeoproterozoic and Caledonian rocks is related to the abundance of magnetic minerals within the rocks and the thermo-mechanical history and geomagnetic field when the rocks formed. Within coarse-grained rocks, the inclination and declination have been aligned to the present-day geomagnetic field (inclination I=79˚, declination D=4.3˚). The induced magnetisation (H) is proportional to the strength of the induced, present-day, geomagnetic field (B) (B = 54000.10^{-9} T or H = 42.97 A/m). Aligning the induced magnetisation and the remanence magnetisation corresponds to adding their respective vectors. This simplification tends to give maximum magnetisation values and we consider the direction of the remanent field to be the same as for the induced field. The relative importance of remanent magnetisation (Mr) vs induced magnetisation (Mi) is expressed by the Koenigsberger ratio (Q-ratio).

$$Koenigsberger\_ratio = Q = \frac{|Mr|}{|Mi|} = \frac{Mr}{\chi H} = \frac{remanence}{\chi * 42.97}$$

With χ = susceptibility.

In order to compute the Q-ratio, both magnetic susceptibility and remanence are considered for each unit. The Q-ratio is computed for each block and geologically interpreted with respect to published values. From the values published by Olesen et al. (1990), a mean remanence of 0.20 A/m for the older Archaean to Palaeoproterozoic rocks and mafic complexes and a remanence value of 0.01 A/m for the Caledonian rocks have been selected, tested and adjusted.

The Curie temperature for magnetite is 580˚C, and therefore we limit the extension of potential magnetic sources to the older Precambrian basement and lower crustal blocks. Sedimentary rocks and rocks below the Moho are assumed to be non-magnetic.

The profiles are compared and correlated with the potential field data (Fig. 2.4) in order to map regional basement units. Before making the interpretation we divided the units into blocks or groups with compatible magnetic properties. The geological interpretation is based on three petrophysical properties: density, magnetic

susceptibility and Q-ratio.

We notice that for some of the eastern Archaean to Palaeoproterozoic crystalline basement blocks modelled with 2750 kg/m^3 and a remanence value 0.20 A/m, the computed Q-ratio value was superior to 1 (Table 2.1). We interpret these inexact estimations of the Q-ratio as an overestimation of the magnetic remanence or an underestimation of the magnetic susceptibility value used in the modelling. We interpret this as an indication of a progressive thickening of the Caledonian nappes.

2.5.2 Modelling results

The models along the IKU_A, B and C transects strike NW-SE (Fig. 2.7A, 2.7B and 2.7C). They are here presented from south to north. (See Fig. 2.2 for location).

2.5.2.1 IKU_C

The transect C is 400 km long (Fig. 2.7C). Starting in the northwest, the first basement high crossed is the Veslemøy High, the second is the outer part of the southwestern corner of the Loppa High and the third is the Finnmark Platform. The basins crossed are the Sørvestsnaget, Tromsø and Hammerfest Basins.

The profile cuts the southern extremity of the ellipsoidal gravity anomaly (Fig. 2.4). The two gravity highs at 145 km and 225 km are mostly associated with basement highs. Nevertheless, the Loppa High block and its well-constrained flanks do not permit a good fit for the western slope of the gravity anomaly. Therefore, a deep high-density body (3200 kg/m^3) is placed in the lower crust (2950 kg/m^3). The northwestern blocks encompass the crust in the vicinity of the margin and the Veslemøy High. They are modelled with a density of 2800 kg/m^3, decreasing to 2790 kg/m^3 towards the Tromsø Basin, and their susceptibility is zero. The three neighbouring blocks constitute the Tromsø Basin basement, the Loppa High and the Hammerfest Basin basement; they are all modelled with an average crustal density of 2750 kg/m^3. The magnetic susceptibility of the basement to the Tromsø Basin is fixed at 0.011 (SI) and those of the Loppa High and the Hammerfest Basin decrease from 0.035 (SI) to 0.001 (SI) towards the southeast. The block of the Finnmark Platform is

modelled with the average crustal density of 2750 kg/m^3 and as its magnetic modelling necessitated the use of the low remanence value 0.01 A/m, its susceptibility is then fixed at 0.003 (SI). To obtain the best fit for the magnetic curve and model the magnetic high at the edge of the Finnmark Platform, a conic body (density = 2750 kg/m^3, magnetic susceptibility = 0.003) is added.
For the non-magnetic blocks the computed Q-ratio is 0. For the blocks modelled with a magnetic remanence of 0.2 A/m, the Q-ratios are 0.41 (normal), 0.13 (very low) and 3.66 (very high). For the block modelled with a remanence value of 0.01, the Q-ratio is 0.07 (very low) and for the conic body modelled with 0.20 A/m, the Q-ratio is 1.47 (high).

2.5.2.2 IKU_B

The B transect is 500 km long (Fig. 2.7B). The model starts in the northwest at the vicinity of the margin, crosses the Vestbakken Volcanic Province, then the Bjørnøyrenna Basin, the Loppa High, the northern part of the Hammerfest Basin and ends on the Finnmark Platform. The profile cuts the middle of the ellipsoidal gravity high at the western edge of the Loppa High. As in the case of IKU_C, it is necessary to create a high-density body (3200 kg/m^3) in the lower crust to fit the western slope of the gravity anomaly related to the Loppa High. Ritzmann and Faleide (2007) proposed a density model along IKU_B where they put a lower crustal body with a flat top of 2980 kg/m^3 to 3050 kg/m^3 density in a lower crust of 2930 kg/m^3 and an upper crust of 2770 kg/m^3. The density contrast was insufficient to fit the computed gravity anomaly to the measured anomaly. The shape and the density of the body proposed in our model is sufficient to produce a gravity effect similar to the measured gravity anomaly, and both its existence and shape are constrained by the high-reflectivity underneath the Loppa High (Ritzmann and Faleide, 2007).

In order to control the edge effect due to the direct contact with the oceanic crust, we modelled a block of basalt (density = 3000 kg/m^3) as part of the oceanic crust. The adjacent block is part of the volcanic province; its density is high (2800 kg/m^3) and its magnetic susceptibility is 0.007 (SI). The rest of the upper crustal blocks are modelled with the average crustal density 2750 kg/m^3. A small rectangular body with a density 3000 kg/m^3 is added to model a little bulge visible along the gravity curve.

At its location, horizontal high reflectors were reported by Ritzmann and Faleide (2007). The modelled magnetic susceptibilities increase from 0.017 (SI) to 0.052 (SI) towards the western flank of the Loppa High. The blocks contributing to making the highest part of the Loppa High (around 190-230 km) are modelled with a susceptibilites of 0.033 (SI) and 0.044 (SI). The block centred on kilometre 280 and responsible for the two adjoining magnetic anomalies (around 380 nT) is modelled with a magnetic susceptibility of 0.085. The dramatic decrease of the magnetic curve requires the use of a low remanence value of 0.01 A/m. The blocks are then modelled using a magnetic susceptibility of 0.035.

For the block close to the margin, the Q-ratio is 0.67. Modelled with a magnetic remanence of 0.20 A/m, the blocks at the western margin of the Bjørnøya Basin present a Q-ratio of around 0.25 and the ones to the east of the Bjørnøya Basin a Q-ratio of around 0.15. In the extreme east, the block modelled with a magnetic remanence of 0.01 A/m presents a Q-ratio of 0.01, which bears witness to a very low magnetisation.

2.5.2.3 IKU_A

The northernmost A transect is about 550 km long (Fig. 2.7A). It starts north of the Vestbakken Volcanic Province, crosses the thick crust of the Stappen High with the Leirdjupet Fault Complex to the south, the Fingerdjupet and the Maud Basins and terminates at the Hoop Fault Complex. Starting with a maximum gravity high of 75 mGal, the gravity anomaly undulates along the profile, locally without correlating to the top basement topography. The strong undulation (from –150 to 265 nT) of the magnetic anomaly in the northwestern gradually becomes smoother, between –35 and 135 nT, along most of the profile.

Several bodies are modelled within the lower crust. Similar to IKU_C and IKU_B, a deep, high-density body of 3200 kg/m^3 is created in the lower crust (x = 225 km, z = 30 km). Contrary to profiles IKU_C and B, no high reflectivity is observed at the place of the high-density body, but instead one can notice the absence of reflectivity within a reflective basement and lower crust. Four other high-density bodies are modelled. Another 3200 kg/m^3 body in the lower crust is necessary to fit the curve at the

eastern edge of the Nordkapp Basin; the others are three intrusions of 3000 kg/m^3 density. The easternmost intrusion (density = 3000 kg/m^3 and apparent magnetic susceptibility = 0.036) is necessary to model the gravity high and associated focused magnetic high at the Norsel High. The remaining two intrusions placed at around 15 km depth in the crust at 305 km and 365 km (density = 3000 kg/m^3 and respective magnetic susceptibility = 0.047 and 0.009) are necessary to model the gravity undulation in the Maud Basin region and the correlated, focused, magnetic highs.
The basement blocks from 0 to 100 km are modelled with a decreasing density from 2990 to 2750 kg/m^3. From there on, all the blocks are modelled with the average crustal density of 2750 kg/m^3. The rather low magnetic susceptibility (0.007, 0.017) of the first blocks is fixed at 0 for the blocks to the east of the Stappen High. From 100 km to 350 km, the blocks have a susceptibility of 0.020 ± 0.005. The block from 350 km to the end of the profile is modelled with the low magnetic remanence value 0.01 A/m and a magnetic susceptibility of 0.006.

For the block closest to the margin, the Q-ratio computation gives a value of 0.60. The adjacent block presents a Q-ratio of 0.27, and the next two blocks are non-magnetic (Q-ratio is 0). The block to the west of the Stappen High shows a Q-ratio of 0.90. The blocks from 100 to 280 km present similar Q-ratios of 0.20 ± 0.05. The first intruded block has a Q-ratio of 0.25 and the two intrusions, respectively, 0.10 (at 305 km) and 0.39 (at 365 km). The last block is modelled with a magnetic remanence of 0.01, its Q-ratio is 0.04 and the last intrusion has a Q-ratio of 0.15.

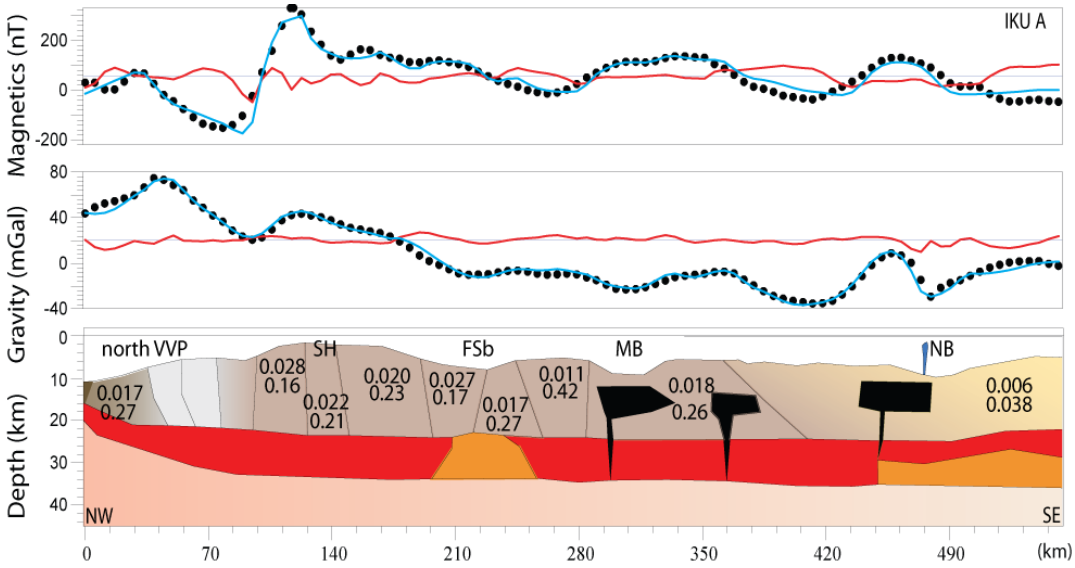
IKU A
Magnetics (nT)
Gravity (mGal)
Depth (km)
north VVP
SH
FSb
MB
NB
0.017
0.27
0.028
0.16
0.022
0.21
0.020
0.23
0.027
0.17
0.017
0.27
0.011
0.42
0.018
0.26
0.006
0.038
NW
SE
0
70
140
210
280
350
420
490
(km)

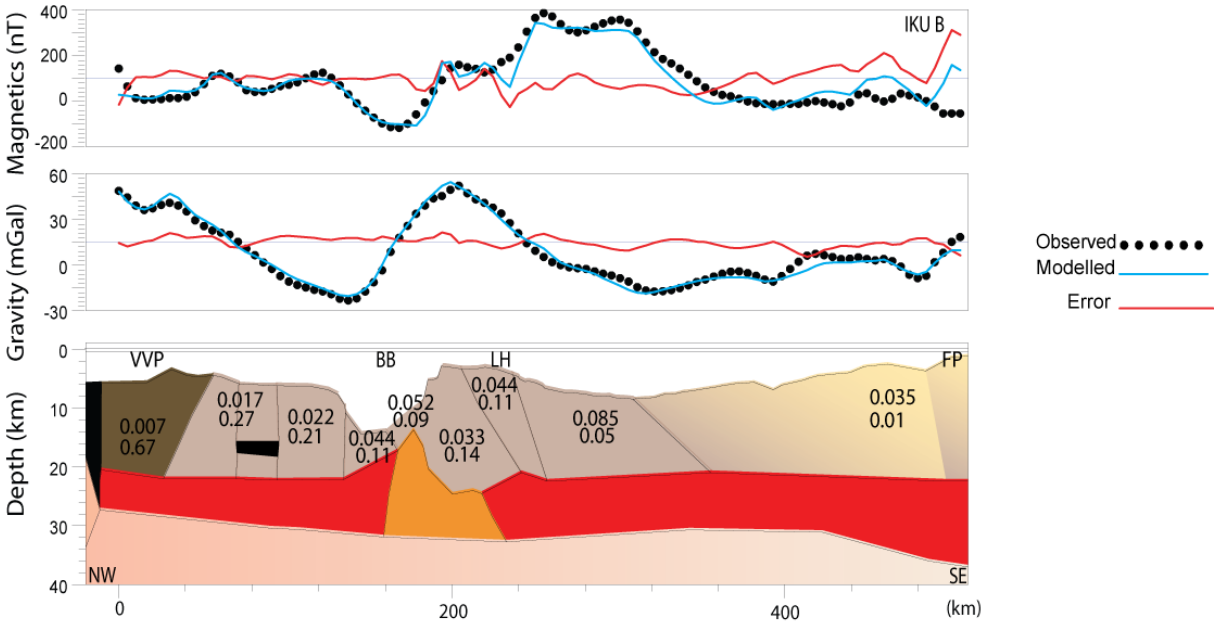
IKU B
Magnetics (nT)
Gravity (mGal)
Depth (km)
VVP
BB
LH
FP
0.007
0.67
0.017
0.27
0.022
0.21
0.044
0.11
0.052
0.09
0.033
0.14
0.044
0.11
0.085
0.05
0.035
0.01
NW
SE
0
200
400
(km)
Observed
Modelled
Error

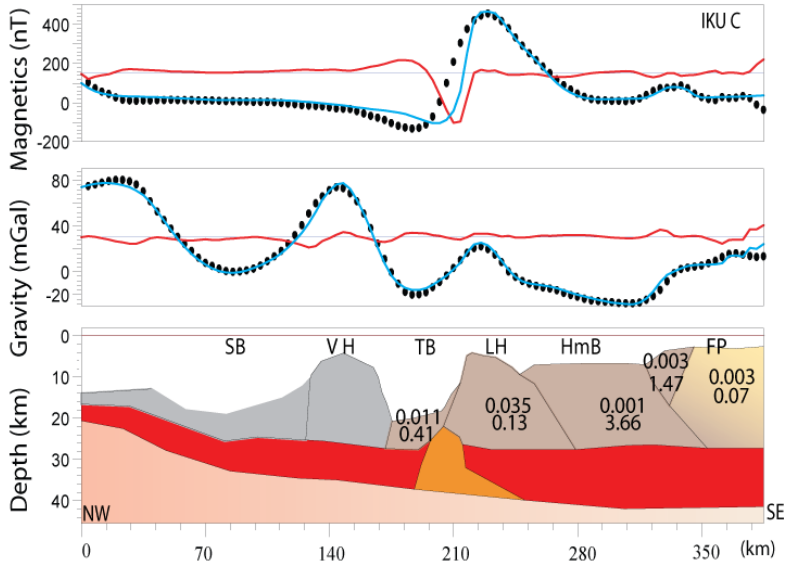
IKU C
Magnetics (nT)
Gravity (mGal)
Depth (km)
SB
V H
TB
LH
HmB
FP
0.011
0.41
0.035
0.13
0.001
3.66
0.003
1.47
0.003
0.07
NW
SE
0
70
140
210
280
350
(km)

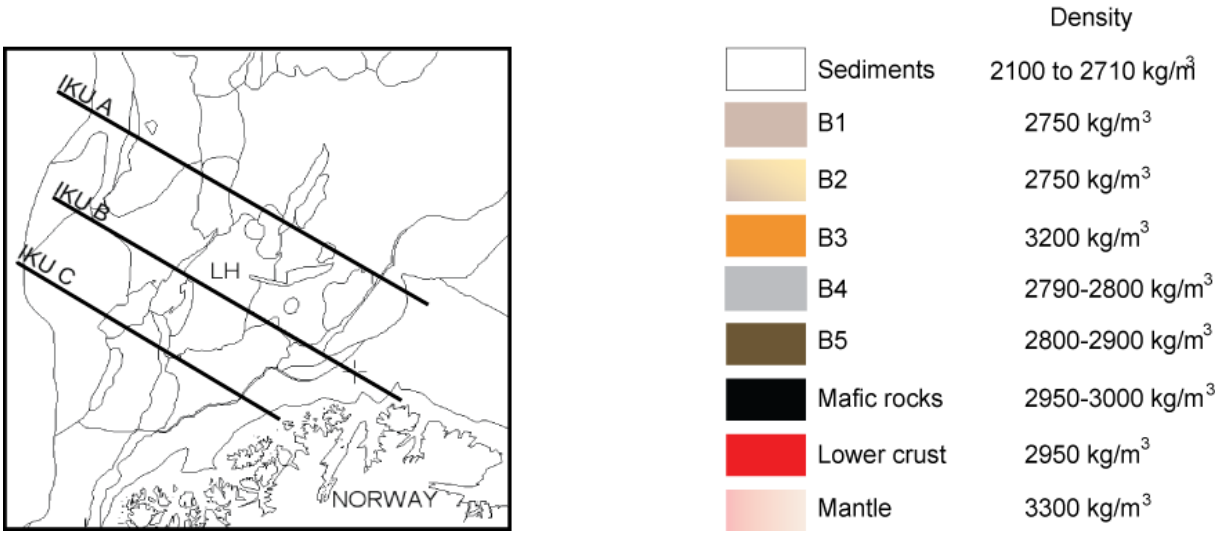

Figure 2.7: Integrated density and magnetic modelling along IKU_A, IKU_B and IKU_C

The crustal structure has been determined by density modelling, and magnetic modelling allows distinguishing blocks of contrasted magnetic properties. The blocks of compatible properties (density, magnetic susceptibility and Q-ratio) are then regrouped under a common basement label (B1, B2, B3, B4, B5, MI, PW). The values on the block are the magnetic susceptibility (top value) and the Q-ratio (bottom value). The density and magnetic properties are constant within a body. Within the GMSYS software, the error between observed and modelled data is represented by a red line respect to a horizontal black line corresponding to the zero error.

2.6 Basement unit map (Fig. 2.8) – southwestern Barents Sea

Five different basement types are distinguished combining information gained from the models and from the magnetic properties measured on rock samples from many part of Troms and Finnmark. The abundance of Archaean to Palaeoproterozoic and Caledonian rocks is determined by the integrated interpretation of potential fields. Mafic intrusions (MI) have also been interpreted.

The B1 basement unit is interpreted Archaean to Palaeoproterozoic basement. The first southernmost field is the Fennoscandian Shield cropping out in northern Norway. Another area of B1 basement is an onshore-offshore strip starting in the Lofoten

Islands, including the outer part of the Troms, and extends towards the northeast. Recently, an isotopic age of 2.8 Ga has been determined on a sample of basement orthogneiss from the well 7120/12-1 (Fig. 2.2) (Davidsen, 2007). It confirms the presence of Archaean basement directly beneath the Palaeozoic sediments at the edge of the Finnmark Platform. Also relevant, in this regard, is the report that a tonalitic gneiss on the island of Vanna (Fig. 2.4), West Troms, has yielded a comparable U-Pb zircon age of 2.88 Ga (Bergh et al., 2007). Therefore, composition and age strongly suggests an onshore-offshore correlation between B1 and the Archaean rocks of Ringvassøya and Vanna in Troms County.
A third B1 block has been mapped in the Stappen High region; it includes the basement beneath the Stappen High and the northern Sørvestsnaget Basin.

The B2 basement unit is interpreted as Caledonian basement on top of Archean to Palaeoproterozoic rocks. This implies that the Caledonian nappes are sufficiently thick to reduce the signal of the underlying crystalline rocks of the Fennoscandian Shield. Onshore, the B2 unit encompasses the Caledonian nappes and underlying Archaean to Palaeoproterozoic basement. Offshore, blocks with a Caledonian signature are modelled at the southeastern ends of profiles IKU_A, B and C.
The B3 unit consists of a high-density body recognised in the deep lower crust along profiles IKU_A, B and C. This body is interpreted as a metamorphic core-complex. Its density is modelled between 3100 and 3200 kg/m^3 and it may be composed of a mixture of high-grade metamorphic rocks and/or mafic lower crust. This high-density body is positioned directly above the Bjørnøyrenna Fault Complex and the Ringvassøy-Loppa Fault Complex. We interpret the deep and curved reflectors (Ritzmann and Faleide, 2007) observed to the east of the Ringvassøy-Loppa and Bjørnøyrenna Fault Complexes as evidence of the emplacement of a core-complex with some modifications of the mineralogy. The profile B crosscuts the N-S trending gravity high related to the high-density body. Along IKU_B, the high density is interpreted to be linked to the Bjørnøyrenna Fault Complex. We consider that the emplacement of this deep crustal body along aligned fault complexes bordering deep basins (here the Tromsø and the Bjørnøya Basins) is associated with the late post-orogenic Scandian collapse and crustal exhumation controlled by large crustal scale detachment. Several studies have reported the development of core-complexes during late to post-orogenic collapse (Burg et al., 2006; Vanderhaeghe, 1999). It is

also possible that a segment of oceanic crust from the former Iapetus Ocean may constitute a part of the lower crust. This interpretation is an alternative to the interpreted Caledonian suture inferred by Ritzmann and Faleide (2007) at that location.

Units B4 and B5 are distinguished along the shelf margin. In the southwest, B4 extends from the oceanic crust to the high-density lower crust of unit B3. The lack of correlation between the gravity high and magnetic high for the basement highs of Veslemøy High and Senja Ridge leads us to consider that the gravity high could have a deeper origin (i.e. crustal underplating, serpentinisation, intrusion of inversed polarised magmatic material), but the poor-quality seismic data do not provide any information in favour of this hypothesis.

B5 encompasses the Vestbakken Volcanic Province and terranes immediately to the north. From the literature (Faleide et al., 1993), the Vestbakken Volcanic Province is characterised seismically by a high reflectivity level interpreted as lava flows covering older sediments. A few associated intrusions have also been reported. Out of the scale of the 3D model, these intra-sedimentary volcanic rocks are not represented and the high-density blocks B5 model all the mass.

High-density bodies that can be interpreted as two stacks of sills are modelled north of the Loppa High (IKU_A). Another high-density body is interpreted at the origin of the focused magnetic high marking the Norsel High. The magnetic highs aligned between the Finnmark Platform and the Hammerfest Basin are interpreted as windows of Precambrian rocks similar to the Alta-Kvænangen Window onshore.

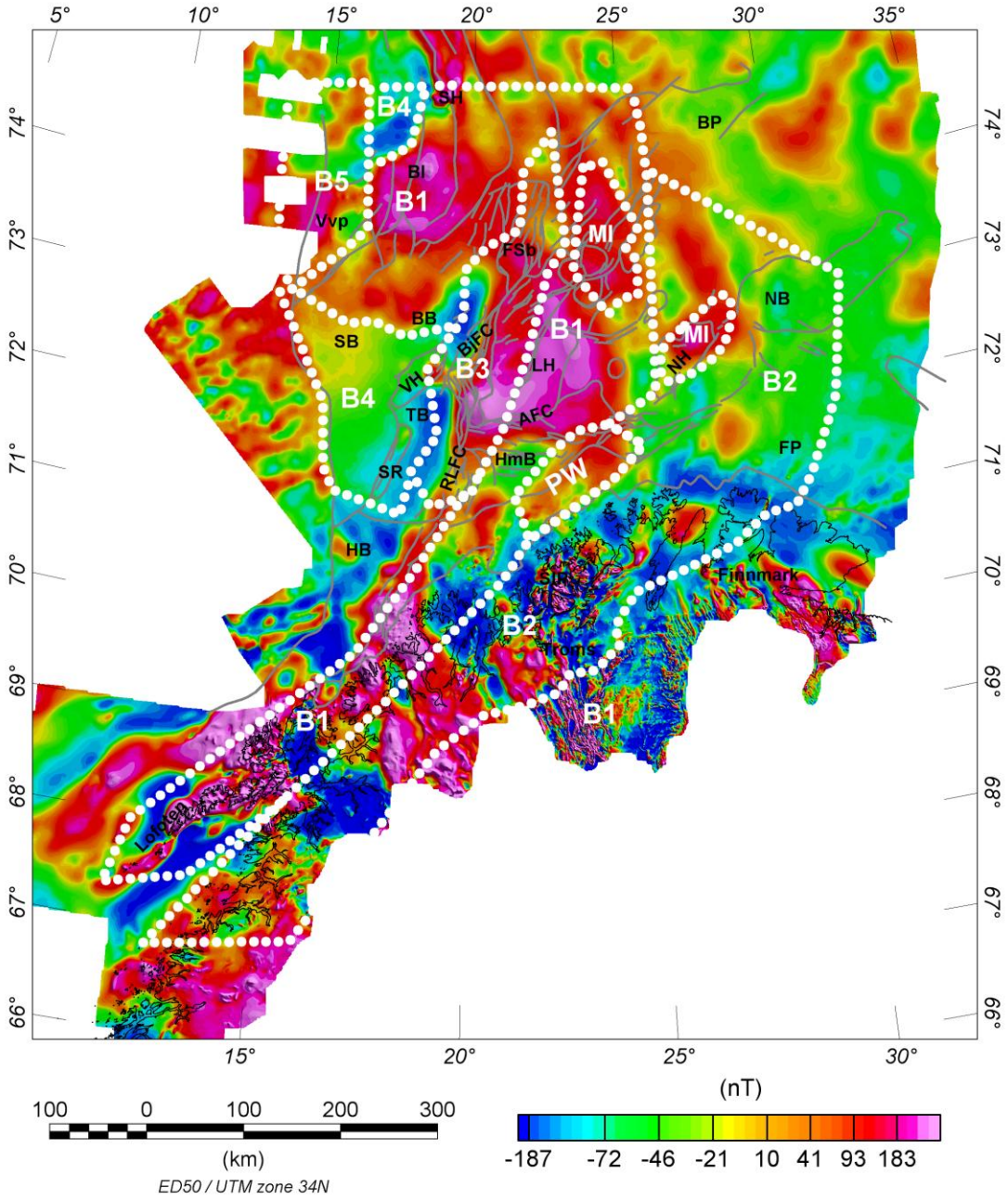

Figure 2.8: Basement units map

Overlay of the TMF (nT) reduced to the pole, the simplified structural map (solid black line) and the basement unit interpreted.

The basement units map is established by interpretation and inter-profile correlations of the 2D density and magnetic models, which allow for discrimination between basement lithologies offshore. Integrating this interpretation with the onshore-offshore correlations of the major lithologies, a map of the different basement units can then be compiled for the southwestern Barents Sea.

B1: Archaean to Paleaoproterozoic rocks

B2: Caledonian nappes over Archaean to Palaeoproterozoic rocks

B3: High-density lower crustal body

B4: Intermediate continental/oceanic crust?

Presence of rocks with a reverse magnetic remanence polarity?

B5: Basement affected by magmatic episode at the origin of the Vestbaken Volcanic Province

(Geological units offshore in black letters, see abbreviation list page 81)

2.7 Regional interpretation

The prolongation of basement lithologies offshore towards the north is still speculative but insights regarding the extension of certain structures are possible. To provide a wider regional interpretation we integrate the present study with the seismic data and the terrane correlations between Svalbard, Bjørnøya and East Greenland (Gee and Tebenkov, 2004).

2.7.1 Revised regional interpretation based on our integration (Fig. 2.9)

The basement structure south of Svalbard is poorly imaged by seismic data; however, information may be gained by integrating the seismic velocity model (Breivik et al., 2005) and crustal reflectivity (Ritzmann and Faleide, 2007) together with our interpretation of the potential field maps.

North of N 74º, Ritzmann and Faleide (2007) interpreted crustal lineaments recognised in previous studies as convergent elements continuing the Laurentia-Baltica collision zone. The lineaments S1, S2, S3 and S4 were inferred from 2D reflection and refraction seismic data (S1, Gudlaugsson et al. (1987); Breivik et al., (2003); S2 and S3, Gudlaugsson et al. (1987) and S4, Breivik et al., (2002)). As these lineaments correlate with magnetic trends, we propose a reorientation of the lineaments following these magnetic trends (Fig. 2.2 and 2.9).

Ritzmann and Faleide (2007) interpreted S1 as the offshore prolongation of the Billefjorden Fault Zone (BFZ) on Svalbard, but on our magnetic data the prolongation

of the BFZ is characterised by a double linear magnetic anomaly trending N-S to the west of the S1 lineament. These linear magnetic anomalies continue to the north of Stappen High. In the present study, the magnetic data (Fig. 2.6A and 2.6B) even support a connection between the southern extension of the BFZ and a northward prolongation of trends coming from the south. The interpretation of the BFZ as a suture by (Breivik et al., 2005; Ritzmann and Faleide, 2007) is questioned as no evidence of a suture has been reported from Svalbard. Moreover, all of Svalbard's terranes from west to east are considered to be Laurentian (Cocks and Torsvik, 2005; Fortey, 1975; Gee, 2005; Gee and Tebenkov, 2004; Torsvik and Cocks, 2005). We suggest that the BFZ and its prolongation along the Leirdjupet, Bjørnøyrenna and Ringvassøy-Loppa Fault Complexes is likely to represent a Caledonian, deep seated, weak zone (Fig. 2.9) rather than a suture.

On our magnetic grid, S1, S2 and S3 correlate with magnetic highs trending NNW-SSE. These trends can be followed towards the SSE to the Norsel High on both the total magnetic field and its tilt derivative. We interpret S1, S2 and S3 as lineaments linking to a Caledonian trend converging towards Svalbard. We propose that these lineaments can be connected one by one to of the Caledonian thrusts mapped onshore. In Fig. 2.9 we indicate preferred paths for these interpreted prolongations of Caledonian thrusts.

S4 is located at the limit of our study area and cannot be interpreted with any confidence; nevertheless, we do not interpret it as a Caledonian structure, mostly because of its convex shape. We link S4 to other convex lineaments in the magnetic domain D4 (Fig. 2.6C).

A lack of seismic data across the hypothetical prolongation of the frontal Caledonian thrusts has precluded their tentative mapping offshore. However, working with high-resolution magnetic data, Gernigon et al. (2007) have interpreted the extension of a Caledonian thrust exposed in the northwestern part of the Varanger Peninsula indicating its northward prolongation towards the Nordkapp Basin. Although, this observation is an element in favour of the idea of Caledonian structures striking northwards, the link between the interpreted northward-striking frontal thrust and its likely propagation towards Svalbard has yet to be proved.

The hypothesis of an arm of the Caledonides branching northwards in the SW Barents Sea was first proposed by Harland and Gayer (1972), Siedlecka (1975) and Ziegler (1988). More recently, Gee and Tebenkov (2004b) have advocated the possibility of a prolongation of the Svalbardian extension of the Caledonides even farther north. Their work established terrane similarities, for example, between Bjørnøya and NE Greenland, west Ny-Friesland and NE Greenland and Svalbard's Nordaustlandet and central east Greenland, and combined with our magnetic trends they support a northward prolongation of the Caledonian structures. The Stappen High appears as a key element at the junction of the proposed weakness zone and the strike-slip fault (with 5 km of offset) necessary to join the BFZ with the sinistral shear zone (Gudlaugsson et al., 1987) separating the thrust sheets from the foreland allochthon of NE Greenland.

The structure developed between Laurentia and Baltica would comprise an extension of Svalbard located at the northeastern corner of the Laurentian plate. The hypothesis of thrusts swinging towards Svalbard implies a change in the tectonic settings in the N-E direction with the limitation of the deformation through the NE and E. This impediment could be due to the existence of more competent blocks or terranes. An explanation for the uncertain tectonic settings along the offshore prolongation of the Caledonides may relate to the idea of the existence of a micro plate or cratonic block within the Iapetus subduction zone and Barents shelf (Breivik et al., 2005; Siedlecka, 1975). However, our preference is for the possible prolongation of the Baltican plate farther north into the Barents Sea. This prolongation does not involve Svalbard (Gee and Tebenkov, 2004; Torsvik and Cocks, 2005) and would extend, across the Barents Shelf, the Timanian terranes reported at the northeastern margin of Baltica (Kostyuchenko et al., 2006). Where it was affected by the Timanian orogeny, the crust would be expected to have been thicker than the rest of the Baltican terranes. The presence of a relatively more competent terrane or craton (e.g. Siedlecka, 1975) to the N and NE of Baltica could explain both the northward bending of the Caledonian thrusts and the contrast in tectonic setting between the southwestern Barents Shelf, where the basins are deep and narrow, and the northwestern Barents Shelf which is mostly made up of platforms. In other words, these Timanian terranes would have limited the

propagation of the Caledonian thrusts and the formation of weakness zones to the east. Consequently, the development of basins during rifting was limited.

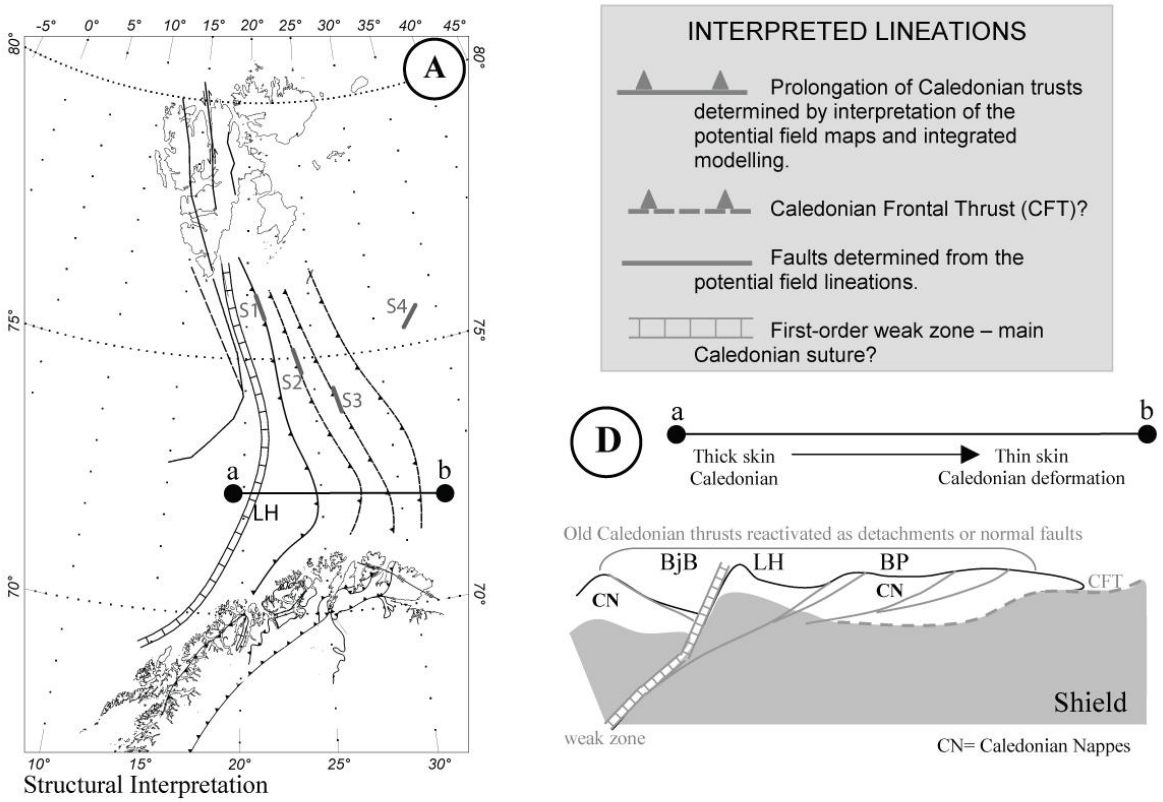

Structural Interpretation

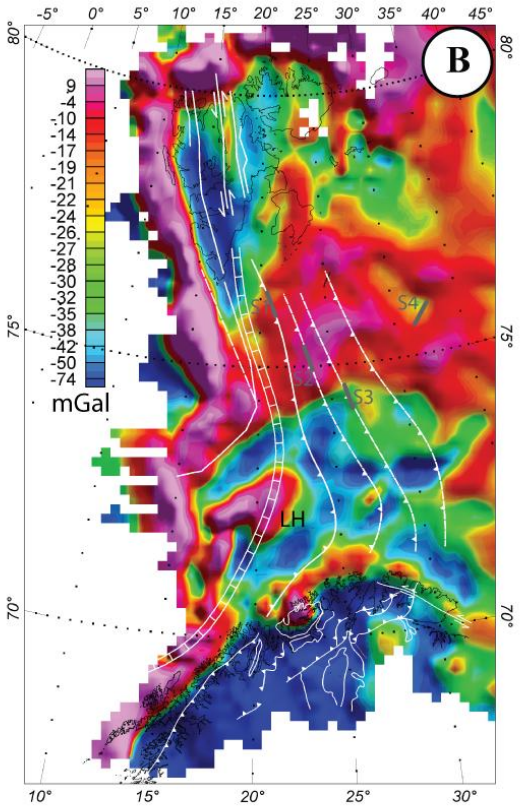

Bouguer Anomaly

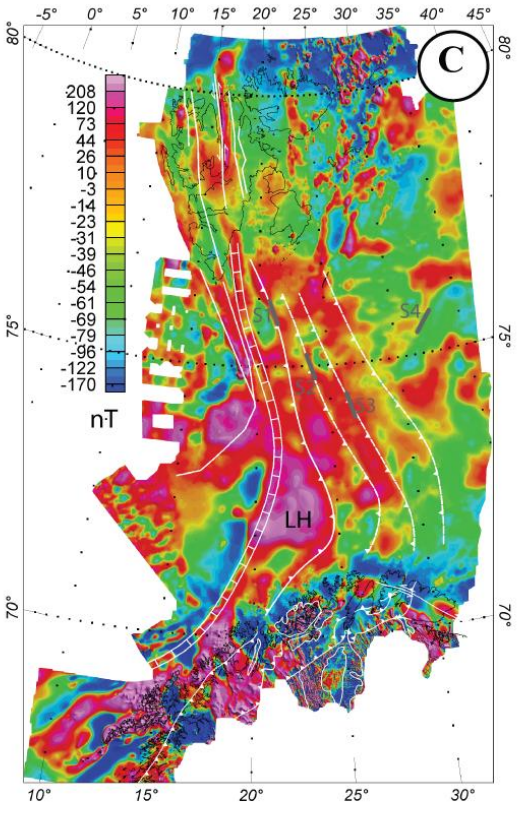

Total Magnetic Field

Figure 2.9: Structural interpretation of the western Barents Sea lineaments. The crustal lineaments S1, S2, S3 and S4 interpreted from seismic data by Gudlaugsson et al. (1987) and Breivik et al. (2002, 2003) are here reoriented based on the integration of magnetic trends.

A. Structural interpretation proposed of the offshore Caledonian structures integrating all published data into a wider regional interpretation. The figure shows the proposed prolongation of Caledonian thrusts and faults related to Billefjorden Fault Zone (Svalbard) as well as a main weak zone (Caledonian suture?).

B. Overlay of the structural map and the Bouguer anomalies (Fig 2.4A).

C. Overlay of the structural map and the total magnetic field anomalies (Fig 2.4B).

D: Schematic EW cross-section across the Bjørnøya Basin (BjB), the Loppa High (LH) and the Bjarmeland Platform (BP). The sketch illustrates the EW evolution of the Caledonian deformation mode: from thick skin in the west with fault cutting through the Shield to progressively thin skin deformation with thrusts rooted at the nappes/shield décollement.

2.8 Caledonian structures and development of the sedimentary basins in the western Barents Sea

The elbow-shaped prolongation (Fig. 2.6C (D5) and 2.9) of the Norwegian Caledonides illustrated here challenges the interpretation of two Caledonian branches proposed by Breivik et al., (2002); Gudlaugsson et al., (1987); Harland and Gayer, (1972); Siedlecka, (1975). When they adopted this theory they took the geometry of the basins as evidence for the existence of these two Caledonian arms. Recent work (Ritzmann and Faleide, 2007) has demonstrated the inhomogeneity of the basement in the southwestern Barents Sea and the existence of a single, large, fan-shaped collision zone diverging to the northeast. Ritzmann and Faleide (2007) suggested that the geometry of the basins was inherited from subjacent Caledonian structures, and their tectonic model located the deep basins (Bjørnøya Basin, Tromsø Basin, Sørvestsnaget Basin) on a continental fragment of Laurentian affinity with a specific rheology.

The fan-shaped collision zone interpreted by Ritzmann and Faleide (2007) in the southwestern Barents Sea is in broad agreement with the elbow-shaped prolongation of the Caledonides suggested in the present study. In our view, the fan-shaped collision zone is the southern part of the elbow, such that a northeastward propagation of the Caledonian thrusts would have been impeded by the presence of more resistant Timanian terranes. We attribute the deep and narrow basins west of the Loppa High to a reactivation of deep detachments inherited from thick-skinned Caledonian allochthons (Fig. 2.9A). Towards the east and northeast, the Caledonian deformation became gradually more thin-skinned with low-angle thrusts and high-angle faults until the deformation waned due to an imbalance between the strength of the deformation stresses and the resistance of the underlying basement. Such a distribution in space and depth of the Caledonian thrusts can explain the observed distribution of the sedimentary basins in the southwestern Barents Sea (Fig. 2.9A). To the west of the Loppa High, subsidence of the deep basin, recorded particularly during the Cretaceous rift phase, was facilitated along the aligned Ringvassøy-Loppa, Bjørnøyrenna and Leirdjupet Fault Complexes, a reactivation of a major high-angle Caledonian thrust. The platform domain to the east and northeast of the Loppa High remains almost non-rifted, providing an argument in favour of the absence of deep, pre-existing, weakness zones. The E-W orientation of the Hammerfest Basin and the segmented Nordkapp Basin oriented N°50 should then be related to the expected complex geometry of lineaments inherited from the Timanian and the Scandian orogenies, in addition to a set of lineaments linked to the margin of the Baltican plate characterised by the TKFZ and its correlated faults in the Timans.

In our view, the Iapetus suture is difficult to define precisely and basal or frontal thrusts are not well constrained. Based on basin geometry and distribution we argue for a limited propagation of the Caledonian thrusts and related deformation towards the northeast (Fig. 2.9). We consider there to have been a thicker and more competent crust in the eastern and northern part of the Barents Sea. We suggest that terranes of contrasting rheology were involved in this region when the Caledonian thrust sheets were emplaced formed and, consequently, we envisage a combination of sutures rather than a simple straight suture between Laurentia and Baltica.

Although we draw the path of the interpreted Caledonian thrusts based on the magnetic data trends (Fig. 2.9C), we did not use the gravity data. Therefore, some comments on the correlations between the traces of the Caledonian thrusts and the Bouguer anomalies (Fig. 2.9B) are pertinent. The overlays of the structural data on top of the Bouguer anomalies reveal that the suggested prolongation of the frontal thrust (dashed grey linein Fig. 2.9D) would separate the rifted southwestern Barents Sea Shelf (Bouguer anomaly lows) from the eastern platform (Bouguer anomaly highs). It is also interesting to see how the segmentation of the Nordkapp Basin correlates with the successive cross-cutting interpreted thrusts. Indeed, a thrust is located perpendicular to the transition between the southern and northern parts of the Nordkapp Basin. Another thrust is interpreted where the northern part of the Nordkapp Basin becomes narrower (73ºN 31ºE). This observation leads us to suggest that the inhomogeneity of the basement has played a role during the rifting and, consequently, impacted the processes that have segmented the shape of the Nordkapp Basin. We also note the closeness of the interpreted thrusts and the large Bouguer high observed north of 74ºN. There is indubitably a dramatic change from the undulating top-basement topography in the south to the rather flat, top-basement topography north of 74ºN. We interpret this change to be related to a contrast in basement rheology and/or a contrast in the stress regime through time. We interpret that this change in the deformation mode is one of the consequences of the interpreted presence of a thicker basement affected by Timanian accretion advocated earlier.

Our potential field study does not unravel the complexity of the Svalbard terrane assemblage. It is, however, compatible with the existence of an elbow-shaped Barentsian Caledonides developed between Laurentia and Baltica. This involves the extension of the Timanian terranes, a northernmost part of Baltica, farther to the northwest than they have usually been mapped. In this model, the strike-slip fault movements that contributed to the formation of Svalbard's terranes would be quite modest as the terranes would have been fairly near to the places where they are observed today with respect to northeast Greenland and Norway.

2.9 Conclusions

(1) Correlating potential fields with the onshore geology shows that Archaean to Palaeoproterozoic medium to high-grade, gneissic and mafic complexes are related to regional magnetic highs whereas Caledonian nappes clearly show lower magnetic anomalies. Corresponding petrophysical data allow a characterisation of the basement rocks by their associated density, magnetic susceptibility and Q-ratio values. The correlations of onshore potential fields and geological information confirm the northwestward prolongation of Fennoscandian, Archaean to Palaeoproterozoic lithologies (gneisses and greenstone belts) beneath the Caledonian nappes.

(2) The study confirms the offshore continuation of the Caledonian nappes and rocks of the Fennoscandian Shield with the Caledonian nappe cover getting thicker to the east of the Loppa High (B2). More locally, we interpret the presence of a Precambrian window, similar to that of Alta-Kvænangen window in western Finnmark and stacks of sills to the northeast of the Loppa High and intruding the Norsel High. The modelling confirms that crust affected by volcanism and with intra-sedimentary volcanic rocks exists along the margin (B5 and B4). To the south of the Loppa High, a low-magnetic basement (B4) requires more investigation before it can be fully interpreted.

(3) One of the most interesting features is the lower-crustal high-density (3100 to 3200 kg/m^3) body (B3) modelled along the western flank of the Loppa High. Features resembling a core-complex (B3) are associated with deep, listric, fault zones and a rather flat Moho. From its geometry, the formation of this inferred core-complex is considered with the late- to post-Caledonian (Scandian) collapse and the consequent development of the fault zones. The modelled flat Moho leads us to suggest that an isostatic re-equilibration push was also involved in the generation of the core complex.

(4) The present study interprets basement lineaments striking towards Svalbard. The hypothesis of an elbow-shaped Caledonian structure propagating northwards is

based on onshore-offshore correlations and a study of magnetic trends. The basement unit map compilation also supports this idea.

(5) The first-order structure aligning the Billefjorden Fault Zone with the Leirdjupet, Bjørnøyrenna and Ringvassøy-Loppa Fault Complexes is here interpreted as a major, deep-seated weak zone.

(6) From our tectonic model, the geometry of the basins is directly linked to the pre-existing Caledonian thrusts and therefore it reflects the deformation mode of the Caledonian orogeny in the region, changing from thick-skinned in the west to thin-skinned in the east.

(7) The correlations between Svalbard, Bjørnøya and Greenland established by other authors, together with our understanding of the geophysical characteristics of the region, suggest to us that the elbow-shaped swing of the strike of the Caledonides is a consequence of the presence of more competent terranes or blocks to the E and NE of Baltica. These terranes are suggested to be of Timanian origin. In our model, the strike-slip fault movements that led to the formation of Svalbard's terrane gathering would have been quite modest.

Acknowledgements

The study was carried out as part of the project “Basement Heat Generation and Heat Flow in the western Barents Sea – Importance for hydrocarbon systems" funded by the PETROMAKS programme of the Research Council of Norway. We thank our project leader Christophe Pascal and also StatoilHydro for providing technical support and databases. We are grateful to the reviewers, Jean Paul Callot and Oliver Ritzmann for their careful review, which profit to the former manuscript. We kindly thank David Roberts for its help correcting the English and together with Jan Reidar Skilbrei, Odleiv Olesen and David Gee for the time spent in fruitful discussions.

References

Alsgaard, P., 1993. Eastern Barents Sea late Palaeozoic setting and potential source rocks. In: T.O. Vorren et al. (Editors), Arctic Geology and Petroleum Potential. Norwegian Petroleum Society, pp. 405-418.

Andersen, T.B., 1998. Extensional tectonics in the caledonides of southern Norway, an overview. Tectonophysics, 285(3-4): 333-351.

Bergh, S., Kullerud, K., Corfu, F., Armitage, P.E.B., Davidsen, B., Johansen, H.W., Pettersen, T. and Knudsen, S., 2007. Lowgrade sedimentary rocks on Vanna, North Norway: a new occurrence of a Palaeoproterozoic (2.4-2.2 Ga) cover succession in northern Fennoscandia. Norwegian Journal of Geology(87): 301-318.

Breivik, A.J., Faleide, J.I. and Gudlaugsson, S.T., 1998. Southwestern Barents Sea margin: late Mesozoic sedimentary basins and crustal extension. Tectonophysics, 293(1-2): 21-44.

Breivik, A.J., Gudlaugsson, S.T. and Faleide, J.I., 1995. Ottar-Basin, Sw Barents-Sea - a Major Upper Paleozoic Rift Basin Containing Large Volumes of Deeply Buried Salt. Basin Research, 7(4): 299-312.

Breivik, A.J., Mjelde, R., Grogan, P., Shimamura, H., Murai, Y. and Nishimura, Y., 2003. Crustal structure and transform margin development south of Svalbard based on ocean bottom seismometer data. Tectonophysics, 369(1-2): 37-70.

Breivik, A.J., Mjelde, R., Grogan, P., Shimamura, H., Murai, Y. and Nishimura, Y., 2005. Caledonide development offshore-onshore Svalbard based on ocean bottom seismometer, conventional seismic, and potential field data. Tectonophysics, 401(1-2): 79-117.

Breivik, A.J., Mjelde, R., Grogan, P., Shimamura, H., Murai, Y., Nishimura, Y. and Kuwano, A., 2002. A possible Caledonide arm through the Barents Sea imaged by OBS data. Tectonophysics, 355(1-4): 67-97.

Bugge, T., Mangerud, G., Elvebakk, G., Mørk, A., Nilsson, I., Fanavoll, S. and Vigran, J.O., 1995. The Upper Palaeozoic succession on the Finnmark Platform, Barents Sea. Norsk Geologisk Tidsskrift(75): 3-30.

Burg, J.-P., Kaus, B.J.P. and Podladchikov, Y.Y., 2006. Domes structures in collision orogens: Mechanical investigation of the gravity/compression interplay. In: D.L. Whitney, C. Teyssier and C.S. Siddoway (Editors), Gneiss domes in orogeny. Boulder, Colorado, Geological Society of America.

Chorowicz, J., 1992. Gravity-Induced Detachment of Devonian Basin Sediments in Northern Svalbard. Norsk Geologisk Tidsskrift, 72(1): 21-25.

Cocks, L.R.M. and Torsvik, T.H., 2005. Baltica from the late Precambrian to mid-Palaeozoic times: The gain and loss of a terrane's identity. Earth-Science Reviews, 72(1-2): 39-66.

Corfu, F., Torsvik, T.H., Andersen, T.B., Ashwal, L.D., Ramsay, D.M. and Roberts, R.J., 2006. Early Silurian mafic-ultramafic and granitic plutonism in contemporaneous flysch, Magerøy, northern Norway: U-Pb ages and regional significance. Journal of the Geological Society, 163: 291-301.

Davidsen, B., 2007. Status report geochronology – project 312700 Basement characterization Barents Sea and Svalbard (HEATBAR); personal communication. Norges Geologiske Undersøkelse Report.

Dimakis, P., Braathen, B.I., Faleide, J.I., Elverhoi, A. and Gudlaugsson, S.T., 1998. Cenozoic erosion and the preglacial uplift of the Svalbard-Barents Sea region Tectonophysics, 300: 311-327.

Doré, A.G., 1991. The Structural Foundation and Evolution of Mesozoic Seaways between Europe and the Arctic. Palaeogeography Palaeoclimatology Palaeoecology(87): 441-492.
Faleide, J.I., Vågnes, E. and Gudlaugsson, S.T., 1993. Late Mesozoic-Cenozoic Evolution of the South-Western Barents Sea in a Regional Rift Shear Tectonic Setting. Marine and Petroleum Geology, 10(3): 186-214.
Filatova, N.I. and Khain, V.E., 2007. Tectonics of the eastern Arctic region. Geotectonics, 41(3): 171-194.
Fortey, R.A., 1975. Early Ordovician Trilobites of Spitzbergen III. Norsk Polarinstitutt Skrifter, 171: 1-263.
Fossen, H., 2000. Extensional tectonics in the Caledonides: synorogenic or postorogenic? Tectonics (19): 213-224.
Gabrielsen, R.H., 1984. Long-lived fault zones and their influence on the tectonic development of the southwestern Barents Sea. Journal of the Geological Society, 141: 651-662.
Gabrielsen, R.H., Færseth, R.B., Jensen, L.N., Kalheim, J.E. and Riis, F., 1990. Structural elements of the Norwegian continental shelf. Part I: The Barents Sea Region. Norwegian Petroleum Directorate Bulletin(6).
Gabrielsen, R.H., Grunnaleite, I. and Rasmussen, E., 1997. Cretaceous and Tertiary inversion in the Bjornoyrenna Fault Complex, south-western Barents Sea. Marine and Petroleum Geology, 14(2): 165-178.
Gee, D.G., 2005. Scandinavian Caledonides (with Greenland). In: R.C. Selley, L.R.M. Cocks and I.R. Plimer (Editors). Encyclopedia of Geology, pp. 64-74.
Gee, D.G., Bogolepova, O.K. and Lorenz, H., 2006. The Timanide, Caledonide and Uralide orogens in the Eurasian high Arctic, and relationships to the palaeo-continents Laurentia, Baltica and Siberia. In: Gee and Stephenson (Editors), European Lithosphere Dynamics. Geological Society of London, pp. 507-521.
Gee, D.G. and Tebenkov, A., 2004. Svalbard: a fragment of the Laurentian margin. In: D.G. Gee and V.L. Pease (Editors), The Neoproterozoic Timanide Orogen of eastern Baltica: introduction. Geological Society London, pp. 191-206.
Gernigon, L., Marello, L., Moogaard, J.O., Werner, S.C. and Skilbrei, J.R., 2007. Barents Sea Aeromagnetic Survey BAS-06-Acquisition-processing report and preliminary interpretation. Geological Survey of Norway, 035.
Grogan, P., Nyberg, K., Fotland, B., Myklebust, R., Dahlgren, S. and Riis, F., 1998. Cretaceous magmatism south and east of Svalbard: evidence from seismic reflection and magmatic data. Polar Research, 68: 11-13.
Grogan, P., Nyberg, K., Fotland, B., Myklebust, R., Dahlgren, S. and Riis, F., 2000. Cretaceous magmatism south and east of Svalbard: evidence from seismic reflection and magmatic data. Polar Research, 68: 11-13.
Gudlaugsson, S.T. and Faleide, J.I., 1994. The continental margin between Spitsbergen and Bjørnøya. In: O. Eiken (Editor), Seismic Atlas of Western Svalbard, Medd. Norwegian Polarinstitut, pp. 11-13.
Gudlaugsson, S.T., Faleide, J.I., Fanavoll, S. and Johansen, B., 1987. Deep Seismic-Reflection Profiles across the Western Barents Sea. Geophysical Journal of the Royal Astronomical Society, 89(1): 273-278.
Gudlaugsson, S.T., Faleide, J.I., Johansen, S.E. and Breivik, A.J., 1998. Late Palaeozoic structural development of the South-western Barents Sea. Marine and Petroleum Geology, 15(1): 73-102.
Harland, W.B. and Gayer, R.A., 1972. The Arctic Caledonides and earlier Oceans. Geological Magazine, 109(4): 289-314.

Higgins, A.K., Elvevold, S., Escher, J.C., Frederiksen, K.S., Gilotti, J.A., Henriksen, N., Jepsen, H.F., Jones, K.A., Kalsbeek, F., Kinny, P.D., Leslie, A.G., Smith, M.P., Thrane, K. and Watt, G.R., 2004. The foreland-propagating thrust architecture of the East Greenland Caledonides 72 degrees-75 degrees N. Journal of the Geological Society, 161: 1009-1026.

Ivanova, N.M., 2001. The geological structure and petroleum potential of the Kola-Kanin Monocline, Russian Barents Sea. Petroleum Geoscience, 7(4): 343-350.

Johansen, S.E., Henningsen, T., Rundhovde, E., Sæther, B.M., Fichler, C. and Rueslatten, H.G., 1994. Continuation of the Caledonides north of Norway - Seismic reflectors within the basement beneath the southern Barents Sea. Marine and Petroleum Geology, 11(2): 190-201.

Kostyuchenko, S.L., Sapozhnikov, R., Egorkin, A., Gee, D.G., Berzin, R. and Solodilov, L.N., 2006. Crustal structure and tectonic model of notheastern Baltica, based on deep seismic and potential field data. In: D.G. Gee and R.A. Stephenson (Editors), European Lithosphere Dynamics. Geological Society, London, Memoirs, 32, pp. 521-539.

Larssen, G.B., Elvebakk, G., Henriksen, L.B., Kristensen, S.-E., Nilsson, I., Samuelsberg, T.J., Svåna, T.A., Stemmerik, L. and Worsley, D., 2005. Upper Palaeozoic lithostratigraphy of the southern part of the Norwegian Barents Sea. Norges Geologiske Undersøkelse Bulletin, 444.

Lind, E., 1987. The Nordkapp Basin, a Major Salt Feature in the Sw Barents Sea. Norsk Geologisk Tidsskrift, 67(4): 435-435.

Lippard, S.J. and Prestvik, T., 1997. Carboniferous dolerite dykes on Magerøya: new age determination and tectonic significance. Norsk Geologisk Tidsskrift (77): 159-163.

Lippard, S.J. and Roberts, D., 1987. Fault systems in Caledonian Finnmark and the southern Barents Sea. Norsk Geologisk Tidsskrift(410): 55-64.

Lundin, E. and Doré, A.G., 2002. Mid-Cenozoic post-breakup deformation in the 'passive' margins bordering the Norwegian-Greenland Sea. Marine and Petroleum Geology, 19(1): 79-93.

Maher, H.D., 2001. Manifestations of the Cretaceous High Arctic Large Igneous Province in Svalbard. Journal of Geology, 109(1): 91-104.

Maher, H.D., Bergh, S., Braathen, A., Manby, G. and Lyberis, N., 2001. Discussion on pre-ocean opening compression of the Northwestern Atlantic margin: evidence from eastern Greenland - Journal, Vol. 157, 2000, 707-710. Journal of the Geological Society, 158: 728-730.

Manby, G. and Lyberis, N., 1992. Tectonic Evolution of the Evonian Basin of Northern Svalbard. Norsk Geologisk Tidsskrift, 72(1): 7-19.

Mjelde, R., Breivik, A.J., Elstad, H., Ryseth, A.E., Skilbrei, J.R., Opsal, J.G., Shimamura, H., Murai, Y. and Nishimura, Y., 2002. Geological development of the Sorvestsnaget Basin, SW Barents Sea, from ocean bottom seismic, surface seismic and gravity data. Norwegian Journal of Geology, 82(3): 183-202.

Nyland, B., Jensen, L.N., Skagen, J.I., Skarpnes, O. and Vorren, T., 1992. Tertiary uplift and erosion in the Barents Sea: magnitude, timing and consequences. In: Larsen, R.M., H. Brekke, B.T. Larsen and E. Talleraas (Editors), Structural and tectonic modelling and its application to petroleum geology. Norsk Petroleum Forening Special Publication - Elsevier, Amsterdam, pp. 153-162.

Olesen, O., Gernigon, L., Ebbing, J., Mogaard, J.O., Pascal, C. and Wienecke, S., 2006. Interpretation of aeromagnetic data along the Jan Mayen Fracture Zone, JAS-05. Geological Survey of Noway (NGU) Report no.2006.018 (confidential to 17.02.2011): 162.

Olesen, O., Roberts, D., Henkel, H., Lile, B.L. and Torsvik, T.H., 1990. Aeromagnetic and gravimetric interpretation of regional structural features in the Caledonides of West Finnmark and North Troms, northern Norway. Norges geologiske undersøkelse Bulletin(419): 1-24.

Olovyanishnikov, V.G., Roberts, D. and Siedlecka, A., 2000. Tectonics and sedimentation of the Meso- to Neoproterozoic Timan-Varanger Belt along the Northeastern Margin of Baltica. Polar Research, 68: 267-274.

Piepjohn, K., von Gosen, W., Estrada, S. and Tessensohn, F., 2007. Deciphering superimposed Ellesmerian and Eurekan deformation, Piper Pass area, northern Ellesmere Island (Nunavut). Canadian Journal of Earth Sciences, 44(10): 1439-1452.

Ramsay, D.M., Sturt, B.A., Zwaan, K.B. and Roberts, D., 1985. Caledonides of northern Norway. The Caledonian Orogen - Scandinavian and related areas, Part 1, edited by Gee, D.G. and B.A. Sturt (John Wiley & Sons, Chichester): 163-184.

Rice, A.H.N., Gayer, R.A., Robinson, D. and Bevins, R.E., 1989. Strike-Slip Restoration of the Barents Sea Caledonides Terrane, Finnmark, North Norway. Tectonics, 8(2): 247-264.

Ritzmann, O. and Faleide, J.I., 2007. Caledonian basement of the western Barents Sea. Tectonics, 26(5).

Ritzmann, O., Maercklin, N., Faleide, J.I., Bungum, H., Mooney, W.D. and Detweiler, S.T., 2007. A three-dimensional geophysical model of the crust in the Barents Sea region: Model construction and basement characterization. Geophysical Journal International, 170(1): 417-435.

Roberts, D., 1983. Devonian tectonic deformation in the Norwegian Caledonides and its regional perspectives. Norges geologiske undersøkelse Bulletin(380): 85-96.

Roberts, D., 2003. The Scandinavian Caledonides: event chronology, palaeogeographic settings and likely modern analogues. Tectonophysics(365): 283-299.

Roberts, D. and Gale, G.H., 1978. The Caledonian-Appalachian Iapetus Ocean. In: D. Tarling (Editor), The evolution of the Earth's crust, pp. 255-341.

Roberts, D. and Olovyanishnikov, V., 2004. Structural and tectonic development of the Timanide orogen. Geological Society London Memoirs, 30: 47-57.

Roberts, D. and Siedlecka, A., 2002. Timanian orogenic deformation along the northeastern margin of Baltica, Northwest Russia and Northeast Norway, and Avalonian-Cadomian connections. Tectonophysics, 352(1-2): 169-184.

Roberts, R.J., Corfu, F., Torsvik, T.H., Ashwal, L.D. and Ramsay, D.M., 2006. Short-lived mafic magmatism at 560-570 Ma in the northern Norwegian Caledonides: U-Pb zircon ages from the Seiland Igneous Province. Geological Magazine, 143(6): 887-903.

Robins, B., 1998. The mode of emplacement of the Honningsvåg Intrusive Suite, Magerøya, northern Norway. Geological Magazine, 135: 231-244.

Sanner, S., 1995. Et seismisk hastighetsstudium i Barentshavet. . Cand. Scient. thesis (in Norwegian), Department of Geology, University of Oslo, Oslo, Norway.

Scott, R.A. and Turton, M.A.K., 2001. Mesozoic tectonic events in the North Atlantic and Arctic: stratigraphic response in an adjacent rift-flank basin (Sverdrup Basin, Arctic Canada). Polar Research, 69: 73-83.

Siedlecka, A., 1975. Late Precambrian Stratigraphy and Structure of the North-Eastern Margin of the Fennoscandian Shield (East Finnmark - Timan Region). Norges geologiske undersøkelse Bulletin, 316(29): 313-348.

Siedlecka, A. and Roberts, D., 1996. Finnmark Fylke, Berggrunnsgeologi M 1:500 000. Norges geologiske undersøkelse,Trondheim.

Skilbrei, J.R., 1991. Interpretation of Depth to the Magnetic Basement in the Northern Barents Sea (South of Svalbard). Tectonophysics, 200(1-3): 127-141.

Skilbrei, J.R., Kihle, O., Gellein, J., Solheim, D. and Nyland, B., 2000. Gravity anomaly map, Norway and adjacent ocean areas. M 1:3 000 000. Geological Survey of Norway.

Skilbrei, J.R., Skyseth, T. and Olesen, O., 1991. Petrophysical Data and Opaque Mineralogy of High-Grade and Retrogressed Lithologies - Implications for the Interpretation of Aeromagnetic Anomalies in Northern Vestranden, Central Norway. Tectonophysics, 192(1-2): 21-31.

Sturt, B.A., Pringle, I.R. and Roberts, D., 1975. Caledonian nappe sequence of Finnmark, northern Norway, and the timing of orogenic deformation and metamorphism. Bull. Geol. Society of America, 86: 710-718.

Torsvik, T.H. and Cocks, L.R.M., 2005. Norway in space and time: A Centennial cavalcade. Norwegian Journal of Geology, 85(1-2): 73-86.

Torsvik, T.H., Smethurst, M.A., Meert, J.G., Van der Voo, R., McKerrow, W.S., Brasier, M.D., Sturt, B.A. and Walderhaug, H.J., 1996. Continental break-up and collision in the Neoproterozoic and Palaeozoic - A tale of Baltica and Laurentia. Earth-Science Reviews, 40(3-4): 229-258.

Tsikalas, F., 1992. A study of seismic velocity, density and porosity in Barents Sea wells (N. Noway). (Unpublished Master Thesis), University of Oslo, Oslo, Norway.

Vanderhaeghe, O., 1999. Pervasive melt migration from migmatites to leucogranite in the Shuswap metamorphic core complex, Canada: control of regional deformation. Tectonophysics, 312(1): 35-55.

Verduzco, B., Fairhead, J.D., Green, C.M. and MacKenzie, C., 2004. New insights into magnetic derivatives for structural mapping. The Leading Edge(23): 116-119.

Ziegler, P.A., 1988. Evolution of the Arctic-North Atlantic and the western Tethys. Am. Assoc. Petrol. Geol. Mem., 48: 198.

Åm, K., 1975. Aeromagnetic basement complex mapping north of latitude 62 N, Norway. Norges geologiske undersøkelse, 316: 351-374.

Abbreviation list (Fig: 2.4A, 2.4B, 2.5A, 2.5B, 2.6, 2.7)

Onshore

AKW:	Alta –Kvænangen Window
BFZ:	Billefjorden Fault Zone
BI:	Bjørnøya Island
CFT:	Caledonian frontal thrust
GN:	Gaissa Nappe Complex
JGC:	Jergol Gneiss Complex
KN:	Kalak Nappe Complex
KuGrB:	Kautokeino Greenstone Belt
KrGRB:	Karasjok Greenstone Belt
LGrB:	Levajok Greenstone Belt
LN:	Laksfjord Nappe Complex
LP:	Lyngen Magmatic Complex
RGC:	Raisædno Gneiss Complex
RW:	Repparfjord-Komagfjord Window
RLFC:	Ringvassøy-Loppa Fault Complex
SI:	Spitsbergen Island
SP:	Seiland Igneous Province
TFFC:	Tromsø-Finnmark Fault Complex
TKFZ:	Trollfjorder-Komagelva Fault Zone
TVG:	Tanaelv and Varanger Complexes
VVFC:	Vestfjorden Vanna Fault Complex

Offshore

AFC:	Asterias Fault Complex
BB:	Bjørnøya Basin
BjFC:	Bjørnøyrenna Fault Complex
BP:	Bjarmeland Platform
EP:	Edgeøya Platform
FFC:	Finnmark Fault Complex
FP:	Finnmark Platform
FSb:	Fingerdjupet Subbasin
GH:	Gardarbanken High
HB:	Harstad Basin
HFC:	Hoop Fault Complex
HmB:	Hammerfest Basin
LFC:	Leirdjupet Fault Complex
LH:	Loppa High
MB:	Maud Basin
MFC:	Måsøy Fault Complex
MI:	Magerøya
NB:	Nordkapp Basin
ND:	Norvarg Dome
NFC:	Nysleppen Fault Complex
NH:	Norsel High
RLFC:	Ringvassøy-Loppa Fault Complex
SB:	Sørvestsnaget Basin
SD:	Samson Dome
SG:	Swaen Grabben
SH:	Stappen High
SR:	Senja Ridge
SvD:	Svalis Dome
SøB:	Sørkapp Basin
TB:	Tromsø Basin
VH:	Veslemøy High
Vvp:	Vestbakken volcanic province

Chapter 3

3D density and magnetic crustal characterisation of the southwestern Barents Shelf: Implications for the offshore prolongation of the Norwegian Caledonides

Cécile Barrère, Jörg Ebbing and Laurent Gernigon

Submitted to Geophysical Journal International, August 2009

Abstract

3D joint gravity and magnetic modelling of the southwestern Barents Shelf provides new information on key geological interfaces and allows characterisation of the crust with respect to its density and magnetic properties. The model presented here is based on a wealth of offshore seismic and onshore geological information. One of the main outcomes of this study is a new top basement map and a crustal units map for the southwestern Barents Sea, which improves our understanding of the tectonic evolution of the region. In the upper crust, a NW-SE trending density contrast is mapped and interpreted as the contact between the terranes inherited from the Caledonian collisional prism and Baltican terranes not affected by Caledonian tectonism. A system with a unique Caledonide branch propagating towards the north and Caledonian nappes emplaced asymmetrically in the western Barents Sea is confirmed, with a geometry interpreted as linked to the palaeogeography of the Baltican Plate. In addition, our crustal units map helps in our understanding of the crustal properties locally and also allows us to propose onshore-offshore links. High-density bodies modelled along the coast of Finnmark suggest a likely offshore prolongation of the Caledonian Middle and Upper Caledonian Allochthons. To the west of the Loppa High, a feature evocative of a core-complex is modelled, associated with fault complexes and strong crustal thinning. A computed crustal thinning ratio map shows that the crustal thinning pattern is complex and suggests a complex deformation mode and timing for the origin of the deep basins. Our study also highlights disparate basin evolution east and west of the Loppa high. To the east, a combination of Timanian and Caledonian faults and weakness zones played an important role in the evolution of the Mesozoic and Cenozoic sedimentary basins. To the west, the basinal evolution was mostly controlled by the reactivated Caledonian suture.

Key words: Composition of the continental crust, Gravity anomalies, Earth structure, Magnetic anomalies: modelling and interpretation, Sedimentary basin processes

3.1 Introduction

The southwestern Barents Shelf north of the Finnmark onshore area of northern Norway (Gabrielsen 1984, Gabrielsen *et al.* 1990), is tectonically complex and represents an ensemble of deep basins, basement highs and platforms (Fig. 1). A large number of seismic profiles have been collected during the last decades south of 74°N, but most of these seismic data do not allow imaging the top basement and below due to a lack of deep seismic penetration and the presence of salt and carbonate in the deep basins. Skilbrei (1991, 1995) presented top basement maps combining magnetic depth estimates and seismic profiles, which until the present study has been the best available compilation. Hitherto, the IKU seismic reflection dataset has been the main resource for deep-crustal imaging (e.g., Gudlaugsson *et al.* 1987, Faleide *et al.* 1993, Gudlaugsson & Faleide 1994, Sanner 1995, Breivik *et al.* 1998, 2005). More specifically, wide-angle data (Breivik *et al.* 2002, 2003, 2005) and the IKU reflectivity have previously been used (Ritzmann & Faleide 2007) to investigate the geometry and extent of the inferred prolongation of the Norwegian Caledonides across the Barents Shelf.

Barrère *et al.* (2009) presented 2D joint density and magnetic modelling along the IKU A, B and C seismic profiles integrated with the geological data and potential field maps that were available onshore and offshore. They presented a preliminary basement unit map for the southwestern Barents Shelf. In our study area of the southwestern Barents Sea (Fig. 3.1), continental crust and a stripe of oceanic crust along the margin are present; an intermediate crustal type may also be present along a sharp Continent-Ocean Transition (COT), previously interpreted as a strike-slip system along the western Barents Sea margin (Ziegler 1988, Faleide *et al.* 1993).
Based on the basement characterisation, Barrère *et al*. (2009) suggested a new regional interpretation for the offshore prolongation of the Norwegian Caledonides, which links the southern part of the west Barents Shelf to an elbow-shaped Caledonian structure propagating towards the north. In the present contribution we describe a new 3D density/magnetic model which is then applied to evaluate, enhance and extend the earlier interpretation regarding the distribution of crustal units and the offshore regional geology.

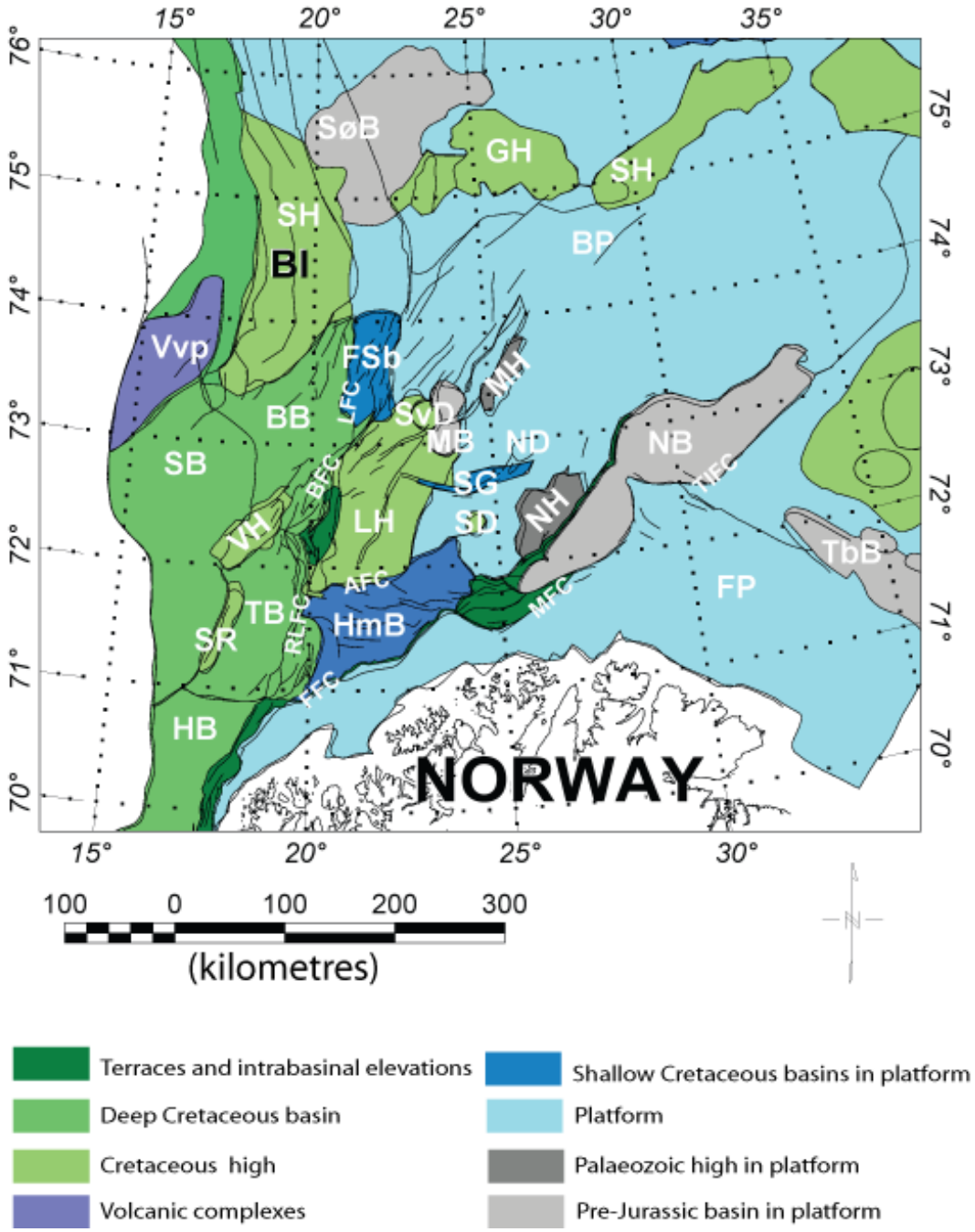

Figure 3.1: Tectonic units and main faults of the study area of the southwestern Barents Sea (see abbreviations list at the end of the paper, page 128).

3.2 Geological and tectonic setting

The southwestern Barents Sea basement composition and structure is inherited from a complex geological history. The basins observed today originate from a succession

of major rifting episodes, which occurred in the Late Palaeozoic and from the Late Jurassic to the Early Cretaceous (Faleide *et al.* 1993, Gudlaugsson *et al.* 1993). Most of the major rift basins on the Barents Shelf were formed during these episodes. A last rifting episode in the latest Cretaceous-Paleocene (Faleide *et al.* 1996) led to continental break-up and onset of seafloor spreading in the Norwegian Greenland Sea.

The basement in the Barents Sea is characterised by the diversity of the terranes involved in its composition. This diversity originates from the successive orogenies that took place from the Palaeoproterozoic to the Caledonian times. The neighbouring terranes to our study area witness on this terranes assemblage.

3.2.1 Adjacent onshore geology to the study area

The outcropping and subcropping Fennoscandian (Baltic) Shield comprises several geological provinces. Six major units can be distinguished (Fig. 3.2) (Gaal & Gorbatschev 1987): the Sveconorwegian (1.25-1 Ga), Svecofennian (1.9-1.8 Ga) and Lapland-Kola-Karelian (2.4-1.9 Ga) terranes constitute the substratum (Gee & Stephenson 2006). A belt of high magnetic granitoid, plutonic and extrusive rocks the Transscandinavian Igneous Belt (TIB) (1.8-1.6 Ga) occurs at the southwestern margin of the Svecofennides. The Caledonian fold belt (450-400 Ma) and sedimentary rocks of the Palaeozoic platform cover the westernmost and easternmost parts of the Archaean to Palaeoproterozoic rocks, respectively. The various terranes of Lapland-Kola-Karelian block and the Caledonian fold belt are known to propagate offshore beneath the Barents Sea. The Lapland-Kola-Karelian block is characterised by a complex association of geological terranes and structures of diverse origin and age (Daly *et al.* 2006, Kostyuchenko *et al.* 2006). The result is a patchwork of greenstone belts and granitic and gneissic complexes, producing a set of characteristic magnetic and gravity anomalies in mainland Finmark (Olesen *et al.* 1990) and neighbouring areas of Russia and Finland (Kostyuchenko *et al.* 2006).

3.2.2 Post Sveconorwegian tectonic events

Baltica's northeastern margin is characterised by structures related to the Late Neoproterozoic Timanian orogeny (Ivanova 2001, Roberts & Siedlecka 2002, Gee & Pease 2004, Siedlecka *et al.* 2004, Gee *et al.* 2006). On the Varanger Peninsula the exposed part of the NW-SE-trending Timanide orogen occurs northeast of the dextral strike-slip Trollfjorden-Komagelva Fault Zone (TKFZ) (Roberts & Gee 1985, Roberts & Siedlecka 2002).

The Caledonian orogen formed as a result of the continent-continent collision between Laurentia and Baltica in Silurian to Early Devonian time, the so-called Scandian orogeny (Roberts & Gale 1978, Torsvik *et al.* 1996, Roberts 2003, Gee 2005, Gee *et al.* 2006). Onshore Norway, Scandian thrust-sheets emplaced onto the autochthonous Fennoscandian Shield are recognised as four major groups of allochthons (Lower, Middle, Upper and Uppermost) (Roberts 1983, Roberts & Gee 1985, Siedlecka *et al.* 2004, Gee 2005, Nystuen *et al.* 2008). The Lower and Middle Allochthons consist of rocks derived from the Baltoscandian-margin shelf (Neoproterozoic to Silurian pericratonic deposits and continental rise, respectively) and their underlying crystalline basement. Mafic intrusions characterise the uppermost units of the Middle Allochthon (Särv and Seve Nappes) with the Seve nappes interpreted as belonging to the outermost part of the pericontinental Baltoscandian margin. The Upper Allochthon comprises thrust sheets (Köli Nappes) of lithologies derived from the Iapetus. Some of the Köli Nappes have Baltican affinities whereas some higher thrust sheets contain faunas of Laurentian origin. The Uppermost Allochthon derives from the Laurentia margin and comprises shelf and slope rise successions, some ophiolites and major granitic batholiths (Stephens & Gee 1989, Gee 2005, Barnes *et al.* 2007, Roberts *et al.* 2007).

In many parts of the Caledonides there is evidence of late Scandian transverse and orogen-parallel extension of the Caledonides (Roberts 1983, Hossack 1984, Andersen 1998, Braathen *et al.* 2002), interpreted as signs of late orogenic gravitational collapse with coeval rapid erosion of the mountains. Broad detachment zones developed obliquely to the recorded Scandian thrust direction have been described (e.g. Braathen *et al.* 2002, Olesen *et al.* 2002, Osmundsen *et al.* 2002, 2003) and are associated with Devonian supra-detachment basins. Extensional

collapse of the Caledonide orogen has been inferred to also have taken place in the Barents Sea Caledonides (Gudlaugsson *et al.* 1998). Gudlaugsson *et al.* (1998) studied the Carboniferous–Permian rifting structures and suggested that weakness zones in the basement were inherited from the Caledonian orogeny. They considered that Carboniferous-Permian rift structures continued along the strike of the North Atlantic rift at least 600 km into the Barents Sea.

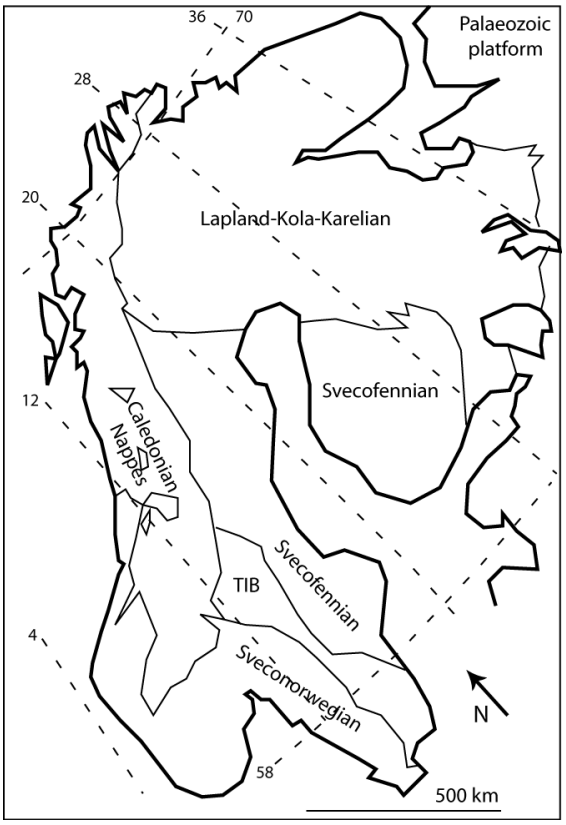

Figure 3.2: Simplified subdivision of the Fennoscandian Shield (after Gaal & Gorbatschev 1987). The Fennoscandian Shield comprises six major geological provinces: the substratum consists of the Sveconorwegian (1.25-1 Ga), Svecofennian (1.9-1.8 Ga) and Lapland-Kola-Karelian (2.4-1.9 Ga) terranes. The Transscandinavian Igneous Belt (TIB) (1.8-1.6 Ga), occurs along the southwestern margin of the Svecofennides; this is an intrusive complex of mostly granitoid composition that is propagating northward underneath the Caledonian nappes. The Caledonian fold belt (450-400 Ma) and the Palaeozoic platform cover occur in the westernmost and easternmost parts of the Fennoscandian shield, respectively.

3.3 Methodology

We have modelled the crustal structure of the SW Barents Sea in order to determine the main crustal characteristics. For this, we established a 3D forward modelling of potential field data integrated with a wealth of seismic information.

3.3.1 3D modelling

The IGMAS software (Götze & Lahmeyer 1988) has been used for forward modelling of the potential field data. Within IGMAS, the geometry is defined along parallel vertical cross-sections (Fig. 3.3). In our model, the line spacing is ranging from 10 to 20 km depending on the complexity of the modelled structures. The geometry is triangulated between the sections in order to define the 3D geometry. The gravity and magnetic fields are then calculated and the resulting field is compared with the observed potential field. Constraints are provided by geometry and petrophysical parameters. A large amount of additional data (e.g. well data, seismic horizons and profiles) was integrated to constrain our 3D model. Note that the resolution of the regional model (> 10 km) is not high enough to allow an integration of smaller intra-sedimentary features (e.g., salt domes).

In order to use absolute densities comparable with the petrophysical database in the modelling, a reference model has to be defined to model the Bouguer anomaly without an arbitrary shift. The densities in the model are defined with respect to reference densities representing the 'normal' crustal column at the coast (Table 3.1).

	Depth to boundaries (km)	Density (kg/m^3)
upper crust	0-15	2750
lower crust	15-32	2950
mantle	32-120	3265

Table 3.1: Reference model description

Magnetisation of crustal rocks is mainly related to the magnetite content in the rock. The Curie temperature of magnetite is 580ºC and at this temperature rocks lose their ability to remain magnetised. Assuming a normal thermal gradient, the Curie temperature is located in the deep crust (e.g., Ebbing *et al.* 2009). Therefore, we can

limit the extension of magnetic sources to the crust. Magnetic field calculations require the definition of an external magnetic field. The Earth magnetic field and the remanent field were modelled parallel to the induced magnetic field. We define the normal inducing magnetic field with constant field strength of 53300 nT, and inclination of 79º and declination of 4.3º.

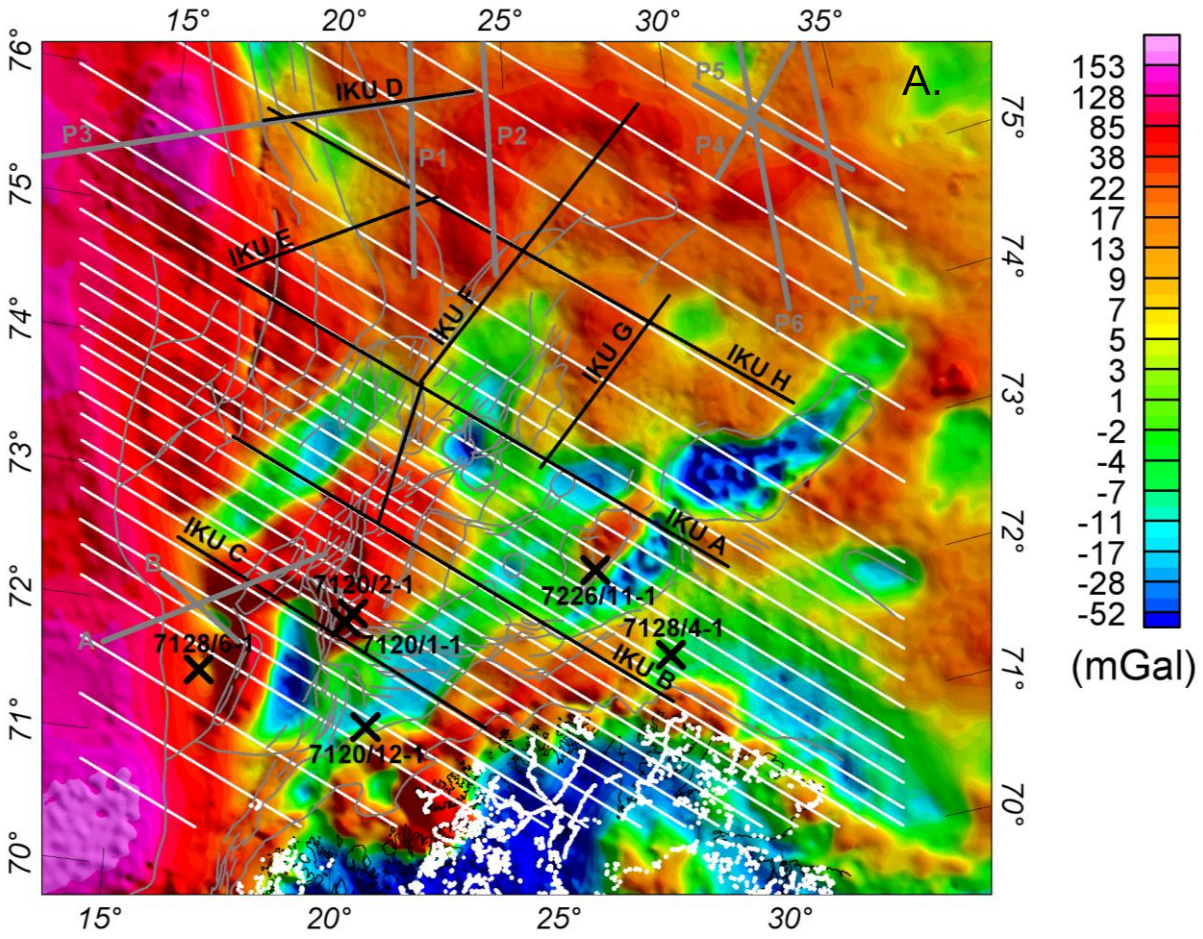

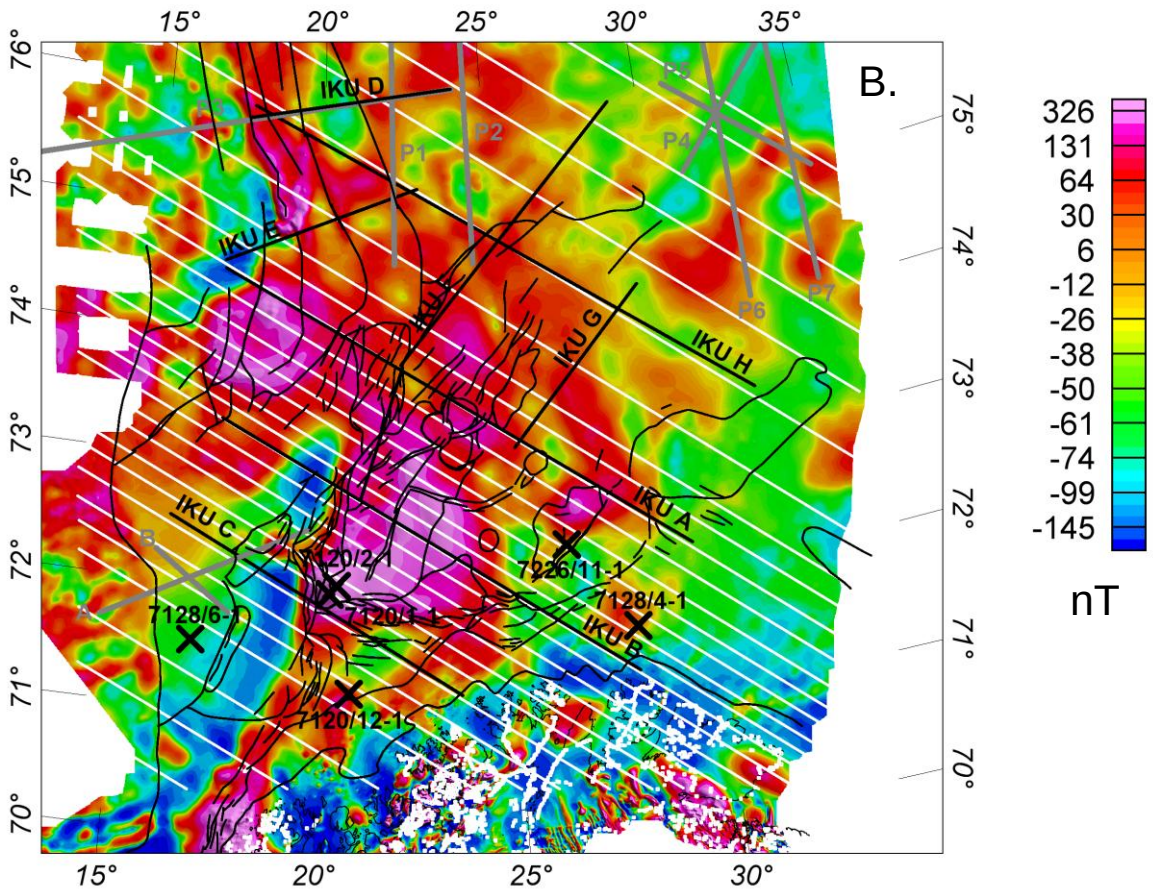

Figure 3.3: (A) Bouguer anomaly and (B) total magnetic field (reduced to the pole) with the main faults superimposed. The white lines indicate the location of the vertical planes defining the 3D model; also represented: the IKU deep-seismic reflection data (thick black lines), the wide-angle data (thick grey lines) and the deep wells reaching the basement (black crosses). The modelling parameters are constrained by the onshore petrophysical database; the measured samples are located by white dots.

3.4 Databases

3.4.1 Potential field data

3.4.1.1 Bouguer anomaly

The Bouguer anomaly (Fig. 3.3A) was calculated from the free air anomaly compilation by Skilbrei *et al.* (2000). The applied bathymetric data are based on the International Bathymetric Chart of the Oceans (IBCAO) (Jakobsson *et al.* 2000) combined with the GTOPO30 grid (onshore data)

(http://edc.usgs.gov/products/elevation/gtopo30/dem_img.html), with resolutions of 2.5 and 1 km, respectively.

A simple Bouguer correction at sea was carried out using a bathymetric grid with a resolution of 2 km and reduction densities of 2200 kg/m^3 and 2670 kg/m^3 for offshore and onshore, respectively.

3.4.1.2 Magnetic anomaly

Aeromagnetic data are available from a magnetic compilation (Fig. 3.3B) of the western Barents Sea by Olesen *et al.* (2006). The dataset is compiled from reprocessed aeromagnetic surveys and line spacing ranges from 0.5 to 2.5 km over mainland Norway and from 3 to 8 km over the continental shelf.

3.4.2 Petrophysical data

In our model the density values from the gravity modelling along IKU profiles A, B and C by Barrère *et al.* (2009) were used as initial parameters. Densities of the sedimentary layers were based on well data (Tsikalas 1992) and published tables based on velocity-density relationships of sedimentary units obtained from seismic refraction and reflection/gravity studies. Bedrock densities are based on direct onshore measurements (Olesen *et al.* 1990, Galitchanina *et al.* 1995); deep-crustal densities are based on published values from refraction data models (Breivik *et al.* 1998, 2002, 2003, 2005, Mjelde *et al.* 2002) inferred from velocity-density relationships and gravity modelling. The errors from the velocity-density relations on these densities are of the order of ±50 kg/m^3 and ±100 kg/m^3 for the upper-crustal layers and deep-crustal layers, respectively.

In the upper crust, the magnetic sources mainly relate to Caledonian and Archaean to Palaeoproterozoic rocks and mafic intrusions within the sedimentary basins (Åm 1975, Olesen *et al.* 1990, Skilbrei 1995, Barrère *et al.* 2009). For the magnetic field, the magnetic susceptibility and remanence from the magnetic modelling along IKU profiles A, B and C by Barrère *et al.* (2009) were used as initial parameters. Those values were derived from onshore samples (Troms and Finnmark regions) (Olesen *et al.* 1990, Slagstad *et al.* 2008). Q-ratios were applied according to the samples and

modified during the modelling. We set a homogeneous and low Q-ratio and magnetic susceptibility for lower crust with Q=0.4 and magnetic susceptibility=1000.10^{-5} (SI). Sedimentary rocks are set to 30.10^{-5} (SI) as they have very low magnetic properties in comparison with the basement rocks (e.g. Olesen *et al.* 1990).

	Breivik et al. (1995) Ottar Basin Nordkapp Basin		Mjelde et al. (2002) Sørvestsnaget Basin	Ritzmann et al. (2007) (Barents50) Average Barents Sea		Breivik et al. (2002) SE Svalbard	Breivik et al. (2003) S. Svalbard	Breivik et al. (2005) S. Svalbard	Clark et al. (2008) SW Barents Sea Loppa High	Barrère et al. (2009) SW Barents Sea	
	Density ($kg.m^{-3}$)	Velocity (m/s)	Density ($kg.m^{-3}$)	Density ($kg.m^{-3}$)	Velocity (m/s)	Velocity (m/s)	Velocity (m/s)	Velocity (m/s)	Velocity (m/s)	Density ($kg.m^{-3}$)	Magnetic properties
Quaternary	1800-2050	1800-2360	2050	1800-2050	1800-2250	-	1800-2250	-	1040-2000	2300	0
Cenozoic	2050	2360	2200	2050-2280	2250-3260	-	2250-3500	-	2000-3000	2300	0
Cretaceous	2140	2750	2300	2240	2750-3600	3200-3360	3500-3600	3200-3600	3000-4500	2450	0
				2370							
			2400	2590		3300-4050	3800-5000				
Triassic	2340	3700	2480	2380-2590	4000-5450	4000-4800	4000	4000-5450	4500-5000	2550	0
	2390	4000		2470-2590		4000-4800	4600-5450				
	2430	4200		2520-2590		4000-4800	4600-5450	4500-5450			
	2500	4600		2520-2590		4500-4950	5100-5450				
Palaeozoic	2610	5200	2620	2640	4500-5900	5100-5520	5650-5900	5100-5900	5000	2600	0
Near top Basement	2660	5500		2710	5500-6000	5800-6000	5920-5950	5800-6000			
Salt	2200		2150								0
Upper Crust	2770	6000	2750-2820	2770	6200-6600	Density ($kg.m^{-3}$) 2800-2990	Density ($kg.m^{-3}$) 2793-2880	Density ($kg.m^{-3}$) 2793-2915	6000-6500	Caledonian Nappes 2750	(0.0001 to 0.01 SI, 0.01 A/m, Q>1)
										Archaean To Proterozoic rocks 2750-2800	(0.010 to 0.200 SI, 0.20 A/m, Q<1)
										Mafic Intrusions 3000	(0.015 to 0.05 SI, 0.2 A/m, Q<1)
Deep Crustal High Density Body			Velocity(m/s) 7400	2980-3050	7100-7600					3100	(0.0001 SI, 0 A/m, Q=0)
Oceanic Layers			Density ($kg.m^{-3}$) 2800-2850				2900-2950	2900-2950			
Lower Crust	2930	>6600	2950			2910-2950	Density ($kg.m^{-3}$) 2900-2950		6500-7000	2950	(0.0001 SI, 0 A/m, Q=0)
Mantle	3330	>8000	3200-3280	3300		3330-3450		3330-3340	7500	3300	

Table 3.2: Compilation of density/velocity laws applied in the Barents Sea and starting value used in this study.

3.4.3 Geometric constraints

To constrain the sedimentary layers we obtained access to three industrial, depth-converted seismic horizons: top Tertiary, base Cretaceous and top Permian. These horizons were produced by depth-conversion of seismic horizons using regional velocity functions calibrated by well data. The sedimentary rocks were then subdivided into four principal units: Quaternary, Neogene-Paleocene-Cretaceous, Jurassic-Triassic and Palaeozoic. In the southwestern Barents region, six wells (black crosses, Fig. 3.2) reach the top basement; they were used to calibrate the modelled top basement and check the reliability of the depth-converted seismic horizons.

We set up our initial model using the Barents50 model of Ritzmann *et al.* (2007) and the top basement reported by Skilbrei (1991, 1995). The former describes a crustal velocity model with a resolution of 50 km, which also provides information along all available regional seismic profiles with 25 km sampling. The top basement of the Barents50 model is roughly similar to the depth to magnetic basement established by Skilbrei (1991, 1995), which provides a locally higher resolution. The IKU deep-seismic reflection profiles and the seismic refraction data (Breivik *et al.* 2002, 2003, 2005, Mjelde *et al.* 2002) were used to refine the crustal structure of our model. The boundary between the upper and lower crust varies between 20 and 22 kilometres depending on the reflectivity along the IKU profiles and the seismic velocities from refraction seismic lines. In addition, a recent OBS profile (Clark *et al.* 2009) has been included in the final phase of the modelling.

3.5 Modelling results

3.5.1 Comparison between observed and modelled potential fields

3.5.1.1 Density modelling

The final differences between the measured and modelled gravity anomalies have a standard deviation of less than ±8.0 mGal. This value is well above the accuracy of the gravity data (±2 mGal). The remaining mismatch can be largely explained as relating to local structures below the resolution of our model (e.g. salt domes). The short-wavelength anomalies (<10 km) onshore have not been modelled and consequently create local deviations from the modelled Bouguer anomalies.

3.5.1.2 Magnetic modelling

The observed and modelled magnetic anomalies show a reasonable match. The anomalies linked to basement topography (wavelengths: 100-200 km) are better matched than the short-wavelength (<100 km) anomalies linked to intra-basement magnetic sources and/or shallow magnetic sources. Because of our simplified settings, the magnetic modelling represents the general magnetic trends but not the absolute amplitudes of the magnetic field.

3.5.2 Density and magnetic properties

Figures 3.4 and 3.5 show the set-up of the model and the main 3D horizons. In Fig. 3.5, the profiles show a good regional fit, but local deviations occur, especially in magnetic modelling.

The model densities and magnetic properties are summarised in Table 3.3. The modelled values are used to distinguish between different basement units, the spatial extensions of which are presented in Figure 3.4A.

			Density (kg/m^3)	Magnetic properties		
				Q-ratio	Susceptibility (.10^{-5} SI) max.	min.
Mantle	continental mantle		3300	0.4	800	
	oceanic mantle		3230			
lower crust	standard lower crust		2950	0.4	800	
	LCB - lower crustal body		3000	0.4	800	
oceanic crust	basalt		2900	1	2000	
Upper crust	onshore zone	BAS1 onshore Fennoscandian Shield	2700-2750	0.5	1500	1000
		CN Caledonian nappes	2750	2	500	
	coastal zone	UCB high-density body	2800	0.5	1000	
	Loppa High zone	BAS1 Loppa High (south & west)	2750	0.5	4500	
		BAS1 Loppa High (east & north)			5000	
		BAS1 Stappen High (south)	2800		3000	
	COT zone	MB1 Hornsund area Sørvestnaget Basin	2850 2880	0.5	2500	1000
		MB3 Harstad Basin	2860	1-0.5	5000	3000
		MB2 Vestbakken volcanic province	2800	0.5	3000	
	eastern zones	BAS2 north of Nordkapp Basin BAS2 south of Nordkapp Basin	2790 2770	0.5	2000	1000
		MI (Norsel High, N-E Loppa High)	2900	0.6	2500	
	northern zones	BAS2 Stappen High north central area	2750	0.5	3000	1000
sedimentary rocks	Quaternary		2300	0.3	30	
	Neogene-Paleogene-Cretaceous		2450	0.3	30	
	Jurassic-Triassic		2550	0.3	30	
	Palaeozoic		2600	0.3	30	

Table 3.3: Modelling parameters: the different crustal units are defined by a combination of petrophysical values obtained by density and magnetic modelling. The association of neighbour crustal units defines the zones geologically interpreted.

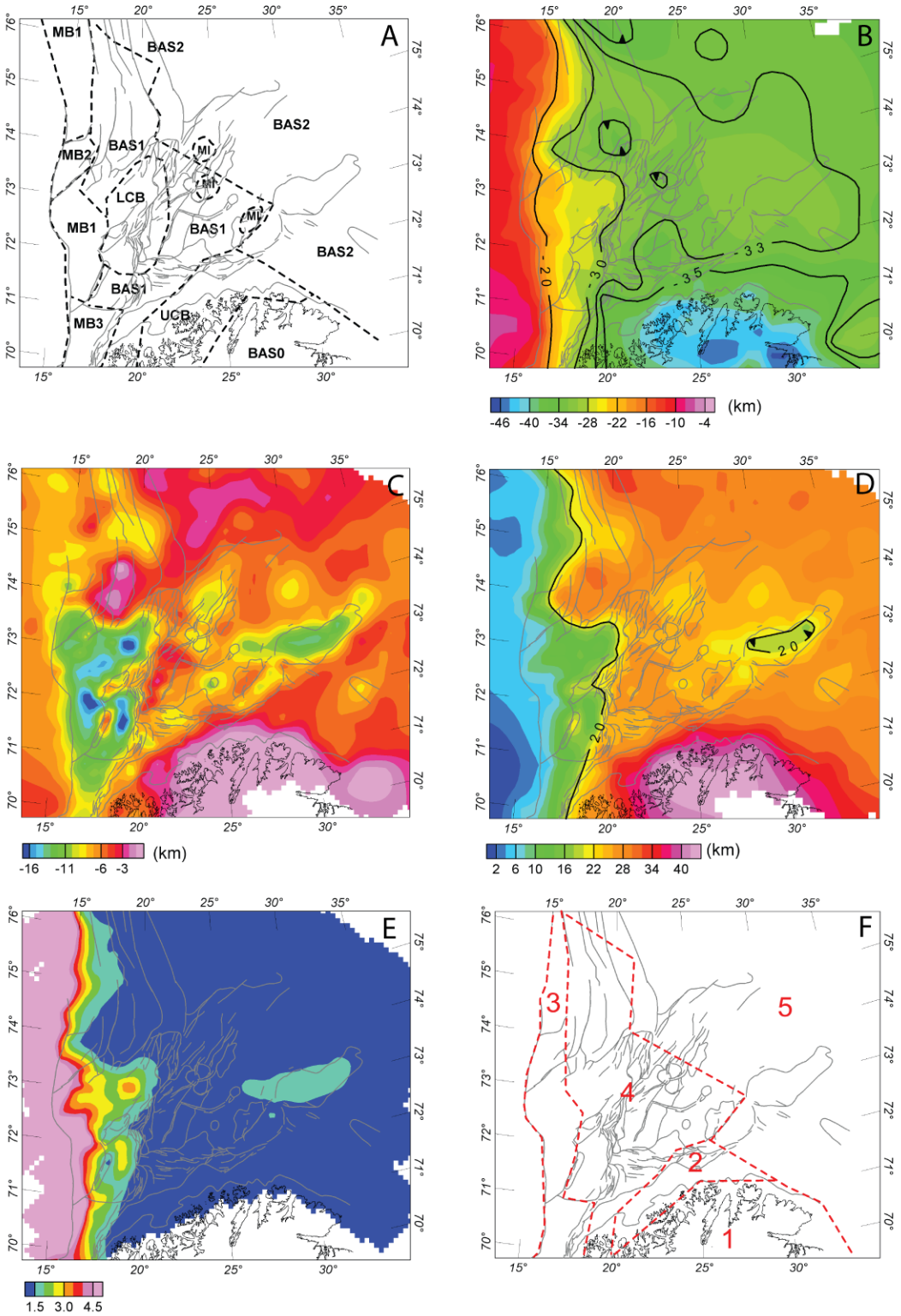

Figure 3.4: (A) Crustal units are established by grouping blocks of comparable density and magnetic properties. LCB = lower crust high-density body; UCB= upper crust high-density body; BAS0= Onshore Fennoscandian Shield; BAS1 = Archaean to Palaeoproterozoic rocks affected by the Caledonian orogeny; BAS2 = Archaean to Palaeoproterozoic rocks weakly affected by the Caledonian orogeny, clearly with

lower magnetisation than the type BAS1; MB1 = high-density/medium-magnetic crust; MB2 = Vestbakken volcanic province; MB3 = high-density/high-magnetic crust. (B) New Moho map from our 3D model. (C) Depth to top basement taken from our 3D model. The depth to top basement coincides over most of the area with the depth to the top of the Caledonian nappes. (D) Crystalline basement thickness map computed from the modelled depth top basement (Fig. 3.4C) to the Moho (Fig. 3.4B), and simplified structural map (solid grey lines). The map shows the intense crustal thinning to the west of the alignment of the Ringvassøy-Loppa and Bjørnøyrenna Fault Complexes. (E) Crustal thinning factor map. This factor is computed dividing the reference thickness of 33 km by the crustal thickness modelled. The map provides a quantitative estimation of the thinning intensity and a qualitative estimation of the main directions of extension. (F) Five ´crustal zones' consisting of one or several basement units are distinguished: (1) onshore zone, (2) offshore coastal zone, (3) marginal zone, (4) central zone and (5) zone covering the eastern and northern areas.

3.5.2.1 Modelled densities (Table 3.3)

On the Bjarmeland Platform (Fig. 3.1), the densities are slightly higher than the 2750 kg/m^3 average values usually considered for the Fennoscandian Shield basement (BAS0) (Galitchanina *et al.* 1995). Also, to produce a Moho depth compatible with the seismic Moho (Ritzmann *et al.* 2007), a lower crustal body (LCB) had to be introduced over the central part of the SW Barents Shelf. The LCB's 3000 kg/m^3 density value contrasts with the surrounding 2950 kg/m^3 density of the regular lower crust density.

Along the western margin, the basement units MB1, MB2 and MB3 are modelled with density values around 2850 kg/m^3. Locally, blocks (MI) of 2900 kg/m^3 density were introduced in the model.

3.5.2.2 Modelled susceptibilities (Table 3.3)

The tops of the magnetic sources are assumed to be the top basement and the top of the oceanic basalts obtained by density modelling, for the continental and oceanic crust, respectively. Due to the resolution of the model and lack of constraining data, no intra-basement magnetic sources are distinguished. Therefore, the resulting

magnetic modelling highlights the main changes in magnetic properties of the upper crust.

The final model shows a variation of the upper-crustal magnetic susceptibility values from 500.10^{-5} (SI) to 5000.10^{-5} (SI).

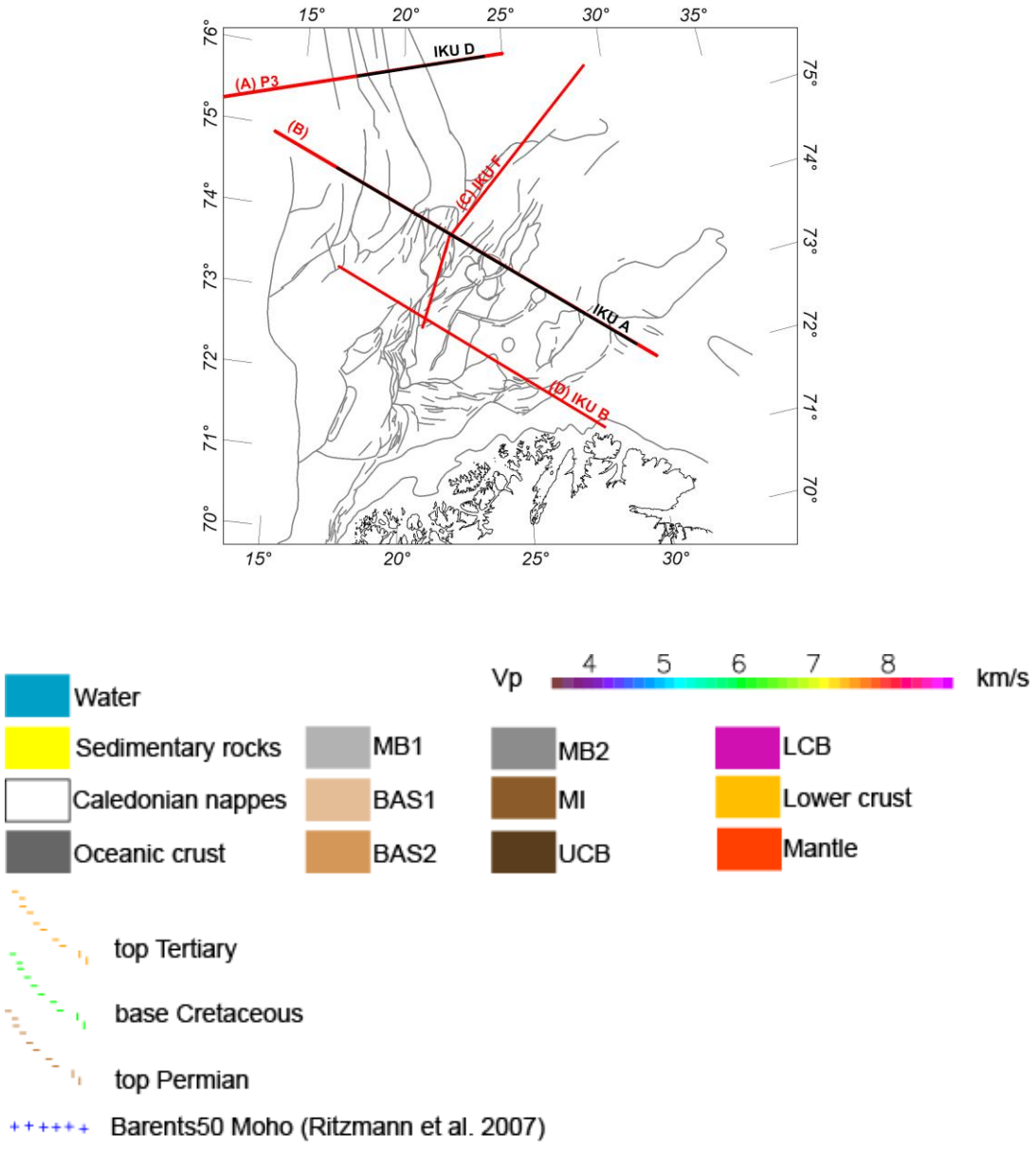

A.

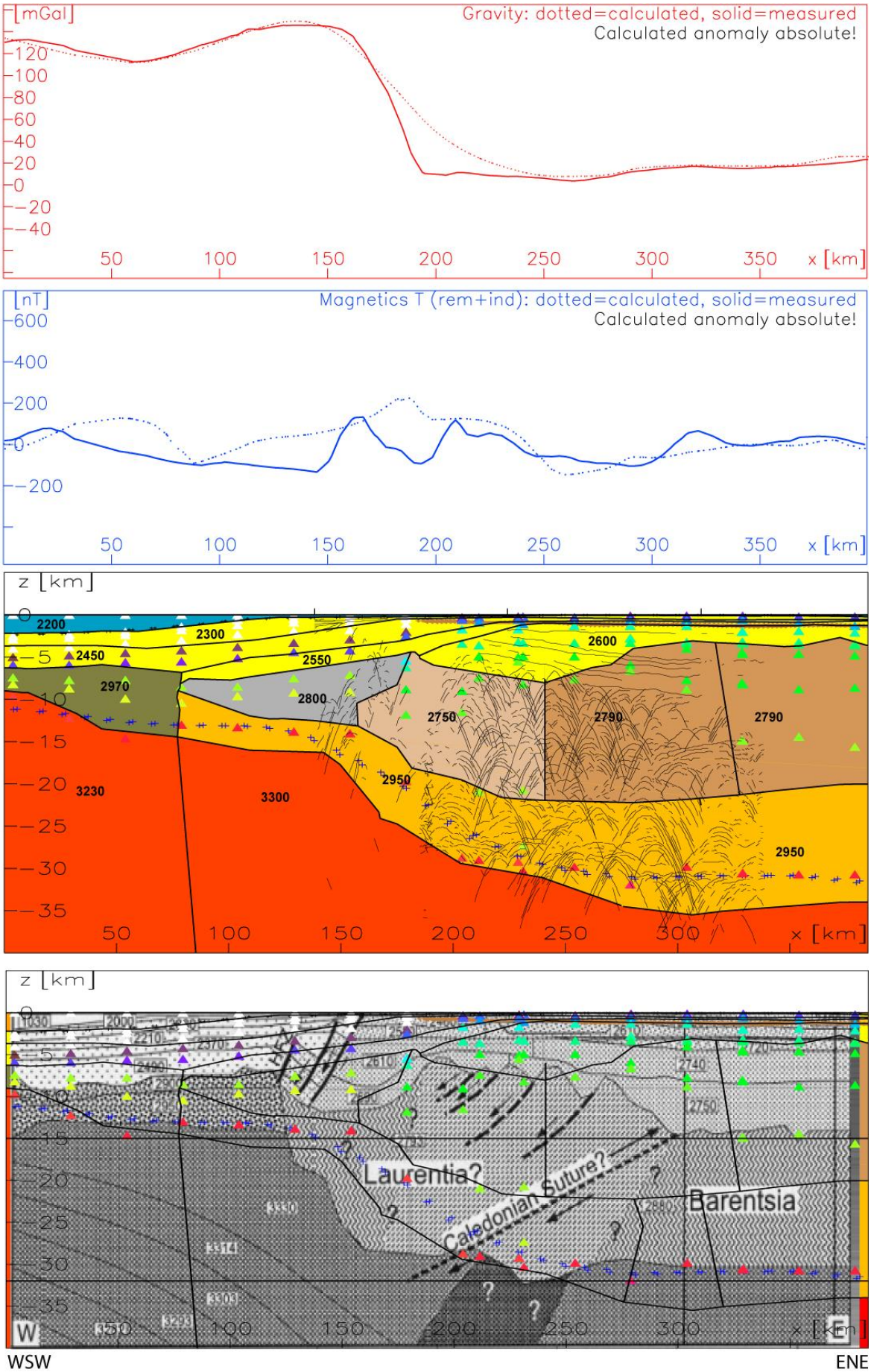
[mGal]
Gravity: dotted=calculated, solid=measured
Calculated anomaly absolute!
120
100
80
60
40
20
0
−20
−40
50
100
150
200
250
300
350
x [km]
[nT]
Magnetics T (rem+ind): dotted=calculated, solid=measured
Calculated anomaly absolute!
600
400
200
0
−200
50
100
150
200
250
300
350
x [km]
z [km]
0
5
10
15
20
25
30
35
2200
2300
2450
2550
2600
2970
2800
2750
2790
2790
2950
3230
3300
2950
50
100
150
200
250
300
x [km]
z [km]
Laurentia?
Caledonian suture?
Barentsia
W
E
50
100
150
200
250
300
x [km]

WSW ENE

B.

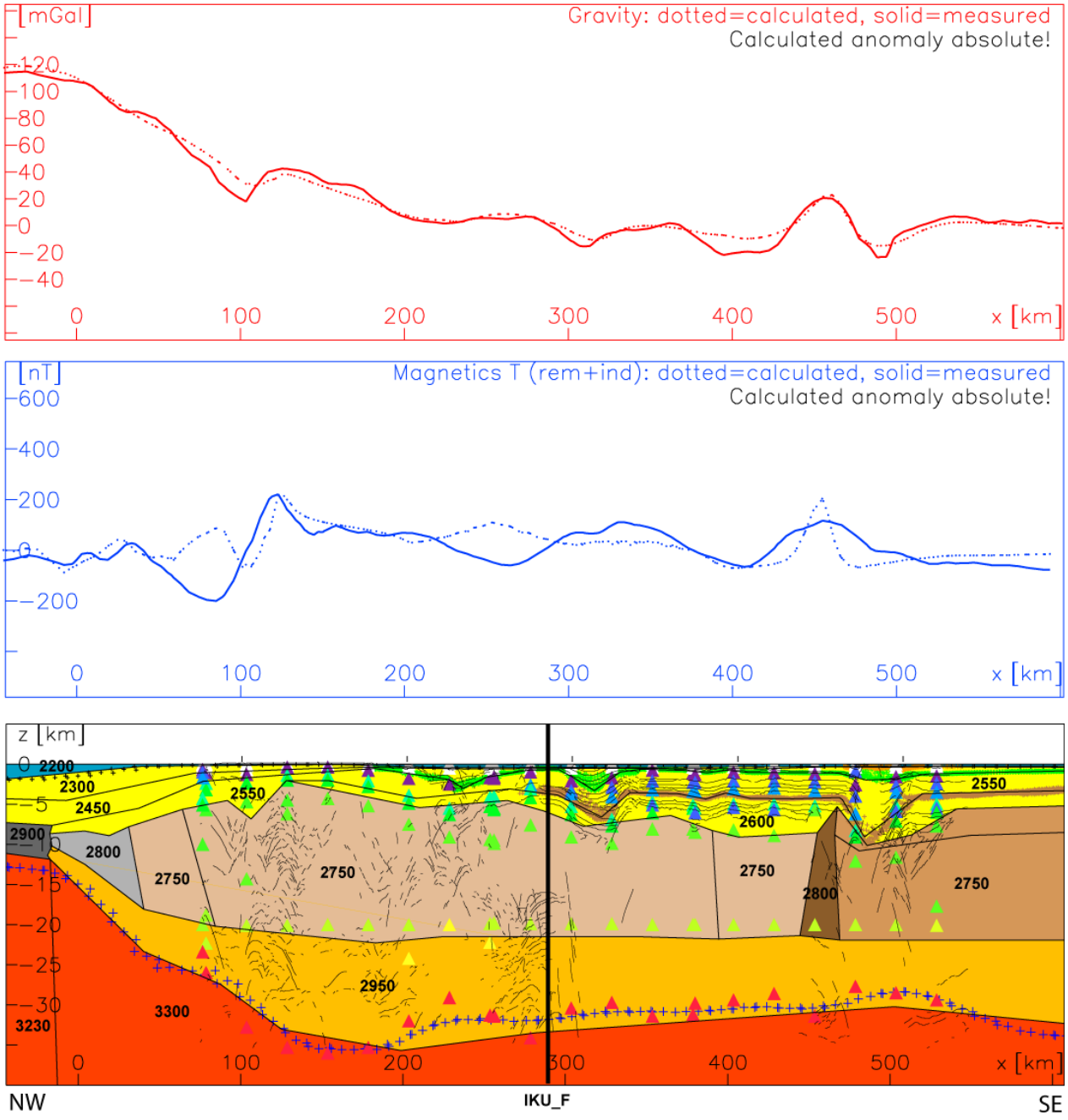
[mGal]
Gravity: dotted=calculated, solid=measured
Calculated anomaly absolute!
120
100
80
60
40
20
0
−20
−40
0
100
200
300
400
500
x [km]
[nT]
Magnetics T (rem+ind): dotted=calculated, solid=measured
Calculated anomaly absolute!
600
400
200
0
−200
0
100
200
300
400
500
x [km]
z [km]
0
5
10
15
20
25
30
2200
2300
2450
2900
2800
2750
2550
2600
2950
3300
3230
0
100
200
300
400
500
x [km]
NW
IKU_F
SE

C.

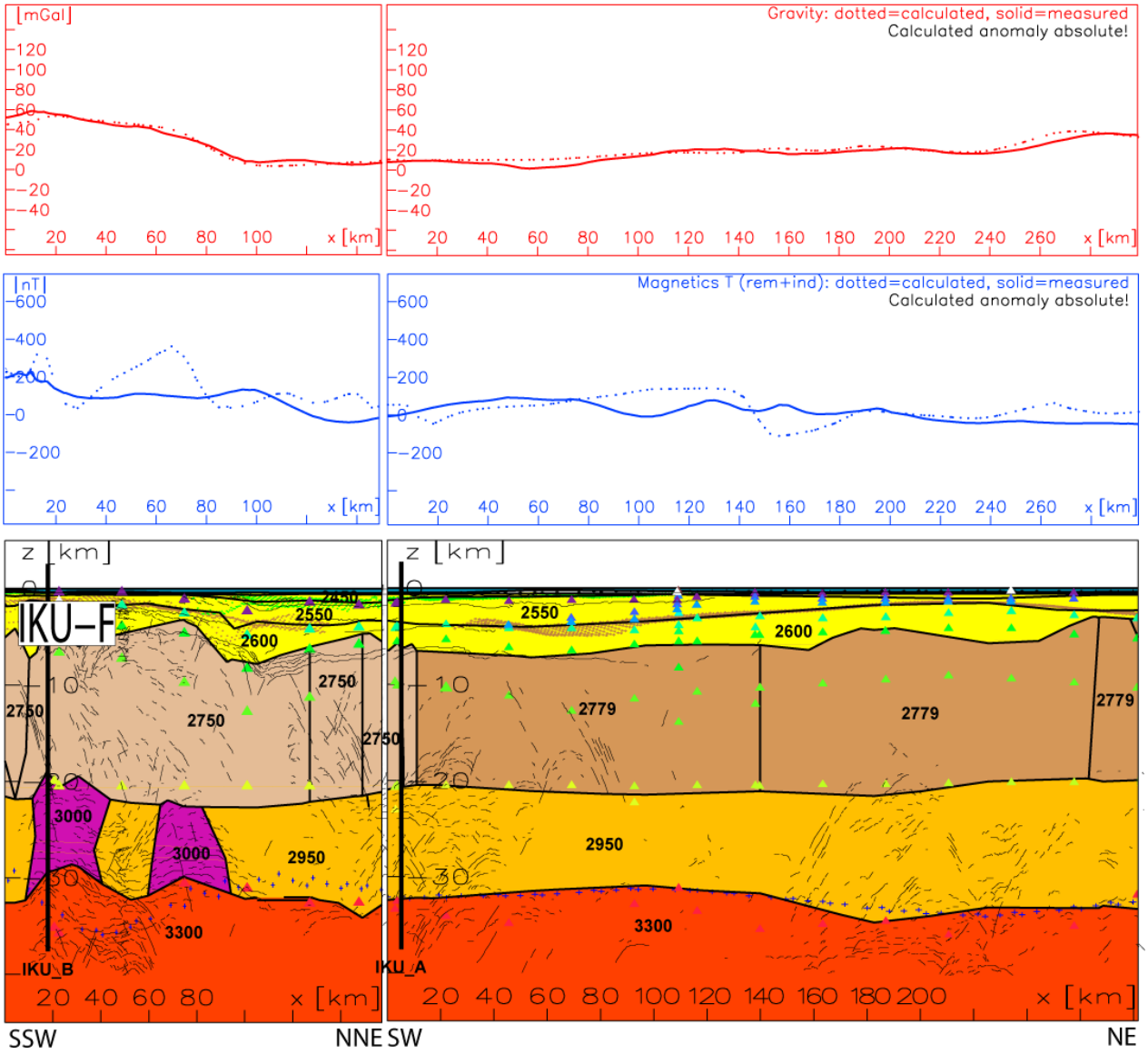
[mGal]
Gravity: dotted=calculated, solid=measured
Calculated anomaly absolute!
x [km]
[nT]
Magnetics T (rem+ind): dotted=calculated, solid=measured
Calculated anomaly absolute!
z [km]
IKU-F
2550
2600
2750
3000
2950
3300
2779
IKU_B
IKU_A
SSW
NNE
SW
NE

D.

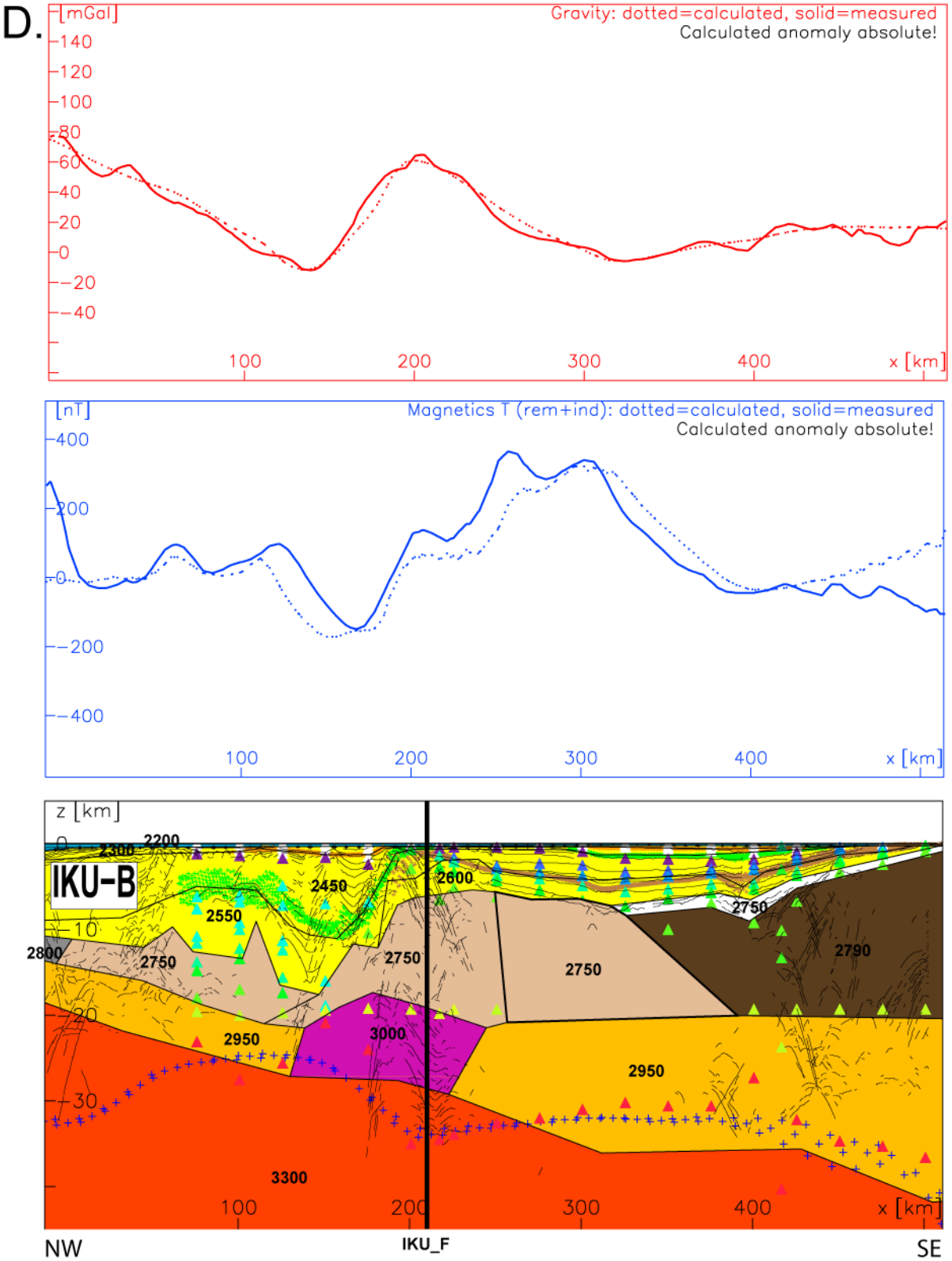
[mGal]
Gravity: dotted=calculated, solid=measured
Calculated anomaly absolute!
140
120
100
80
60
40
20
0
−20
−40
100
200
300
400
x [km]
[nT]
Magnetics T (rem+ind): dotted=calculated, solid=measured
Calculated anomaly absolute!
400
200
0
−200
−400
100
200
300
400
x [km]
z [km]
IKU-B
2200
2300
2450
2600
2550
2750
2790
2800
2750
2750
2750
2950
3000
2950
3300
10
20
30
100
200
300
400
x [km]
NW
IKU_F
SE

Figure 3.5: Location map: integrated modelling cross sections A, B, C and D (red solid lines) parallel to existing seismic data: (A) P3 and IKU D, (B) IKU A, (C) IKU F and (D) IKU B. Cross sections: the two top frames show the modelled (dash line) and observed (solid line) Bouguer (red) and magnetic (blue) anomalies. The bottom frames display the model; black numbers represent densities in kg/m^3 and basement units are interpreted. The model is overlain by the line drawings reflectivity of the IKU data. The triangles represent Vp velocities extracted from the Barent50 model (Ritzmann *et al.* 2007). In figure (A) the fourth frame presents a comparison of our model with the model of Breivik *et al.* (2002) along P3. In figure (D), the model does not reflect the Barents50 constraints (Vp velocities) but rather a recent seismic refraction dataset named Petrobar-07 (Clark *et al.* 2009).

3.5.3 3D Crustal configuration

Our 3D model allows us to define and present key elements of the southwestern Barents Sea crustal architecture. As a result we have compiled maps of the depth to Moho (Fig. 3.4B), the top basement (Fig. 3.4C) and crystalline crust thickness (Fig. 3.4D) extracted from the 3D model.

3.5.3.1 Depth to the crust-mantle boundary (Moho)

The Moho (Fig. 3.4B) is, in general, associated with a density contrast of 350 kg/m^3 between the lower crust and the upper mantle. Only across the lower crustal body (LCB) is this contrast slightly smaller (Fig. 3.4A). The resulting Moho geometry reflects the Moho of the Barents50 model at the continental margin and onshore. Over most of the margin, the Moho is similar to the Barents 50 model, but varies significantly in the trend of anomalies. Along the IKU profiles (Fig. 3.2) the Moho depths (Fig. 3.4B) are essentially the same with the exception of IKU-B where a new OBS interpretation suggests a deeper Moho and provides an update of the Barents50 model (Clark *et al.* 2009).

The Moho (Fig. 3.4B) undulates over the continental shelf between depths of 20 and 35 km. In the central study area, an E-W shallowing trend correlates with the location of basins and highs. We also observe a steep deepening of the Moho, from 20 km to

30 km, between the continent-ocean transition and the Ringvassøy-Loppa and Bjørnøyrenna Fault Complexes. Interestingly, the depth to the Moho is in the order of 30-32.5 km below the Bjarmeland Platform and northwards and shows a gradual shallowing from north to south offshore.

3.5.3.2 Depth to top basement

The density contrast between the crystalline basement and Palaeozoic sedimentary rocks is at least 50 kg/m^3. In our model, sedimentary rocks are considered to be relatively non-magnetic and the top basement (Fig. 3.4C) was regarded as the upper limit of the magnetic sources. Over large parts of the shelf, this interface is located at depths between 4 and 8 km. The shallowest crystalline basement (<2 km) occurs at the Gardarbanken High, north of the Stappen High and on Bjørnøya, where it outcrops (Fig. 3.1).

In the northern part of the Nordkapp Basin, where the depth to crystalline basement reaches 12 km, there is a deep graben. Much deeper basins to the west of the Loppa High and south of the Stappen High were modelled with a depth to basement locally reaching >15 km.

3.5.3.3 High-density lower crustal body (LCB)

We have modelled the LCB in 3D (Fig. 3.4A), a body previously interpreted in the deep lower crust at the western rim of the Loppa High along profile IKU B (Barrère *et al.* 2009). The presence of this deep buried high-density body was necessary to model correctly the Bouguer high at the location of the Loppa High. The 3D modelling allowed us to evaluate the northward and southward extension of this LCB (Fig. 3.4A), but the lack of good seismic constraints did not allow us to determine its exact thickness.

3.5.3.4 High-density bodies in the upper crust (UCB and MI)

A basement stripe of high-densities (UCB) about 2800 kg/m^3 and magnetic susceptibility of 1000.10^{-5} (SI) has been modelled along most of the coast of Finnmark (Fig. 3.4A, UCB). Local high-density bodies (Fig. 3.4A, MI) with a density of

2900 kg/m^3 and a magnetic susceptibility of up to 2500.10^{-5} (SI) have also been modelled between two profiles at the Norsel High and northeast of the Loppa High.

3.5.3.5 Crystalline crust thickness and thinning factor maps

The crystalline basement thickness map (Fig. 3.4D) is computed from the difference between the modelled Moho and top basement. The 20 km isopach contour separates a narrow thin crust (10 to 20 km) between the continental margin and the alignment of the Ringvassøy-Loppa and Bjørnøyrenna Fault Complexes from a large eastern area with a crustal thickness between 20 and 28 km.

An estimation of the apparent crustal thinning through a crustal thinning factor (β-factor) (McKenzie 1978) was computed (Fig. 3.4E) from the crustal thickness grid inferred from our 3D model. The 33 km thickness of the Bjarmeland Platform is considered as the reference crystalline basement thickness before basin formation:

$$\beta_{factor} = 33 / crystallin\,e\_basement\_thickness$$

β-factors greater than or equal to 2 are mapped west of the Ringvassøy-Loppa and Bjørnøyrenna Fault Complexes (at the location of Sørvestsnaget Basin >3; Harstad Basin >3; Tromsø Basin 2 to 3 and Bjørnøya Basin 0.5 to 3.5). The North Nordkapp Basin shows a maximum β-value of 2.5 and in the Hammerfest Basin β-values <1.5. Apart from along the continent-ocean transition, the maximum crustal thinning seems to follow the trend of two fault alignments; (1) the ENE-WSW alignment of the Finnmark, Måsøy and Thor Iversen Fault Complexes and (2) the N-S alignment of the Ringvassøy Loppa and Bjørnøyrenna Fault Complexes.

In addition to the strong crustal thinning along the margin, the zone between 74°N and the Finnmark and Måsøy Fault Complexes shows β-values of about 1.5. One can observe that this area correlates with a shallower Moho (30-32 km) compared to the platform areas. Towards the east the crustal thickness increases to 32 km, and is clearly associated with the transition from the Eastern to the Western Barents Sea.

3.6 Interpretations and discussion

3.6.1 Comparison with previous top basement estimates

In Fig. 3.6, the new top basement model is compared with the compilations by Ritzmann *et al.* (2007) (Fig. 3.6A) and the depth to magnetic basement maps published by Skilbrei (1991, 1995) (Fig. 3.6B). North and east of the Loppa High, differences greater than 5 km are observed, where the low-amplitude magnetic anomaly and lack of seismic data prevented Skilbrei (1991, 1995) from obtaining magnetic depth estimates. North of 74°N our model shows a shallower top basement than Skilbrei (1991, 1995). Here, the low amplitude magnetic anomalies have been interpreted by him as a consequence of a deepening of the top basement. In our model, the magnetic susceptibility in the basement changes to lower values, which consequently leads to a shallower top basement.

The Barents50 model integrates the refraction data north of 74°N and we expected the correlation between our modelled top basement and the Barents50 top basement to be reasonable. However, the difference map between the two (Fig. 3.6A) shows a significant underestimation (i.e., 6 to 10 km) of the top basement in the Barents50 model despite seismic constraints. Comparing the seismic refraction model and our geological model (Fig. 3.5A), it appears that a layer with a density of 2750 kg/m^3 is interpreted as sedimentary rocks in the refraction model. In our model, sedimentary rocks have densities <2750 kg/m^3 whilst crystalline rocks have densities greater than 2750 kg/m^3. The misfit can consequently be attributed to differing definitions of the top basement. From the density tables established by Tsikalas (1992) for the sedimentary rock samples and from measurements of onshore basement samples (Olesen *et al.* 1990, Galitchanina *et al.* 1995), we regard a density higher than 2750 kg/m^3 to be more appropriate for basement rocks.

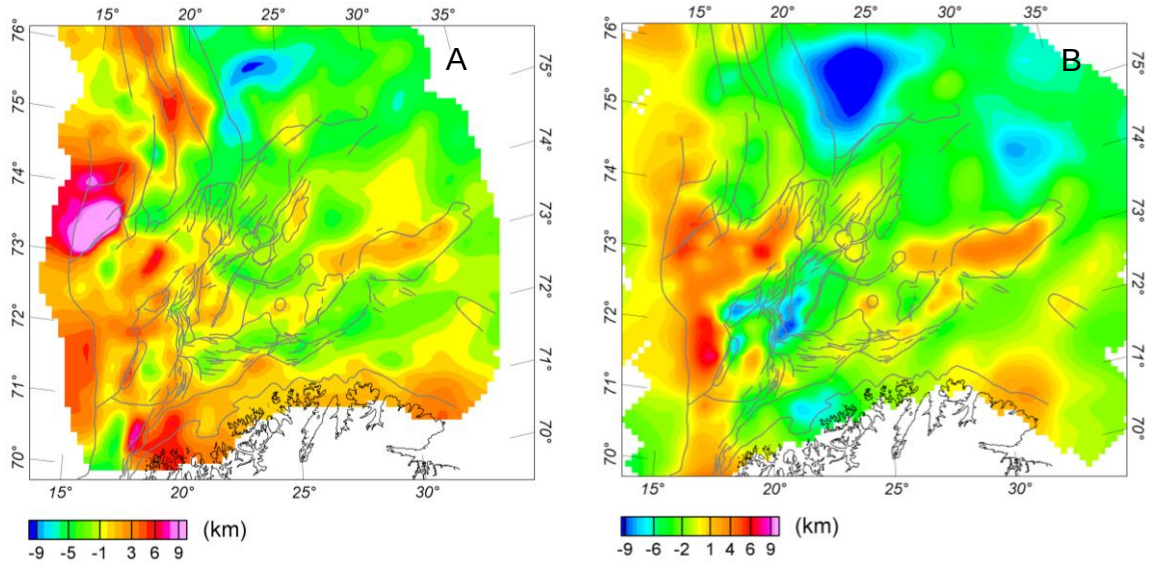

Figure 3.6: Difference map between our new top basement estimates (Fig. 3.4C) and the top basement (A) from the basement grid based on estimates of depth to magnetic basement. (Skilbrei 1991, 1995) and from the Barents 50 model (Ritzmann *et al.* 2007) (B).

3.6.2 Interpretation of the crustal units map

The densities allow us to distinguish between different basement units but resolve the Caledonian nappes only in general terms. In fact, except for exotic terranes the Norwegian Caledonian nappes correspond to a low-magnetic basement on top of an Archaean to Palaeoproterozoic basement with higher magnetisation properties (Olesen *et al.* 1990). The northward extension of the Caledonian nappes is based on the assumption of the offshore propagation of the nappes that occur in northern Norway (Åm 1975, Olesen *et al.* 1990, Skilbrei 1995, Siedlecka & Roberts 1996, Gernigon *et al.* 2007). Estimations of their extension and thicknesses from our model are difficult as the density and magnetisation contrasts between the nappes and the Archaean to Palaeoproterozoic basement are low.

After interpretation and correlation, five crustal zones consisting of one or several units (Fig. 3.4F) have been distinguished: (1) an onshore zone, (2) an offshore coastal zone, (3) a zone along the continent-ocean transition, (4) a central zone and (5) a zone covering the eastern and northern parts of the study area.

3.6.2.1 Onshore Zone

For the BAS0 onshore zone (Fig. 3.4A), the Fennoscandian Shield was divided into two bodies, one of 2750 kg/m^3 density interpreted as Archaean to Palaeoproterozoic, high-grade metamorphic rocks (potential granulites), and the second with a slightly lower density (2700 kg/m^3) which is interpreted as lower-grade metamorphic rocks such as Archaean to Palaeoproterozoic granitic gneisses.

3.6.2.2 Coastal zone

Offshore, along the coast, the high-density upper crustal body (UCB) (Figs. 3.4, 3.5D) with intermediate magnetic properties is considered to be related to rocks within the Middle and Upper Allochthons intruded by major mafic-ultramafic, plutonic complexes similar to the onshore Vendian-age (570-560 Ma) Seiland Igneous Province (Roberts *et al.* 2006) and the Early Silurian, Honningsvåg Igneous Complex (Robins 1998, Corfu *et al.* 2006). In compliance with the onshore observations and the samples of Caledonian nappes samples taken from drillcores (Slagstad *et al.* 2008), we have modelled a body consisting of Caledonian nappes at the top of the upper crustal body.

3.6.2.3 External margin

In the western part of the study area, four bodies are distinguished which correlate with distinctive structural elements: (1) the Harstad Basin, (2) the Vestbakken Volcanic Province, (3) the Sørvestsnaget Basin and (4) the Hornsund Area west of the Stappen High. The four bodies have high densities of around 2850 kg/m^3 and very variable magnetic susceptibilities from 1000.10^{-5} to 5000.10^{-5} (SI). The good correlation between basement units and tectonic units reflects the strong relationships between the different basement types and the evolution of the continental margin.

Over the Sørvestsnaget Basin, the Bouguer anomaly high and the low magnetic signature may be comparable with a 'quiet zone' that has been described from the vicinity of some margins (Gunn 1997). This 'quiet zone' could be interpreted either as

extremely thinned crust or as attenuated crust with an intermediate character between true continental and true oceanic crust that developed close to the continent-ocean transition. Alternatively, it could possibly be due to a specific chronostratigraphic period of reverse polarity. Whatever the case, both a better seismic imaging and a more focused study of the Sørvestnaget Basin are necessary in order to understand this very complex area.

3.6.2.4 Central zone

This elongate zone encompasses the Loppa High, the Bjørnøya Basin and the southern part of the Stappen High. Several units with the same density value (2750 kg/m^3) and high susceptibility were distinguished in the upper crust. Compared to the onshore geology, the relatively high susceptibility is interpreted as indicating a crust consisting of magnetic gneisses comparable to the ones mapped and sampled onshore Norway (Olesen *et al.* 1990). They are here grouped under the label BAS1.

In the lower crust, a high-density body (LCB) of 3000 kg/m^3 is modelled to the west of the Loppa High (Figs. 3.4, 3.5D). The modelling indicates its approximate extension along the Ringvassøy-Loppa and Bjørnøyrenna Fault Complexes. Locally, it reveals the existence of a lower crustal bulge. The elongation of the high-density body suggests a close genetic link to the development of these major faults. It suggests that the crustal thinning was accommodated along the Ringvassøy Loppa and/or the Bjørnøyrenna Fault Complexes in a manner comparable to the major detachments documented onshore (Braathen *et al.* 2002, Osmundsen *et al.* 2002, 2003) and offshore Norway (Olesen *et al.* 2002). In addition to changes in the reflectivity and density, the LCB modelled along profile IKU-F correlates with a steep jump in Moho depth (Ritzmann & Faleide 2007) below the central Loppa High (Fig. 3.5C, kilometre 85). The structural and geophysical characteristics of this LCB strengthens our interpretation of it as a core complex (Barrère *et al.* 2009) but better seismic imaging is needed in order to understand how the structures are linked to each other.

3.6.2.5 Eastern and northern zones

East and north of the Loppa High the upper crust (BAS2) consists of two bodies that are different from the upper crust type BAS1. On a regional scale, the BAS1/BAS2 (Figs. 3.4A, 3.5) boundary clearly separates a northeastern zone of platforms from a deeply rifted southwestern zone. The BAS2 crust appears to have a slightly lower magnetic susceptibility (< 3500.10^{-5} SI) to the east and north of the Loppa High and a little higher density (2790 kg/m^3) in the northern areas of the study area.

In the East Barents Sea, the NW-SE striking trends have been interpreted as related to Timanian structures formed in Late Neoproterozoic times (Ivanova 2001), but the northwestern limit of the Timanides, as well as the interactions between Timanian and Caledonian structures remains unclear. Although the western boundary of the BAS2 crustal unit (Fig. 3.4A) is schematic in its definition of the geometry along the vertical sections, the seismic profiles P3 (Fig. 3.5A) and IKU A (Fig. 3.5B) confirm the presence of both a reflectivity change and a possible structural boundary coinciding with contrasting density/magnetisation values. Local basement units (MI bodies, Figs. 3.4A, 3.5B) are interpreted as mafic intrusions; they could be sheets emplaced between the Caledonian nappes or bodies linked to the formation of the Mesozoic basins.

3.6.3 Interpretation of the crustal thinning factor map

Breivik *et al.* (1998) showed a previous crustal thinning factor map highlighting the complexity of the β-ratio pattern over the Tromsø, Bjørnøya and Sørvestsnaget basins, which led them to the theory of a margin formed by continental transform faulting rather than by rifting. Our new map (Fig. 3.4E) shows the composite pattern of the β-ratio over the entire southwestern Barents Sea. High β-factors and an extension mostly N-S to NNE-SSW are confirmed for the basins initiated in Palaeozoic and Cenozoic times along the margin and a E-W to ENE-WSW extension and lower β-factors are mapped for the North Nordkapp and Hammerfest basins that were initiated in Palaeozoic times (Rønnevik & Jacobsen 1984, Gudlaugsson *et al.* 1987, 1998, Faleide *et al.* 1991, 1993, 1996, Breivik *et al.* 1998). The trends of the extension, as well as the intensity of crustal thinning, do not correlate with the ages of the basins. This mismatch is an argument in favour of pre-existing weakness zones

locally controlling the development of the basin architecture. It may also be due to interplay of successive, complex, crustal thinning episodes.

3.6.4 Tectonic Framework

3.6.4.1 The Laurentian/Baltican suture

No evidence of a suture between Laurentia and Baltica has been observed on Svalbard and the Svalbard Caledonian terranes are recognized as the northerly continuation of the Caledonides of eastern Greenland (Gee *et al.* 1995, Witt-Nilsson *et al.* 1998). In addition, all of Svalbard's terranes from west to east are generally considered to be Laurentian (Fortey 1975, Gee & Tebenkov 2004, Cocks & Torsvik 2005, Gee 2005, Torsvik & Cocks 2005), and since the Billefjorden Fault Zone N-S strike-slip system (n°1, Fig. 3.7) occurred between two Laurentian-affinity terranes we disagree with the interpretation of a Caledonian suture along the Billefjorden Fault Zone as suggested by Ritzmann & Faleide (2007). Furthermore, recent studies on Nordaustlandet (eastern Svalbard) (n°2, Fig. 3.7) (Tebenkov *et al.* 2002, Johansson *et al.* 2004, Johansson *et al.* 2005) have reported an increasing metamorphic gradient and intensity of deformation from west to east (Tebenkov *et al.* 2002). High-grade complexes with widespread migmatisation have proven to be Caledonian, high-temperature, low-pressure terranes (Harland 1997) and Caledonian migmatisation has been documented as far northeast as Kvitøya (n°3, Fig. 3.7) (Gee 2004).

For these reasons, we placed the Caledonian suture between Nordaustlandet and Franz Josef Land, in agreement with studies by Gee *et al.* (2006), Mazur *et al.* (2009). We observe a NNE-SSW alignment of strongly focused magnetic anomalies correlating with positive Bouguer anomalies east of Spitsbergen. Despite the fact that these focused magnetic anomalies most likely relate to Late Mesozoic intrusions linked to the significant magmatic event (Grogan *et al.* 1998) at the origin of a Large Igneous Province (Maher 2001), we interpret these intrusions to be controlled in depth by an older weakness zone (n°4, Fig. 3.7) which may coincide with the Caledonian suture.

Consequently, we interpret the offshore path of the Caledonian suture to occur along the outer part of Lofoten, west of the Hammerfest Basin, the Loppa High and the Gardarbanken High (n°5, Fig. 3.7) and then to propagate north-northeastwards towards Kvitøya (n°5, Fig. 3.7). The N-S alignment of the Ringvassøy Loppa, Bjørnøyrenna and Fingerdjupet Fault Complexes and the proposed link to the Billefjorden Fault Zone on Svalbard were consequently interpreted as associated with a deep-seated weakness zone (Skilbrei 1991; Barrère *et al.* 2009) instead of a suture (Breivik *et al.* 2005, Ritzmann & Faleide 2007).

The location of the Caledonian suture between Nordaustlandet and Franz Josef Land (Gee *et al.* 2006) implies the existence of Caledonian thrust sheets in this area. Because the Svalbard Caledonian terranes are direct northerly continuations of the Caledonides of East Greenland (Gee & Tebenkov 2004, Higgins *et al.* 2004), the westward thrusting of the Nordaustlandet Terrane (Gee 2005) is in agreement with the expected general geometry. If the Caledonian suture lies east of Svalbard and if no other mega structure separates the suture and the BFZ it is most likely that the BFZ originated from a mechanism of terrane extrusion linked to an oblique collision of Laurentia and Baltica in that region.

3.6.4.2 Interaction between Timanian and Caledonian structures

In a previous study we interpreted a branch of the Caledonian thrust belt propagating towards the north from NE Finnmark (Barrère *et al.* 2009), with nappes emplaced asymmetrically in the western Barents Sea (n°6, Fig. 3.7). The new 3D model and information derived from the potential fields allow us to elaborate on this scenario and on the complexity of crustal structures.

The major NW trending BAS1/BAS2 boundary in the centre of the southwestern Barents Shelf (n°7, Fig. 3.7) challenges the concept of a Caledonian branch propagating north-eastward (Breivik *et al.* 2002) or a collision fan widening towards the NE (Ritzmann & Faleide 2007).

Empirical and numerical modelling of fold-thrust belt geometry (Macedo & Marshak 1999) have tested the relationship between thrust geometry and geological setting in which the fold belt formed. The hypothetic geometry combining a unique northward

branch and asymmetric nappes emplacement would imply an oblique convergent model and the presence of an asymmetric basin at pre-Caledonian times in the southwestern Barents Sea. In this concept of oblique convergent model, a strike-slip fault forms parallel to the direction of backdrop movement at the vicinity of the fold belt long limb foreland boundary (Macedo & Marshak 1999). Following this model, we interpret the distribution of the nappes as inherited from the Baltica plate geometry. More precisely, the geometry of the Caledonian thrusts is probably due to the existence of an asymmetric Neoproterozoic basin or at least a relatively low area through the southwestern Barents Sea with respect to the NW-SE trending Timanian structures. The following elements are in favour of that interpretation:

(1) The presence of Neoproterozoic pericratonic deposits and deep-water basinal successions in the Parautochthon and Lower Allochthons in Finnmark (Fig. 3.7) (Roberts & Siedlecka 2002, Siedlecka *et al.* 2004, Nystuen *et al.* 2008) have demonstrated the existence of a Neoproterozoic basin along the northeastern Timanian margin.

2) The boundary between the two basement types BAS1 and BAS2 (green solid line, Figs. 3.7B, 3.7C) may be interpreted as the approximate position of the Proterozoic basin border. Due to its position, the immediate surroundings of the basin border were likely of Timanian nature. We interpreted the BAS1/BAS2 boundary (green solid line, Fig.s 3.7B, 3.7C) as a contact between the Caledonian collision prism and Baltica terranes accreted at Late Proterozoic. Thus, we suggest a propagation of the Timanides northwestward until the Caledonian suture (n°7, Fig. 3.7).

(3) The alignment of the Finnmark, Måsøy and Thor Iversen Fault Complexes is interpreted as inherited from a strike-slip fault dextral (n°8, Fig. 3.7) developed parallel to the direction of oblique convergence.

(4) On the Varanger Peninsula, the ENE-WSW-trending frontal Caledonian thrust is mapped overriding the TKFZ (n°9, Fig. 3.7) and truncates the NW-SE-trending Timanian structures.

A. Crustal thickness and basement units

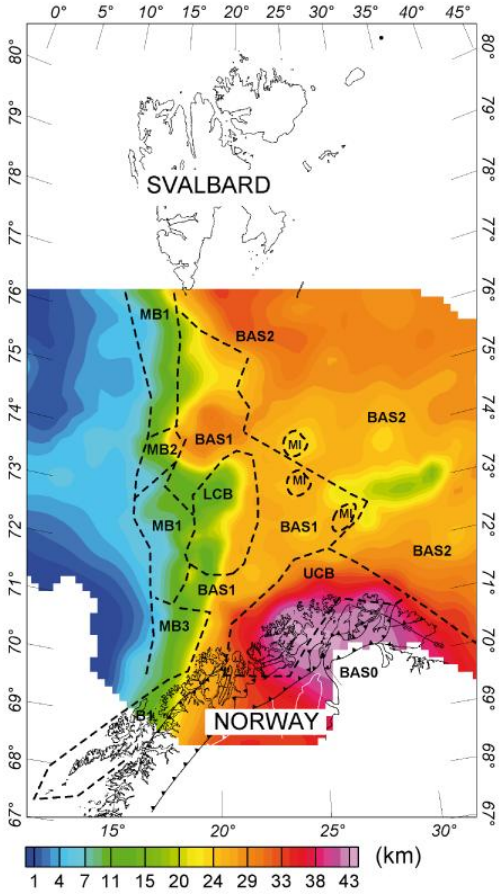

B. Total magnetic field and interpreted lineaments

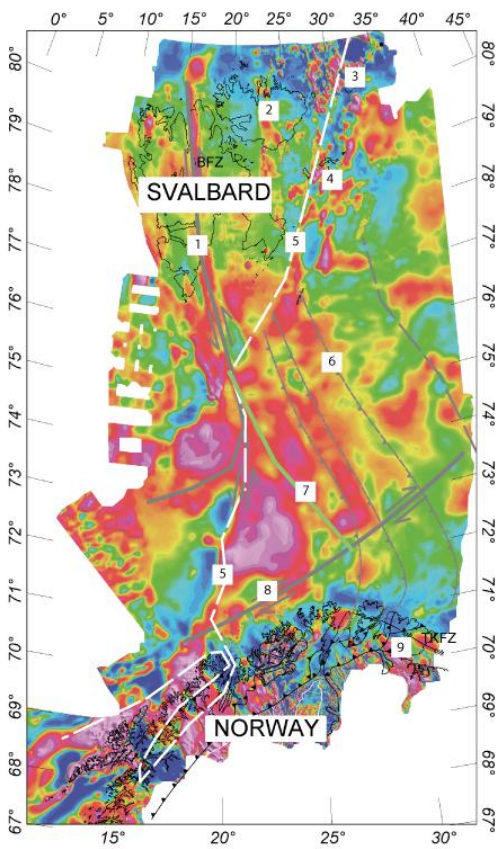

C. Regional geological interpretation

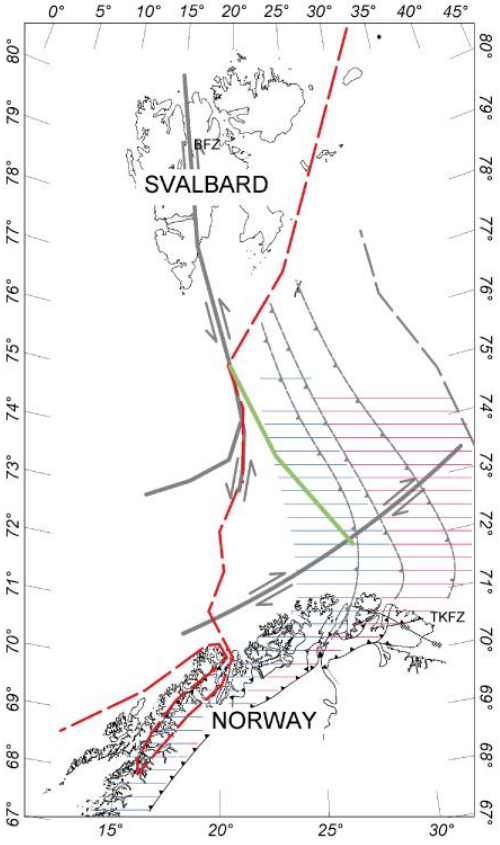

2 Nordaustlandet

3 Kvitøya

TKFZ Trollfjorden-Komagelva Fault Zone

BFZ Billefjorden Fault Zone

Interpreted Caledonian suture

Onshore Caledonian thrusts

Interpreted prolongation of the Caledonian thrusts (Barrère et al. 2009a)

Proposed Caledonian deformation front

Weakness zone inherited from the Caledonian orogeny

Interpreted onshore-offshore prolongation of the Lower Allochthon

Interpreted onshore-offshore prolongation of the Middle/Upper Allochthon

Boundary between BAS1 and BAS2 basement units

Figure 3.7:

A. The map shows interesting correlations between the known structural elements, the modelled crustal thickness and the interpreted basement units.

B. The map presents the interpreted structural lineaments after integration of our 3D density/magnetic model with the geophysical and geological information available on top of the magnetic data modelled. We show the suggested locations of a Caledonian suture, the offshore prolongation of the Caledonian thrusts, main Caledonian weakness zones as well as the delimitation of a Palaeoproterozoic basin part of the Baltica Plate. The map also shows that the magnetic anomalies are closely related to both basement lithology and structural elements. For further explanation and reference to numbers, see text.

C. The structural map shows the interpreted lineaments and offshore prolongations of the Caledonian nappes. This map summarises our regional geological interpretation presenting our vision of the distribution of the Caledonian orogenic extension and associated weakness zones. Our study also suggests the existence of a Palaeoproterozoic basin that controlled the Caledonian trend of the thrusts and the later suture geometry.

3.6.5 Evolution of sedimentary basins

We now discuss the relationship between the weakness zones (n°1, 4, 5, 6, 7 and 8 Fig. 3.7) and the crustal thickness (Figs. 3.4C, 3.7).

The Ringvassøy-Loppa and Bjørnøyrenna Fault Complexes to the west of the Loppa High (Figs. 3.1, 3.4D, 3.7) dip westwards and are interpreted as structures controlling the crustal thinning that created the Tromsø and Bjørnøya Basins. The existence of important fault complexes bounding these two basins provides arguments in favour of a crustal thinning controlled by pre-existing large-scale faults. Nevertheless, the fact that shallow deformation (i.e., at crustal scale) was focused along pre-existing weakness zones does not necessarily mean that this scenario is valid at lithospheric scale. More complex depth- and/or time-dependent, lithospheric thinning processes may also be involved (e.g., Kuzsnir *et al.* 2004).

Previously, we highlighted the fact that the trends of the offshore prolongation of the Caledonian thrusts correlate with the segmentation of the Nordkapp Basin,

suggesting a direct link between ancient Caledonian weakness zones trending NNW-SSE and changes in the shape of the Nordkapp Basin (Gernigon *et al.* 2007, Barrère *et al.* 2009). The new 3D modelling suggests that the Nordkapp Basin developed within both the BAS1 and the BAS2 crustal units. Thus, we interpret the Nordkapp Basin to be located at the meeting point of the Timanian and Caledonian trends. Ancient Caledonian thrusts and older Timanian weakness zones may have facilitated rifting. In that concept, the NW-SE magnetic trends east of the Loppa High have an uncertain origin; (1) they may be linked to susceptibility contrasts between Caledonian nappes or (2) to susceptibility variations within the Timanides similar to the strong linear magnetic anomalies observed in association with the Timanian terranes in the Timan Range and Pechora Basin farther southeast.

3.7 Conclusions

In this contribution, we present a new 3D model for the SW Barents Shelf that provides new insights into the complex 3D crustal architecture.

(1) The new top basement map highlights the regional differences between the platforms, the deep basins and the transition to the North Atlantic Ocean. The resulting crustal thickness and crustal thinning ratio maps show the occurrence of significant thinning processes in the western part of the Barents Sea. Furthermore, the trends of the extensions, as well as the intensity of crustal thinning, do not correlate with the ages of the basins, a feature that favours the pre-existence of crustal weakness zones, which controlled the initiation of the basin architecture and ensuring complex basin evolution. On the one hand, we suggest that pre-existing Caledonian and Timanian weakness zones exerted a strong control on basin evolution east of the Loppa High. On the other hand, formation of the western basins (i.e., the Tromsø and Bjørnøya Basins) was controlled mostly by the reactivation of the Caledonian suture, which coincides with the alignment of the Bjørnøyrenna and Ringvassøy-Loppa Fault Complexes.

(2) Our new crustal units map proposes a noticeable NW-SE trending upper crustal boundary interpreted as the contact between terranes inherited from the Caledonian

fold and thrust belt and Baltican terranes only weakly affected by the Caledonian orogeny.

(3) The regional interpretation integrating the 3D model with the interpreted weakness zones shows a very asymmetric Caledonian collisional extension with an unique Caledonian arm, and a Caledonian suture to the west of the Loppa High propagating northwards between Svalbard and Franz Josef Land. East of this suture, there is a fan of nappes thrusted eastward in the southwestern Barents Sea and bounded to the south by a fault zone parallel to the oblique convergence between Baltica and Laurentia. This strike-slip fault system lies along the alignment of the Finnmark and Måsøy and Thor Iversen Fault Complexes. West of the suture, we observe the development of a complex fault system involving the transport of Laurentia terranes along strike slip systems such as the Billefjorden Fault Zone. These transported terranes would be the origin of the Svalbard assemblage.

Acknowledgements

The study was carried out as part of the projects “Basement Heat Generation and Heat Flow in the western Barents Sea – Importance for hydrocarbon systems" (Petromaks project 169438) funded by the PETROMAKS programme of the Research Council of Norway and StatoilHydro. We thank Jan Reidar Skilbrei for initiating the project and our project leader Christophe Pascal for administrating it. Laurent Gernigon's contribution is part of the Petrobar project, also funded by the PETROMAKS programme of the Research Council of Norway. We thank also StatoilHydro and particularly Peter Midbøe and Trond Zakariassen for providing us with the seismic depth converted horizons. We also thank Oliver Ritzmann and Stoney Clark from the university of Oslo for information on the Barents50 model and new OBS data. We are very grateful to Odleiv Olesen and David Roberts for discussions and comments on earlier versions of the manuscript. We are very grateful to David Roberts for editorial review before paper submission.

References

Andersen, T.B., 1998. Extensional tectonics in the Caledonides of southern Norway, an overview, Tectonophysics, 285, 333-351.

Barnes, C.G., Frost, C.D., Yoshinobu, A.S., McArthur, K., Barnes, M.A. Allen, C.M., Nordgulen, Ø. & Prestvik, T., 2007. Timing of sedimentation, metamorphism, and plutonism in the Helgeland Nappe Complex, north-central Norwegian Caledonides. *Geosphere* 3, 683–703.

Barrère, C., Ebbing, J. & Gernigon, L., 2009. Offshore prolongation of Caledonian structure and basement characterisation in the western Barents Sea from geophysical modelling, *Tectonophysics*, 470, 71-88.

Breivik, A.J., Gudlaugsson, S.T. and Faleide, J.I., 1995. Ottar-Basin, Sw Barents-Sea - a Major Upper Paleozoic Rift Basin Containing Large Volumes of Deeply Buried Salt. *Basin Research*, 7(4): 299-312.

Breivik, A.J., Faleide, J.I. & Gudlaugsson, S.T., 1998. Southwestern Barents Sea margin: late Mesozoic sedimentary basins and crustal extension, *Tectonophysics,* 293**,** 21-44.

Breivik, A.J., Mjelde, R., Grogan, P., Shimamura, H., Murai, Y. & Nishimura, Y., 2003. Crustal structure and transform margin development south of Svalbard based on ocean bottom seismometer data, *Tectonophysics,* 369**,** 37-70.

Breivik, A.J., Mjelde, R., Grogan, P., Shimamura, H., Murai, Y. & Nishimura, Y., 2005. Caledonide development offshore-onshore Svalbard based on ocean bottom seismometer, conventional seismic, and potential field data, *Tectonophysics,* 401**,** 79-117.

Breivik, A.J., Mjelde, R., Grogan, P., Shimamura, H., Murai, Y., Nishimura, Y. & Kuwano, A., 2002. A possible Caledonide arm through the Barents Sea imaged by OBS data, *Tectonophysics,* 355**,** 67-97.

Braathen, A., Osmundsen, P.T., Nordgulen, O., Roberts, D. & Meyer, G.B., 2002. Orogen-parallel extension of the Caledonides in northern Central Norway: an overview, *Norwegian Journal of Geology,* 82**,** 225-241.

Clark**,** S. A., Faleide, J. I., Ritzmann, O. and Mjelde, R. 2009. Multi-stage rift evolution of the SW Barents Sea from wide-angle seismic velocity modeling. EGU2009-12559.

Cocks, L.R.M. & Torsvik, T.H., 2005. Baltica from the late Precambrian to mid-Palaeozoic times: The gain and loss of a terrane's identity, *Earth-Science Reviews,* 72**,** 39-66.

Corfu, F., Torsvik, T.H., Andersen, T.B., Ashwal, L.D., Ramsay, D.M. & Roberts, R.J., 2006. Early Silurian mafic-ultramafic and granitic plutonism in contemporaneous flysch, Magerøy, northern Norway: U-Pb ages and regional significance, *Journal of the Geological Society,* 163**,** 291-301.

Daly, V.V. Balagansky, M.J. Timmerman and M.J. Whitehouse, The Lapland-Kola Orogen: Palaeoproterozoic collision and accretion of the northern Fennoscandian lithosphere. In: D.G. Gee and R. Stephenson, Editors, European Lithosphere Dynamics, *Geological Society, London Memoir* vol. 32 (2006), pp. 579–597.

Dibner, V.D., 1998. Geology of Franz Josef Land, *Norsk Polarinstitut, Oslo, Meddelelse,* 146.

Ebbing, J., Gernigon, L., Pascal, C., Olesen, O. and Osmundsen, P.T., 2009. A discussion of structural and thermal control of magnetic anomalies on the mid-Norwegian margin. *Geophysical Prospecting*, 57, 665-681.

Faleide, J.I., Gudlaugsson, S.T., Eldholm, O., Myhre, A.M. & Jackson, H.R., 1991. Deep Seismic Transects across the Sheared Western Barents Sea-Svalbard Continental-Margin, *Tectonophysics,* 189**,** 73-89.

Faleide, J.I., Vågnes, E. & Gudlaugsson, S.T., 1993. Late Mesozoic-Cenozoic Evolution of the South-Western Barents Sea in a Regional Rift Shear Tectonic Setting, *Marine and Petroleum Geology,* 10**,** 186-214.

Faleide, J.I., Solheim, A., Fiedler, A., Hjelstuen, B.O., Andersen, E.S. & Vanneste, K., 1996. Late Cenozoic evolution of the western Barents Sea-Svalbard continental margin, *Global and Planetary Change,* 12**,** 53-74.

Fortey, R.A., 1975. Early Ordovician Trilobites of Spitzbergen III, *Norsk Polarinstitutt Skrifter,* 171**,** 1-263.

Gaal, G. & Gorbatschev, R., 1987. An outline of the Precambrian evolution of the Baltic Shield, *Precambrian Research,* 35**,** 15-52.

Gabrielsen, R.H., 1984. Long-lived fault zones and their influence on the tectonic development of the southwestern Barents Sea., *Journal of the Geological Society,* 141**,** 651-662.

Gabrielsen, R.H., Færseth, R.B., Jensen, L.N., Kalheim, J.E. & Riis, F., 1990. Structural elements of the Norwegian continental shelf. Part I: The Barents Sea Region., *Norwegian Petroleum Directorate Bulletin*.

Galitchanina, L.D., Glaznev, V.N., Mitrofanov, F.P. & Olesen, O., 1995. Surface density characteristics of the Baltic Shield and adjacent territories, *Norwegian Journal of Geology,* Special Publi.**,** 349-354.

Gee, D.G., 2004. The Barentsian Caledonides: death of the High Arctic Barents Craton. *in Arctic Geology, Hydrocarbon Resources and Environmental Challenges. NGF Abstracts and Proceedings, 2*, pp. 48-49, eds. Smelror, M. & Bugge, T.

Gee, D.G., 2005. Scandinavian Caledonides (with Greenland). pp. 64-74, eds Selley, R. C., Cocks, L. R. M. & Plimer, I. R. Encyclopedia of Geology.

Gee, D.G., Johansson, A., Ohta, Y., Tebenkov, A.M., Krasilschikov, A.A., Balashov, Y.A., Larionov, A.N., Gannibal, L.F. & Ryungenen, G.I., 1995. Grenvillian Basement and a Major Unconformity within the Caledonides of Nordaustlandet, Svalbard, *Precambrian Research,* 70**,** 215-234.

Gee, D.G., Bogolepova, O.K. & Lorenz, H., 2006. The Timanide, Caledonide and Uralide orogens in the Eurasian high Arctic, and relationships to the palaeo-continents Laurentia, Baltica and Siberia. *in European Lithosphere Dynamics*, pp. 507-521, eds Gee & Stephenson. Geological Society of London.

Gee, D.G. & Pease, V.L., 2004. The Neoproterozoic Timanide Orogeny of Eastern Baltica, *Geological Society London Memoirs,* 30**,** 191-207.

Gee, D.G. & Tebenkov, A., 2004. Svalbard: a fragment of the Laurentian margin. *in The Neoproterozoic Timanide Orogen of eastern Baltica: introduction*, pp. 191-206, eds Gee, D. G. & Pease, V. L. Geological Society London.

Gernigon, L., Marello, L., Mogaard, J.O., Werner, S.C. and Skilbrei, J.R., 2007. Barents Sea Aeromagnetic Survey BAS - 06: Acquisition-processing report and preliminary interpretation. NGU Report 2007.035, Geological Survey of Norway, Trondheim, 142 p.

Grogan, P., Nyberg, K., Fotland, B., Myklebust, R., Dahlgren, S. & Riis, F., 1998. Cretaceous magmatism south and east of Svalbard: evidence from seismic reflection and magmatic data., *Polar Research,* 68**,** 11-13.

Gudlaugsson, S.T. & Faleide, J.I., 1994. The continental margin between Spitsbergen and Bjørnøya. *in Seismic Atlas of Western Svalbard, Medd*, pp. 11-13, ed Eiken, O. Norwegian Polarinstitut.

Gudlaugsson, S.T., Faleide, J.I., Fanavoll, S. & Johansen, B., 1987. Deep Seismic-Reflection Profiles across the Western Barents Sea, *Geophysical Journal of the Royal Astronomical Society,* 89**,** 273-278.

Gudlaugsson, S.T., Faleide, J.I., Johansen, S.E. & Breivik, A.J., 1998. Late Palaeozoic structural development of the South-western Barents Sea, *Marine and Petroleum Geology,* 15**,** 73-102.

Gunn, P.J., 1997. Application of aeromagnetic surveys to sedimentary basin studies, *Journal of Australian Geology & Geophysics,* 17**,** 133-144.

Götze, H.J. & Lahmeyer, B., 1988. Application of 3-Dimensional Interactive Modeling in Gravity and Magnetics, *Geophysics,* 53**,** 1096-1108.

Harland, W.B., 1997. The Geology of Svalbard, *Geological Society London Memoirs,* 17.

Higgins, A.K., Elvevold, S., Escher, J.C., Frederiksen, K.S., Gilotti, J.A., Henriksen, N., Jepsen, H.F., Jones, K.A., Kalsbeek, F., Kinny, P.D., Leslie, A.G., Smith, M.P., Thrane, K. & Watt, G.R., 2004. The foreland-propagating thrust architecture of the East Greenland Caledonides 72 degrees-75 degrees N, Journal of the Geological Society, 161, 1009-1026.

Hossack, J. R. 1984. The geometry of listric normal faults in the Devonian basins of Sunnfjord, Western Norway. *Journal of the Geological Society of London 141*, 629-637.

Ivanova, N.M., 2001. The geological structure and petroleum potential of the Kola-Kanin Monocline, Russian Barents Sea, *Petroleum Geoscience,* 7**,** 343-350.

Jakobsson, M., Cherkis, N.Z., Woodward, J., Macnab, R. & Coakley, B., 2000. New grid of Arctic bathymetry aids scientists and mapmakers, *Eos, Transactions, American Geophysical Union,* 81**,** 89-96.

Johansson, A., Larionov, A.N., Gee, D.G., Ohta, Y., Tebenkov, A.M. & Sandelin, S., 2004. Grenvillian and Caledonian tectonomagmatic activity in northeasternmost Svalbard. *in The Neoproterozoic Timanide Orogeny of Eastern Baltica*, pp. 207-233, eds. Gee, D. G. & Pease, V. L. Geological Society, London, Memoirs, 30.

Johansson, A., Gee, D.G., Larionov, A.N., Ohta, Y. & Tebenkov, A.M., 2005. Grenvillian and Caledonian evolution of eastern Svalbard - a tale of two orogenies, *Terra Nova,* 17**,** 317-325.

Kapland, A.A., Copeland, P. & Bro, E.G., 2001. New radiogenic age of igneous and metamorphic rocks from the Russian Arctic *in In: VIIGRI/AAPG International Conference 'Exploration and Production Operations in Difficult and Sensitive Areas', St. Petersburg, 06-2.*

Kostyuchenko, S.L., Sapozhnikov, R., Egorkin, A., Gee, D.G. , Berzin R. & Solodilov, L.N. , 2006. Crustal structure and tectonic model of notheastern Baltica, based on deep seismic and potential field data. In: D.G. Gee and R.A. Stephenson, Editors, *European Lithosphere Dynamics*, Memoirs vol. 32, Geological Society, London (2006), pp. 521–539.

Kusznir, N. J., Hunsdale, R. & Roberts, A. M. 2004. Timing of depth-dependent lithosphere stretching on the S. Lofoten rifted margin offshore Mid-Norway: Pre-breakup or post-breakup? Basin Research, 16, 279–296.

Macedo, J. & Marshak, S., 1999. Controls on the geometry of fold-thrust belt salients, *Geological Society of America Bulletin,* 111**,** 1808-1822.

Maher, H.D., 2001. Manifestations of the Cretaceous High Arctic Large Igneous Province in Svalbard, *Journal of Geology,* 109**,** 91-104.

McKenzie, D., 1978. Some remarks on the development of sedimentary basins, *Earth Planet Scientific Letters,* 40**,** 25-32.

Mjelde, R., Breivik, A.J., Elstad, H., Ryseth, A.E., Skilbrei, J.R., Opsal, J.G., Shimamura, H., Murai, Y. & Nishimura, Y., 2002. Geological development of the Sorvestsnaget Basin, SW Barents Sea, from ocean bottom seismic, surface seismic and gravity data, *Norwegian Journal of Geology,* 82**,** 183-202.

Nystuen, J.P., Andresen, A., Kumpulainen, R.A. & Siedlecka, A., 2008. Neoproterozoic basin evolution in Fennoscandia, East Greenland and Svalbard, *Episodes,* 31.

Olesen, O., Roberts, D., Henkel, H., Lile, B.L. & Torsvik, T.H., 1990. Aeromagnetic and gravimetric interpretation of regional structural features in the Caledonides of West Finnmark and North Troms, northern Norway. *Norges geologiske undersøkelse Bulletin 419***,** 1-24.

Olesen, O., Torsvik, T.H., Tveten, E., Zwaan, K.B., Løseth H. & Henningsen, T. 1997. Basement structure of the continental margin in the Lofoten-Lopphavet area, northern Norway: constraints from potential field data, on-land structural mapping and palaeomagnetic data. *Nor. Geol. Tidsskr. 77,* 15-33.

Olesen, O., Lundin, E., Nordgulen, Ø., Osmundsen, P.T., Skilbrei, J.R., Smethurst, M.A., Solli, A. & Fichler, C., 2002. Bridging the gap between the onshore and offshore geology in Nordland, northern Norway, *Norwegian Journal of Geology,* 82, 243-262.

Olesen, O., Gernigon, L., Ebbing, J., Mogaard, J.O., Pascal, C. & Wienecke, S., 2006. Interpretation of aeromagnetic data along the Jan Mayen Fracture Zone, JAS-05., *Geological Survey of Noway (NGU)* Report 2006.018 (confidential to 17.02.2011)**,** 162.

Osmundsen, P.T., Sommaruga, A., Skilbrei, J.R. & Olesen, O., 2002. Deep structure of the Mid Norway rifted margin, *Norwegian Journal of Geology,* 82**,** 205-224.

Osmundsen, P.T., Braathen, A., Nordgulen, O., Roberts, D., Meyer, G.B. & Eide, E., 2003. The Devonian Nesna shear zone and adjacent gneiss-cored culminations, North-Central Norwegian Caledonides, *Journal of the Geological Society,* 160**,** 137-150.

Ritzmann, O. & Faleide, J.I., 2007. Caledonian basement of the western Barents Sea, *Tectonics,* 26.

Ritzmann, O., Maercklin, N., Faleide, J.I., Bungum, H., Mooney, W.D. & Detweiler, S.T., 2007. A three-dimensional geophysical model of the crust in the Barents Sea region: Model construction and basement characterization, *Geophysical Journal International,* 170**,** 417-435.

Roberts, D., 1983. Devonian tectonic deformation in the Norwegian Caledonides and its regional perspectives., *Norges geologiske undersøkelse Bulletin***,** 85-96.

Roberts, D., 2003. The Scandinavian Caledonides: event chronology, palaeogeographic settings and likely modern analogues, *Tectonophysics***,** 283-299.

Roberts, D. & Gale, G.H., 1978. The Caledonian-Appalachian Iapetus Ocean. in The evolution of the Earth's crust, pp. 255-341, ed. Tarling, D.

Roberts, D. & Gee, D.G., 1985. An introduction to the structure of the Scandinavian Caledonides. In Gee, D.G. & Sturt, B.A. (eds) The Caledonide Orogen – Scandinavia and related areas. John Wiley & Sons,Chichester, 55-68.

Roberts, D. & Nordgulen, Ø. (editors) 1995. Geology of the eastern Finnmark–western Kola Peninsula region. Norges geologiske undersøkelse Special Publication 7, 378 pp.

Roberts, D. & Lippard, S.J., 2005. Inferred Mesozoic faulting in Finnmark: current status and offshore links., *Norges Geologiske Undersøkelse Bulletin,* 443**,** 55-60.

Roberts, D. & Olovyanishnikov, V., 2004. Structural and tectonic development of the Timanide orogen., *Geological Society London Memoirs,* 30**,** 47-57.

Roberts, D. & Siedlecka, A., 2002. Timanian orogenic deformation along the northeastern margin of Baltica, Northwest Russia and Northeast Norway, and Avalonian-Cadomian connections, *Tectonophysics,* 352**,** 169-184.

Roberts, D., Torsvik, T.H., Andersen, T.B. & Rehnström, E.F., 2003. The Early Carboniferous Magerøy dykes, northern Norway: palaeomagnetism and palaeogeography., *Geological Magazine,* 140**,** 443-451.

Roberts, R.J., Corfu, F., Torsvik, T.H., Ashwal, L.D. & Ramsay, D.M., 2006. Short-lived mafic magmatism at 560-570 Ma in the northern Norwegian Caledonides: U-Pb zircon ages from the Seiland Igneous Province, *Geological Magazine,* 143**,** 887-903.

Roberts, D., Nordgulen, Ø. and Melezhik, V., 2007. The Uppermost Allochton in the Scandinavian Caledonides: From a Laurentian ancestry through Taconian orogeny to Scandian crustal growth on Baltica. In: Hatcher, R.D.J., Carlson, M.P., McBride, J.H. and Martinez-Catalan, J.R., (Eds.), 4-D framework of continental crust, Geological Society of America Memoir, 200, 357-377.

Robins, B., 1998. The mode of emplacement of the Honningsvåg Intrusive Suite, Magerøya, northern Norway, *Geological Magazine,* 135**,** 231-244.

Rønnevik, H.C. & Jacobsen, H.P., 1984. Structures and Basins in the Western Barents Sea. *in Petroleum Geology of the North European Margin.*, pp. 19-32, ed Spencer, A. M. e. a. Norwegian Petroleum Society.

Sanner, S., 1995. Et seismisk hastighetsstudium i Barentshavet. C*and. Scient. thesis (in Norwegian), Department of Geology, University of Oslo, Oslo, Norway*.

Siedlecka, A., 1975. Late Precambrian Stratigraphy and Structure of the North-Eastern Margin of the Fennoscandian Shield (East Finnmark - Timan Region), *Norges geologiske undersøkelse Bulletin,* 316**,** 313-348.

Siedlecka, A. & Roberts, D., 1996. Finnmark Fylke, Berggrunnsgeologi M 1:500 000, *Norges geologiske undersøkelse,Trondheim.*

Siedlecka, A., Roberts, D., Nystuen, J.P. & Olovyanishnikov, V.G., 2004. Northeastern and northwestern margins of Baltica in Neoproterozoic time: evidence from the Timanian and Caledonian Orogens. *in The Neoproterozoic Timanide Orogen of Eastern Baltica*, pp. 169-190, eds. Gee, D. G. & Pease, V. L. Geological Society, London, Memoirs.

Skilbrei, J.R., 1991. Interpretation of Depth to the Magnetic Basement in the Northern Barents Sea (South of Svalbard), *Tectonophysics,* 200**,** 127-141.

Skilbrei, J.R., 1995. Aspects of the geology of the southwestern Barents sea from aeromagnetic data. *Norges geologiske undersøkelse Bulletin* 427, 64-67.

Skilbrei, J.R., Skyseth, T. & Olesen, O., 1991. Petrophysical Data and Opaque Mineralogy of High-Grade and Retrogressed Lithologies - Implications for the Interpretation of Aeromagnetic Anomalies in Northern Vestranden, Central Norway, Tectonophysics, 192, 21-31.

Skilbrei, J.R., Kihle, O., Gellein, J., Solheim, D., Nyland, B., 2000. Gravity anomaly map, Norway and adjacent ocean areas. M 1:3 000 000. Geological Survey of Norway.

Slagstad, T., Barrère, C., Davidsen, B. & Ramstad, R.K., 2008. Petrophysical and thermal properties of pre-Devonian basement rocks on the Norwegian continental margin, Geological Survey of Norway Bulletin, 448, 1-6.

Stephens, M.B., & Gee, D.G., 1989. Terranes and polyphase accretionary history in the Scandinavian Caledonides, in Dallmeyer, R.D. (ed) Terranes in the Circum-Atlantic Paelozoic Orogens. *Geological Society of America* Special Paper 230, 17–30.

Tebenkov, A.M., Sandelin, S., Gee, D.G. & Johansson, A., 2002. Caledonian migmatization in central Nordaustlandet, Svalbard, *Norwegian Journal of Geology,* 82**,** 15-28.

Torsvik, T.H. & Cocks, L.R.M., 2005. Norway in space and time: A Centennial cavalcade, *Norwegian Journal of Geology,* 85**,** 73-86.

Torsvik, T.H., Smethurst, M.A., Meert, J.G., Van der Voo, R., McKerrow, W.S., Brasier, M.D., Sturt, B.A. & Walderhaug, H.J., 1996. Continental break-up and collision in the Neoproterozoic and Palaeozoic - A tale of Baltica and Laurentia, *Earth-Science Reviews,* 40**,** 229-258.

Tsikalas, F., 1992. A study of seismic velocity, density and porosity in Barents Sea wells (N. Noway). (Unpublished Master Thesis), Master, University of Oslo, Oslo, Norway.

Witt-Nilsson, P., Gee, D.G. & Hellman, F.J., 1998. Tectonostratigraphy of the Caledonian Atomfjella Antiform of northern Ny Friesland, Svalbard, *Norsk Geologisk Tidsskrift,* 78**,** 67-80.

Ziegler, P.A., 1988. Evolution of the Arctic-North Atlantic and the western Tethys, *Am. Assoc. Petrol. Geol. Mem.,* 48**,** 198.

Åm, K., 1975. Aeromagnetic basement complex mapping north of latitude 62 N, Norway, *Norges geologiske undersøkelse,* 316**,** 351-374.

Abbreviation list:

AFC:	Asterias Fault Complex
BB:	Bjørnøya Basin
BFC:	Bjørnøyrenna Fault Complex
BI:	Bjørnøya
BP:	Bjarmeland Platform
FFC:	Finnmark Fault Complex
FP:	Finnmark Platform
FSb:	Fingerdjupet Subbasin
GH:	Gardarbanken High
HB:	Harstad Basin
HmB:	Hammerfest Basin
LFC:	Leirdjupet Fault Complex
LH:	Loppa High
MB:	Maud Basin
MFC:	Måsøy Fault Complex
MI:	Magerøya
NB:	Nordkapp Basin
ND:	Norvarg Dome
NH:	Norsel High
RLFC:	Ringvassøy-Loppa Fault Complex
SB:	Sørvestsnaget Basin
SD:	Samson Dome
SG:	Swaen Graben
SH:	Stappen High
SR:	Senja Ridge
SvD:	Svalis Dome
SøB:	Sørkapp Basin
TB:	Tromsø Basin
TbB:	Tiddlybanken Basin
TIFC:	Thor Iversen Fault Complex
VH:	Veslemøy High
Vvp:	Vestbakken volcanic province

Chapter 4

Tectonic evolution of the Bjørnøya Basin and Loppa High, southwestern Barents Sea

- new insights into post-Caledonian features

Cécile Barrère, Laurent Gernigon and Jörg Ebbing

Submitted to Geological Society of America Bulletin, August 2009

Is not included due to copyright

Chapter 5

Integrated modelling and heat flow estimations, case study along a 2D profile across the southwestern Barents Shelf

Cécile Barrère and Hermann Zeyen

Manuscript in preparation

Is not included due to copyright

Chapter 6. Synthesis

6.1 Workflow

The different chapters in this thesis present the different steps necessary to understand the lithospheric and thermal structure of the Western Barents Sea. 2D forward gravity and magnetic models (Paper I) constrained by industrial seismic profiles, well data and onshore geological and petrophysical database are used as a preliminary work providing modelling parameters, hypothesis for the interpretation of the potential field maps and an initial crustal architecture to the 3D modelling presented (Paper II). The 3D forward gravity and magnetic modelling benefits of new constraints as industrial depth converted sedimentary horizons enhances and extends the crustal structure. The 3D model provides key elements as the top basement and Moho depth and highlights the complexity of the deep crust to the west of the Loppa High and a contrast in density and particularly magnetic properties within the southwestern Barents Sea basement rocks. More particularly, it provides a regional geological interpretation.

The papers III and IV further assist in increasing our geological knowledge about the southwestern Barents Shelf. The modelling presented in paper III follows basically the same workflow presented within paper I but the high quality 2D seismic profile offers very good constraints on the top basement and crustal reflectivity enhancing details in the gravity and magnetic model, which allow to develop new concepts regarding the tectonic relationship between the Loppa High and Bjørnøya Basin.

The modelling in paper IV further extends the modelling from gravity and magnetic data to geoid, topography and heat flow data. The modelling uses crustal structures from paper III as input and changes the crustal model in a lithospheric scale model allowing to model the lithosphere asthenosphere boundary (LAB). Although the heat flow modelling is poorly constrained due to a sparse heat flow database offshore, the relative effect of the Caledonian nappes on top of the Archaean to Palaeoproterozoic rocks on surface heat flow is investigated. Moreover, geoid and topography modelling provide an interesting picture of the geometry of the LABsupporting geological and geodynamical interpretations. Finally, together with the topography modelling, elastic thickness modelling allows to discuss

the isostatic state of the Barents Sea region.

6.2 Main results of the thesis

6.2.1 2D potential field modelling and map interpretation: A first step towards a review of the Caledonian thrusts geometry

We constructed 2¾D density and magnetic models, which allowed a preliminary basement characterisation and insight into deep crustal structures. We propose a new regional interpretation with an elbow shaped prolongation of the Caledonian orogene into the southwestern Barents Sea. Furthermore, an east-west gradient of the Caledonian deformation is proposed with thick-skinned deformation to the west of the Loppa High becoming thin-skinned towards east.

6.2.2 Integrated 3D modelling: Evolution of the western Barents Shelf

Our 3D potential field model produces a revised set of maps for top basement, Moho, crustal thickness and related thinning-ratio. These maps reveal an appreciable thinning of the crust to the west of the Ringvassøy-Loppa and Bjørnøyrenna Fault Complexes. Our 3D model allowed to classify basement units. The basement units distribution and potential field maps support the hypothesis of a swing toward Svalbard of the Caledonian thrusts mapped onshore. This leads to a re-evaluation of the tectonic framework and triggers a discussion about sedimentary basin evolution. Pre-existing Caledonian and Timanian weakness zones have probably exerted a strong control on basin evolution east of the Loppa High. However, formation of the western basins (i.e., the Tromsø and Bjørnøya Basins) was also heavily controlled by the reactivation of the Caledonian suture, which coincides with the alignment of the Bjørnøyrenna and Ringvassøy-Loppa Fault Complexes. We further propose a very asymmetric Caledonian collisional prism with an unique Caledonian arm, and a Caledonian suture to the west of the Loppa High propagating northwards between Svalbard and Franz Josef Land.

6.2.3 The Bjørnøya Basin formation: Crustal structure and rifting processes

The seismic interpretation and joint magnetic and gravity modelling along the NBR07-232948 seismic reflection transect precise the crustal structure that has led to the

severe crustal thinning highlighted to the west of the Loppa High. This high quality seismic data highlight the tectonic relationships between the Bjørnøya Basin and the Loppa High. Post Caledonian structures comparable to the ones typically observed of mid-Norway seismic data are observed. An updated scenario for the Bjørnøya Basin/Loppa High tectonic evolution is proposed. Also, the crustal structure is discussed in terms of stretching model.

6.2.4 Thermal Modelling: Lithosphere and tectonics

A 2D lithospheric scale model across the southwestern Barents Shelf was developed using the well constrained geometry of profile NBR07-232948 combined with the IKU_B profile as input into a heat flow modelling software (CAGES).

The model shows that Caledonian nappes contribute to the surface heat flow with 10 mW/m^2. The elevation modelling required a high flexural rigidity for the compensation of the load in the southwestern Barents Shelf. We recommend an elastic plate thickness of about 30 km for our model. Finally, the model analysis suggests that the Loppa High is situated at the transition between the Archaean to Palaeoproterozoic and Palaeozoic lithospheres. This result supports our previous regional interpretations, which place the Loppa High at the boundary of the Baltica Plate and suggests that the elbow shaped geometry of the Caledonian thrusts originates from the palaeogeography of the Baltica Plate in Silurian time.

6.3 Conclusions

The integration of geophysical modelling, geological information and the potential field maps leads to a re-evaluation of the tectonic framework of the western Barents Shelf. In this thesis, I propose an offshore prolongation of the Caledonian orogen with a swing towardSvalbard with respect to the Caledonian thrusts mapped onshore. Also, the Caledonian suture is placed to the west of the Loppa High and its northward propagation between Svalbard and Franz Josef Land. These Caledonian structures greatly impact the evolution of the southwestern Barents Sea basins. Variation in the crustal composition correlate with variation of lithosphere thickness: The Loppa High appears at a key location with Palaeozoic lithosphere inherited from the Caledonian orogeny to its west and Precambrian lithosphere inherited from the Timanian orogeny

to the east. The contrast in lithosphere characteristics (i.e., temperature and related rheology) appears to be caused by a limited propagation of the Caledonian deformation towards the east. The diversity of basin orientations and crustal structures is related to the complex association of ancients Caledonian weakness zones, crustal composition and lithosphere age. The high elastic thickness estimated for the study area implies a flexural component in the compensation for the sedimentary load and consequently in the basin formation supporting the formation of asymmetric basins.

6.4 Closing remarks

As every research work in applied geophysics, this large scale study of the southwestern Barents Shelf should be improved including more detail and accuracy in the interpretations using the most modern and high-quality data available. I think a significant improvement of the 3D joint density and magnetic model is possible by using models based on the entire NBR07 dataset as constraints. The high quality of the NBR07 dataset would allow the restoration and balancing of the geological structures interpreted along the profile. Even better, a complete restoration of the Loppa High in 3D could be achieved. Introducing thermal calculations in the modelling process opens the way to reconstruct the entire present-day lithospheric structure.

Based on the presented work, 3D thermal modelling from the southwestern Barents Shelf is currently being carried out at NGU. Interesting results including an estimation of well constrained surface heat flow and heat flow maps at the base of the sedimentary basins and at Moho are expected.

APPENDIX

GEOLOGICAL NOTE

Petrophysical and thermal properties of pre-Devonian basement rocks on the Norwegian continental margin

Trond Slagstad[1], Cécile Barrére[1], Børre Davidsen[1], Randi K. Ramstad[1,2]

[1]Geological Survey of Norway (NGU), 7491 Trondheim, Norway
[2]Present address: Asplan Viak AS, Pb 6723, 7031 Trondheim, Norway
E-mail: trond.slagstad@ngu.no

This Geological note presents petrophysical and thermal properties of pre-Devonian basement rocks along the Norwegian continental margin. The dataset is the first to present ground-truth data from basement rocks along the continental margin, and can be used to constrain future geophysical and thermal models of the margin's structure.

Introduction

Gravimetric and magnetic surveys along the Norwegian continental margin has significantly improved our understanding of the margin's crustal architecture and has allowed correlations between the onshore and offshore realms (e.g., Doré et al. 1997, Olesen et al. 2002, Skilbrei et al. 2002, Lyngsie et al. 2006), in addition to yielding important information to the petroleum industry. Furthermore, the location of hydrocarbon accumulations is believed to depend on the temperature structure of the subsurface (*e.g., Bjørkum and Nadeau 1998*), which in turn varies with variations in thermal conductivity and radiogenic heat production. However, models based on gravimetric, magnetic and thermal methods are hampered by a lack of ground-truth data, and at present, the petrophysical and thermal properties of basement rocks along the Norwegian continental margin have to be inferred from onshore datasets and educated estimates. Here, we present new data that help characterise the basement along the Norwegian continental margin (defined here as the dominantly pre-Devonian crystalline rocks underlying the ubiquitous Mesozoic cover) in terms of mineralogical and chemical composition, and petrophysical/thermal properties. The work is based on samples from 22 wells that have penetrated basement rocks, made available by the Norwegian Petroleum Directorate and Statoil. The purpose of this brief communication is to present petrophysical data from 12 wells (15 samples) in the North Sea, 4 wells (6 samples) in the Norwegian Sea and 6 wells (12 samples) in the

Slagstad, T., Barrére, C., Davidsen, B. and Ramstad, R. K. (2008) Petrophysical and thermal properties of pre-Devonian basement rocks on the Norwegian continental margin. Geological Survey of Norway Bulletin, 448, xxx–xxx

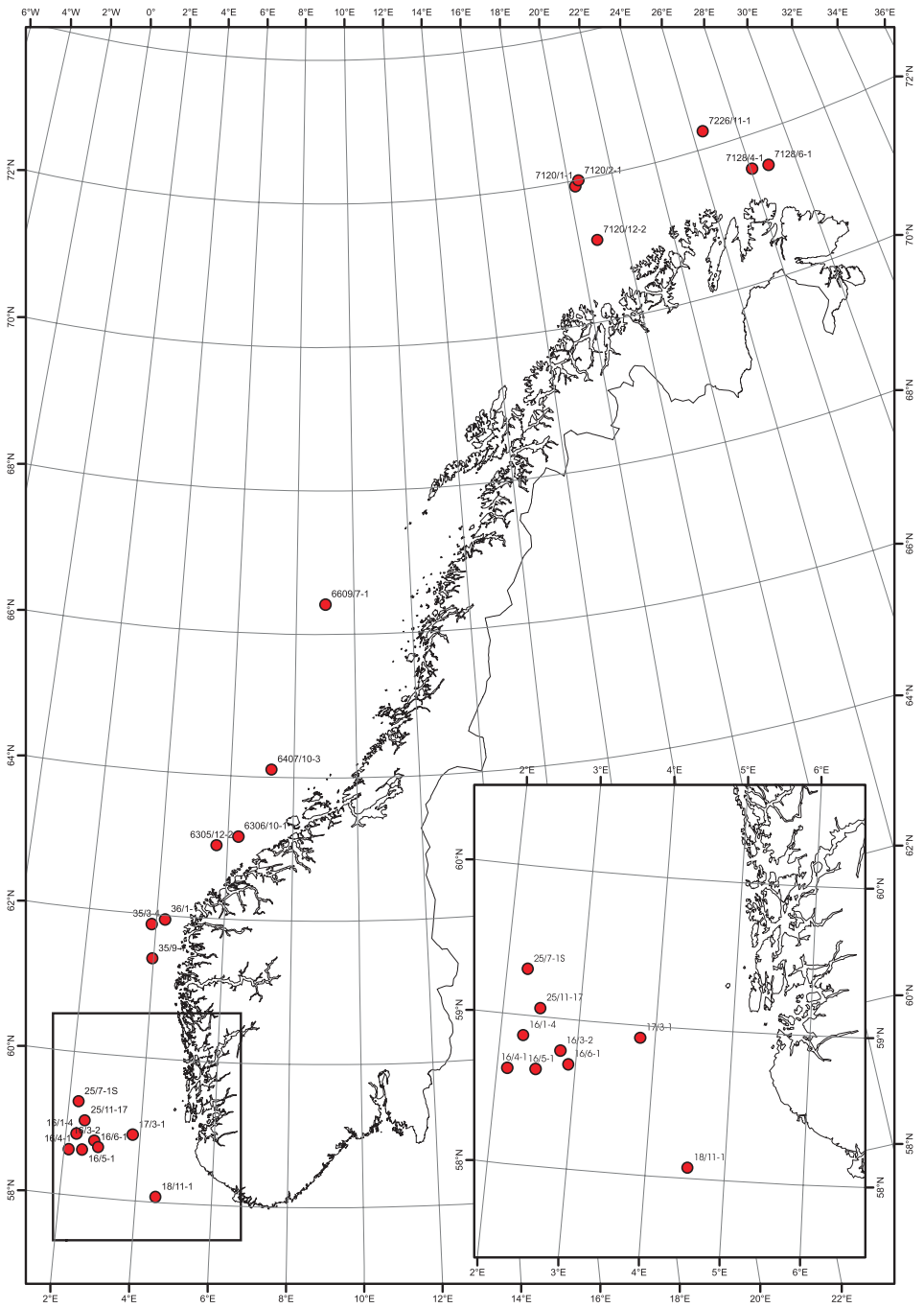

Figure 1. Overview of the Oslo Rift and distribution of larvikite and similar rocks. Modified from NGU digital maps of the Oslo region.

Barents Sea (Figure 1). The analyses include determination of density, magnetic remanence, magnetic susceptibility, thermal conductivity and radiogenic heat production. The samples are described in Appendix 1 and a discussion on the geological significance of a subset of the samples is presented by Slagstad and Davidsen in Olesen et al. (*2007*). A few super-basement samples were also analysed for petrophysical properties. These samples are described in Appendix 2 and the data presented in Table 1.

Analytical methods

Petrophysical properties

Measurements of density, remanence and magnetic susceptibility are conducted following procedures described by Torsvik and Olesen (1988) and Olesen (1988).

Thermal conductivity

Measurements of thermal conductivity are conducted on 2 cm thick circular disks. A constant heat flow is induced to the top of the sample by placing a heat source with a constant tempera-

Table 1. Petrophysical data from offshore basement samples, and some super-basement samples.

Well name	Sample depth (m)	Area	Top Basement Depth (m)	Sample depth below Top Basement (m)	North	East	Lithology	Density (kg m^{-3})	Magnetic suscept. (10^{-6} SI)	Magnetic remanence (10-3 A m^{-1})	Electrical resistivity (ohm*m)
16/1-4	1937.0	North Sea	1864.0	73.0	58° 51` 55.20`` N	2° 17` 56.12`` E	Gabbro	2765	448.4	32.1	130
16/3-2	2017.7	North Sea	2015.0	2.7	58° 47` 12.80`` N	2° 47` 34.70`` E	Granite	2680	949.7	48.8	39845
16/4-1	2907.4	North Sea	2885.0	22.4	58° 38` 18.33`` N	2° 8` 17.03`` E	Altern. qtzite/siltstone	2778	221.3	2.8	3829
16/4-1	2908.6	North Sea	2885.0	23.6	58° 38` 18.33`` N	2° 8` 17.03`` E	Granite	2646	88	6.9	11075
16/5-1	1929.3	North Sea	1925.0	4.3	58° 38` 53.66`` N	2° 29` 39.69`` E	Granite	2662	179.8	11.3	403
16/6-1	2059.7	North Sea	2055.0	4.7	58° 42` 06.00`` N	2° 54` 44.00`` E	Porph. volcanic rock	2591	181.1	9.5	768
17/3-1	2849.5	North Sea	2811.0	38.5	58° 55` 02.50`` N	3° 48` 21.33`` E	Breccia	2750	553.3	10.3	1100
17/3-1	2850.7	North Sea	2811.0	39.7	58° 55` 02.50`` N	3° 48` 21.33`` E	Breccia	2661	58.3	0	14854
18/11-1	2082.3	North Sea	2060.0	22.3	58° 4` 21.30`` N	4° 32` 00.10`` E	Porph. volcanic rock	2639	207.4	22	1465
25/7-1S	3548.2	North Sea	n.a.	n.a.	59° 18` 35.23`` N	2° 16` 05.37`` E	Brecciated siltstone	2883	1406.8	68.7	110
25/7-1S	3554.3	North Sea	n.a.	n.a.	59° 18` 35.23`` N	2° 16` 05.37`` E	Qtz-rich sandstone	2722	48.8	9.2	553
25/11-17	2259.5	North Sea	2243.0	16.5	59° 3` 26.66`` N	2° 29` 06.59`` E	Metasiltstone	2656	291.6	0	415
35/3-4	4088.3	North Sea	4069.0	19.3	61° 51` 54.54`` N	3° 52` 26.99`` E	Bt-gneiss	2773	234.1	0	2288
35/9-1	2313.6	North Sea	2313.6	0.0	61° 23` 07.95`` N	3° 59` 03.72`` E	Breccia	2619	286.4	0	38
36/1-1	1588.7	North Sea	1568.0	20.7	61° 56` 40.36`` N	4° 15` 43.86`` E	Granitic gneiss	2676	104.3	5.2	835
6305/12-2	3158.3	Norwegian Sea	3145.0	13.3	63° 1` 11.39`` N	5° 40` 06.44`` E	Brecciated siltstone	2740	456.8	9.6	198
6306/10-1	3158.5	Norwegian Sea	2989.0	169.5	63° 9` 26.32`` N	6° 19` 41.45`` E	Quartz diorite	2767	2836.2	58.6	363
6306/10-1	3159.2	Norwegian Sea	2989.0	170.2	63° 9` 26.32`` N	6° 19` 41.45`` E	Quartz diorite	2732	1001.7	20	1403
6407/10-3	2972.1	Norwegian Sea	2959.0	13.1	64° 6` 11.66`` N	7° 18` 11.43`` E	Granite	2631	1186.7	108.9	11622
6609/7-1	1944.7	Norwegian Sea	1912.0	32.7	66° 24` 56.49`` N	9° 1` 14.91`` E	Brecciated silt-/ sandstone	2622	14.7	0	958
6609/7-1	1945.8	Norwegian Sea	1912.0	33.8	66° 24` 56.49`` N	9° 1` 14.91`` E	Altern. silt-/ sandstone	2580	24.6	11	1121
7120/1-1	4002.2	Barents Sea	3947.0	55.2	71° 55` 00.83`` N	20° 18` 07.13`` E	Amphibolite	3085	777.1	27.2	n.a.
7120/2-1	3478.0	Barents Sea	3471.0	7.0	71° 58` 57.94`` N	20° 28` 35.09`` E	Diabase	2762	42281	475.4	n.a.
7120/2-1	3479.0	Barents Sea	3471.0	8.0	71° 58` 57.94`` N	20° 28` 35.09`` E	Diabase	2727	34025.5	291.6	n.a.
7120/12-2	4675.8	Barents Sea	4664.0	11.8	71° 7` 30.30`` N	20° 48` 19.00`` E	Qtz-rich augen gneiss	2676	177.8	5	15060
7120/12-2	4678.2	Barents Sea	4664.0	14.2	71° 7` 30.30`` N	20° 48` 19.00`` E	Qtz-rich augen gneiss	2656	181.3	10.1	37368
7128/4-1	2527.0	Barents Sea	2503.0	24.0	71° 32` 27.33`` N	28° 4` 54.08`` E	Altern. silt-/ sandstone	2640	207	0	n.a.
7128/4-1	2527.2	Barents Sea	2503.0	24.2	71° 32` 27.33`` N	28° 4` 54.08`` E	Altern. silt-/ sandstone	2638	242.8	28.6	95
7128/4-1	2528.1	Barents Sea	2503.0	25.1	71° 32` 27.33`` N	28° 4` 54.08`` E	Altern. silt-/ sandstone	2617	260.4	46.1	177
7128/6-1	2540.5	Barents Sea	2534.0	6.5	71° 31` 04.99`` N	28° 49` 03.41`` E	Metasandstone	2689	124.8	11	1722
7128/6-1	2541.73	Barents Sea	2534.0	7.7	71° 31` 04.99`` N	28° 49` 03.41`` E	Metasandstone	2622	125.8	0	n.a.
7226/11-1	5198.3	Barents Sea	5137.0	61.3	72° 14` 18.16`` N	26° 28` 44.78`` E	Biotite-rich schist/gneiss	2783	315.8	5	n.a.
7226/11-1	5198.8	Barents Sea	5137.0	61.8	72° 14` 18.16`` N	26° 28` 44.78`` E	Biotite-rich schist/gneiss	2794	337.9	6.5	2295

Continued next page

Table 1. Contined

Non-basement samples

Well name	Sample depth (m)	Area	Top Basement Depth (m)	Sample depth below Top Basement (m)	North	East	Lithology	Density (kg m^{-3})	Magnetic suscept. (10^{-6} SI)	Magnetic remanence (10-3 A m^{-1})	Electrical resistivity (ohm*m)
7120/2-1	2239.35	Barents Sea	n.a.	n.a.	71° 58` 57.94`` N	20° 28` 35.09`` E	Polymict conglomerate	2738	444.6	10.7	n.a.
7120/2-1	2242.35	Barents Sea	n.a.	n.a.	71° 58` 57.94`` N	20° 28` 35.09`` E	Polymict conglomerate	2495	345.9	0	n.a.
7120/2-1	2230.65	Barents Sea	n.a.	n.a.	71° 58` 57.94`` N	20° 28` 35.09`` E	Polymict conglomerate	2642	241.8	2.8	**n.a.**
7120/2-1	**2235**	**Barents Sea**	**n.a.**	**n.a.**	**71° 58` 57.94`` N**	**20° 28` 35.09`` E**	**Reddish brown, fine-grained conglomerate or ignimbrite???**	**2656**	**328.5**	**8.4**	**n.a.**
7120/2-1	**2645**	**Barents Sea**	**n.a.**	**n.a.**	**71° 58` 57.94`` N**	**20° 28` 35.09`` E**	**Conglomerate, silty and sandy matrix**	**2556**	**151.2**	**0**	**n.a.**
7120/2-1	**2641.35**	**Barents Sea**	**n.a.**	**n.a.**	**71° 58` 57.94`` N**	**20° 28` 35.09`` E**	**Breccia**	**2587**	**421.4**	**3.9**	**n.a.**

ture approximately 10 mm above the top surface of the sample. The heat is transferred as radiation. The sample is insulated on all other surfaces and the temperature is measured at the base of the sample. The thermal conductivity (K) is calculated from Equation 1 based on measured thermal diffusivity (α) and density (ρ), and assumed specific heat (Cp) of the sample. The specific heat capacity is assumed to be 850 J kg^{-1} K^{-1} for all rock types.

$$K = \rho C_p \alpha \qquad (1)$$

Radiogenic heat production

Radiogenic heat production is calculated from U, Th and K concentrations determined by standard XRF and LA–ICP–MS techniques at NGU and measured densities (δ) using Equation 2 (Rybach 1988).

$$A = \delta * (9.52C_U + 2.56C_{Th} + 3.48C_K) * 10^{-5} \qquad (2)$$

where C_U and C_{Th} represent U and Th concentrations in ppm, respectively, and C_K represents K concentration in wt.%.

Petrophysical and thermal properties

The petrophysical and thermal data are presented in Tables 1 and 2, respectively. Compilations of onshore petrophysical data show that most geological units display highly varied magnetic properties, typically ranging between 2 and 3 orders of magnitude (Skilbrei 1989), greatly limiting the value of a small dataset with poor geological control (due to pinprick offshore sampling). However, despite the difficulties in extending these very localised measurements to a larger rock volume, they represent additional information to the onshore petrophysical database at NGU. The main purpose of this contribution is therefore to disseminate the available data so that they are available to other researchers who may find them useful. For the same reason, we limit ourselves to a very brief and general discussion.

Most of the offshore samples are relatively low-magnetic, which is compatible with the geological information (Slagstad and Davidsen, in Olesen et al. 2007) suggesting that the shallow basement along much of the continental margin consists of rock types that may be correlated with the Caledonian Uppermost Allochthon on land (cf., Olesen et al. 2002). In particular, the granites encountered in wells 16/3-2, 16/4-1, 16/5-1 and 6407/10-3 yield Caledonian ages and may be correlated with the low-magnetic Bindal batholith (Olesen et al. 2002). The diabase from well 7120/2-1 confirms the presence of thick mafic dykes within the basement of the Loppa High. This is in agreement with the joint interpretation of potential field modelling (Barrére et al. 2007) that proposes a tongue of basement affected by mafic dykes all along the fault complexes bordering the west of the Loppa High.

Table 2. Thermal data from offshore basement samples.

Well name	Depth (m)	Area	Top Basement Depth (m)	Sample depth below Top Basement (m)	North	East	Lithology	Thermal conduct-ivity ($W\ m^{-1}K^{-1}$)	n	K (wt.%)	Th (ppm)	U (ppm)	Heat production (µW m-3)
16/1-4	1937.0	North Sea	1864.0	73.0	58° 51` 55.20`` N	2° 17` 56.12`` E	Gabbro	2.38	1	2.80	2.83	8.37	2.7
16/3-2	2017.7	North Sea	2015.0	2.7	58° 47` 12.80`` N	2° 47` 34.70`` E	Granite	3.12	1	2.25	8.70	2.62	1.5
16/4-1	2907.4	North Sea	2885.0	22.4	58° 38` 18.33`` N	2° 8` 17.03`` E	Altern. qtzite/ siltstone	2.51 (2.17–2.94)	4	3.82	10.8	3.64	2.1
16/4-1	2908.6	North Sea	2885.0	23.6	58° 38` 18.33`` N	2° 8` 17.03`` E	Granite	3.18	1	3.11	11.5	1.11	1.3
16/5-1	1929.3	North Sea	1925.0	4.3	58° 38` 53.66`` N	2° 29` 39.69`` E	Granite	3.23	1	2.89	10.7	2.89	1.7
16/6-1	2059.7	North Sea	2055.0	4.7	58° 42` 06.00`` N	2° 54` 44.00`` E	Porph. volcanic rock	2.89	1	2.26	0.34	0.96	0.5
17/3-1	2849.5	North Sea	2811.0	38.5	58° 55` 02.50`` N	3° 48` 21.33`` E	Breccia	2.69	1	0.04	1.81	0.60	0.3
17/3-1	2850.7	North Sea	2811.0	39.7	58° 55` 02.50`` N	3° 48` 21.33`` E	Breccia	3.93	1	0.05	1.59	0.55	0.3
18/11-1	2082.3	North Sea	2060.0	22.3	58° 4` 21.30`` N	4° 32` 00.10`` E	Porph. volcanic rock	3.25	1	0.11	7.14	2.12	1.0
25/7-1S	3548.2	North Sea	n.a.	n.a.	59° 18` 35.23`` N	2° 16` 05.37`` E	Brecciated siltstone	2.42	1	0.11	2.96	0.91	0.5
25/7-1S	3554.3	North Sea	n.a.	n.a.	59° 18` 35.23`` N	2° 16` 05.37`` E	Qtz-rich sandstone	4.69	1	2.67	3.65	0.96	0.8
25/11-17	2259.5	North Sea	2243.0	16.5	59° 3` 26.66`` N	2° 29` 06.59`` E	Metasiltstone	2.04	1	4.81	9.00	1.56	1.5
35/3-4	4088.3	North Sea	4069.0	19.3	61° 51` 54.54`` N	3° 52` 26.99`` E	Bt-gneiss	2.00	1	3.16	9.13	2.22	1.5
35/9-1	2313.6	North Sea	2313.6	0.0	61° 23` 07.95`` N	3° 59` 03.72`` E	Breccia	2.34 (2.25–2.47)	3	1.27	3.31	1.19	0.6
36/1-1	1588.7	North Sea	1568.0	20.7	61° 56` 40.36`` N	4° 15` 43.86`` E	Granitic gneiss	2.70 (2.54–2.80)	3	3.89	11.9	1.75	1.6
6305/12-2	3158.3	Norwegian Sea	3145.0	13.3	63° 1` 11.39`` N	5° 40` 06.44`` E	Brecciated siltstone	2.85	1	0.72	0.11	0.29	0.2
6306/10-1	3158.5	Norwegian Sea	2989.0	169.5	63° 9` 26.32`` N	6° 19` 41.45`` E	Quartz diorite	2.76	1	1.29	4.66	2.68	1.2
6306/10-1	3159.2	Norwegian Sea	2989.0	170.2	63° 9` 26.32`` N	6° 19` 41.45`` E	Quartz diorite	2.94	1	1.60	7.08	1.96	1.2
6407/10-3	2972.1	Norwegian Sea	2959.0	13.1	64° 6` 11.66`` N	7° 18` 11.43`` E	Granite	3.56	1	4.41	58.3	2.65	5.0
6609/7-1	**1944.7**	**Norwegian Sea**	**1912.0**	**32.7**	**66° 24` 56.49`` N**	**9° 1` 14.91`` E**	**Brecciated silt-/ sandstone**	**5.15 (4.95–5.44)**	**3**	**1.66**	**3.25**	**0.92**	**0.6**
6609/7-1	**1945.8**	**Norwegian Sea**	**1912.0**	**33.8**	**66° 24` 56.49`` N**	**9° 1` 14.91`` E**	**Altern. silt-/ sandstone**	**3.58**	**1**	**2.76**	**7.84**	**2.34**	**1.3**
7120/1-1	**4002.2**	**Barents Sea**	**3947.0**	**55.2**	**71° 55` 00.83`` N**	**20° 18` 07.13`` E**	**Amphibolite**	**2.69**	**1**	**0.93**	**3.42**	**1.07**	**0.7**
7120/2-1	**3478.0**	**Barents Sea**	**3471.0**	**7.0**	**71° 58` 57.94`` N**	**20° 28` 35.09`` E**	**Diabase**	**n.a.**	**0**	**n.a.**	**n.a.**	**n.a.**	**n.a.**
7120/2-1	**3479.0**	**Barents Sea**	**3471.0**	**8.0**	**71° 58` 57.94`` N**	**20° 28` 35.09`` E**	**Diabase**	**n.a.**	**0**	**n.a.**	**n.a.**	**n.a.**	**n.a.**
7120/12-2	**4675.8**	**Barents Sea**	**4664.0**	**11.8**	**71° 7` 30.30`` N**	**20° 48` 19.00`` E**	**Qtz-rich augen gneiss**	**2.72 (2.60–2.82)**	**3**	**1.69**	**16.2**	**4.85**	**2.5**
7120/12-2	**4678.2**	**Barents Sea**	**4664.0**	**14.2**	**71° 7` 30.30`` N**	**20° 48` 19.00`` E**	**Qtz-rich augen gneiss**	**2.94**	**1**	**2.90**	**4.29**	**0.40**	**0.7**
7128/4-1	**2527.0**	**Barents Sea**	**2503.0**	**24.0**	**71° 32` 27.33`` N**	**28° 4` 54.08`` E**	**Altern. silt-/ sandstone**	**n.a.**	**0**	**n.a.**	**n.a.**	**n.a.**	**n.a.**
7128/4-1	**2527.2**	**Barents Sea**	**2503.0**	**24.2**	**71° 32` 27.33`` N**	**28° 4` 54.08`` E**	**Altern. silt-/ sandstone**	**n.a.**	**0**	**4.18**	**21.2**	**5.51**	**3.2**
7128/4-1	**2528.1**	**Barents Sea**	**2503.0**	**25.1**	**71° 32` 27.33`` N**	**28° 4` 54.08`` E**	**Altern. silt-/ sandstone**	**n.a.**	**0**	**3.68**	**19.3**	**4.62**	**2.8**
7128/6-1	**2540.5**	**Barents Sea**	**2534.0**	**6.5**	**71° 31` 04.99`` N**	**28° 49` 03.41`` E**	**Metasandstone**	**4.90**	**1**	**1.47**	**2.58**	**0.87**	**0.5**
7128/6-1	**2541.73**	**Barents Sea**	**2534.0**	**7.7**	**71° 31` 04.99`` N**	**28° 49` 03.41`` E**	**Metasandstone**	**n.a.**	**0**	**n.a.**	**n.a.**	**n.a.**	**n.a.**
7226/11-1	**5198.3**	**Barents Sea**	**5137.0**	**61.3**	**72° 14` 18.16`` N**	**26° 28` 44.78`` E**	**Biotite-rich schist/gneiss**	**n.a.**	**0**	**n.a.**	**n.a.**	**n.a.**	**n.a.**
7226/11-1	**5198.8**	**Barents Sea**	**5137.0**	**61.8**	**72° 14` 18.16`` N**	**26° 28` 44.78`` E**	**Biotite-rich schist/ gneiss**	**3.75 (3.70–3.81)**	**3**	**2.43**	**12.6**	**2.55**	**1.8**

References

Barrére, C., Ebbing, J., Skilbrei, J.R. and Zeyen, H. (2007) Lithospheric characterisation by joint interpretation of potential fields and thermal modelling - southwestern Barents Sea, Norway. *In EGM 2007 International Workshop Innovation in EM, Grav and Mag Methods: a new Perspective for Exploration*, Capri, Italy.

Bjørkum, P.A. and Nadeau, P.H. (1998) Temperature controlled porosity/permeability reduction, fluid migration, and petroleum exploration in sedimentary basins. *Australian Petroleum Production and Exploration Journal,* **38**, 453-464.

Doré, A.G., Lundin, E., Fichler, C. and Olesen, O. (1997) Patterns of basement structure and reactivation along the NE Atlantic margin. *Journal of the Geological Society of London*, **154**, 85-92.

Lyngsie, S.B., Thybo, H. and Rasmussen, B.L. (2006) Regional geological and tectonic structures of the North Sea area from potential field modelling. *Tectonophysics*, **413**, 147-170.

Olesen, O. (1988) Petrofysiske undersøkelser, Finnmark. *NGU Rapport 88.222*, 154 pp.

Olesen, O., Lundin, E., Nordgulen, Ø., Osmundsen, P.T., Skilbrei, J.R., Smethurst, M.A., Solli, A., Bugge, T. and Fichler, C. (2002) Bridging the gap between the onshore and offshore geology in Nordland, northern Norway. *Norsk Geologisk Tidsskrift*, **82**, 243-262.

Olesen, O., Balling, N., Barrère, C., Breiner, N., Davidsen, B., Ebbing, J., Elvebakk, H., Gernigon, L., Koziel, J., Lutro, O., Midttømme, K., Nordgulen, Ø., Olsen, L., Osmundsen, P.T., Pascal, C., Ramstad, R.K., Rønning, J.S., Skilbrei, J.R., Slagstad, T. and Wissing, B. (2007) KONTIKI Final Report, CONTInental Crust and Heat Generation In 3D. *NGU Report 2007.042*, 438 pp.

Rybach, L. (1988) Determination of heat production rate. In Hänel, R., Rybach, L. and Stegena, L. (eds.) *Handbook of Terrestrial Heat-Flow Determination*, Kluwer Academic Publishers, Dordrecht, pp. 125-142.

Skilbrei, J.R. (1989) Petrofysiske undersøkelser, Midt-Norge. *NGU Rapport 89.164*, 109 pp.

Skilbrei, J.R., Olesen, O., Osmundsen, P.T., Kihle, O., Aaro, S. and Fjellanger, E. (2002) A study of basement structures and onshore-offshore correlations in Central Norway. *Norwegian Journal of Geology*, **82**, 263-279.

Torsvik, T.H. and Olesen, O. (1988) Petrophysics and palaeomagnetism initial report of the Norwegian Geological Survey Laboratory. *NGU Report 88.171*, 108 pp.